Water Research X 31 (2026) 100527

Contents lists available at ScienceDirect

Water Research X

journal homepage: www.sciencedirect.com/journal/water-research-x

Pristine and modified biochar comparison for environmental micro(nano)plastic removal: adsorption dynamics, influencing factors, mechanisms, and regeneration potential

Muhammad Junaid [a,*], Stuart Cairns [a], Iain Robertson [a], Peter J. Holliman [b]

[a] Department of Geography, Faculty of Science and Engineering, Swansea University, Swansea SA2 8PP, UK
[b] Chemistry Engineering Materials Environment Group (CEMEG), Faculty of Science and Engineering, Swansea University, Swansea SA1 8EN, UK

ARTICLE INFO

Keywords:
Magnetic biochar
Micro(nano)plastics
Adsorption mechanisms
Biochar regeneration
Plastic degradation

ABSTRACT

Micro(nano)plastics (MNPs) are plastic particles ranging in size from < 1 μm to 5 mm, posing immense challenges owing to their ubiquitous and polydisperse nature, ecological and human health risks, and environmental remediation challenges. Biochar is a promising tool to remove legacy and emerging environmental pollutants, including MNPs, from aquatic and terrestrial matrices. This review systematically collates studies on pristine and modified biochar in terms of their potential to remove MNPs from laboratory and environmental samples (freshwater, seawater, wastewater, and soil), factors affecting MNP-biochar interactions, adsorption mechanisms, biochar regeneration methods, and research gaps. Our data analyses showed that the modified biochar (8.25–897.7 m^2/g, $p = 0.035$) exhibited significantly higher surface area than that of pristine biochar (1.30–540.36 m^2/g). Similarly, the adsorption capacity of modified biochar (10.92–1723 mg/g, $p = 0.030$) was significantly higher than that of the pristine biochar (0.56–80.3 mg/g). Pearson correlation analysis showed a significantly positive correlation between surface area and pyrolysis temperature for pristine biochar ($r = 0.81$, $p < 0.05$); and adsorption capacity showed a significantly positive correlation with the size of MNPs ($r = 0.78$, $p < 0.05$) for modified biochar. Further, properties of MNPs, biochar, and environmental conditions were the major factors affecting the MNP-biochar interface, plastic removal, and biochar regeneration. Removal mechanisms mainly involved pore filling, physical trapping, electrostatic interaction, hydrophobic interaction, hydrogen bonding, and π-π interactions. Depending on the type of MNPs and biochar, either single or multiple removal mechanisms can be involved in the adsorption of MNPs on biochar. Pyrolysis, ultrasonication, chemical methods, and hydrothermal degradation were mainly used individually or in combination to regenerate biochar with high reuse efficiencies. Lack of field studies; polymer mixture and environmental MNP removal; aging of biochar and MNPs; optimization and sustainable modification and regeneration of biochar; MNP-biochar-specific interaction mechanisms; scale-up applications; and fate of spent MNP-biochar complexes are the major research gaps and future research perspectives.

1. Introduction

In recent decades, the use of carbonaceous materials, such as biochar, carbon nanotubes, activated carbon, and graphene, has immensely increased to remove legacy and emerging pollutants from the environment (Cairns et al., 2024; Haziq et al., 2020; Soffian et al., 2022; Singh et al., 2024). Considering sustainability and economic feasibility, biochar is deemed the most promising carbonaceous material for environmental remediation. Biochar, a porous carbon-rich material, is produced as an oxygen-depleted byproduct through pyrolysis of renewable biomass at temperatures between 350 °C and 1000 °C (Afraz et al., 2024; Schmidt et al., 2016). The estimated cost of biochar is USD 246 per tonne, which is about one-sixth the price of commercial activated carbon and far lower than that of graphene and carbon nanotubes (Amalina et al., 2024). Moreover, the feedstock source for biochar production is more adaptable than the alternatives. Biochar is a sustainable, cost-effective material with a high adsorption capacity and chemical stability, making it an effective and eco-friendly adsorbent for immobilising or adsorbing contaminants (Amalina et al., 2023). Biochar is a compelling choice for ecological rehabilitation and waste management

* Corresponding author.
E-mail addresses: muhammad.junaid@swansea.ac.uk, junaidyaha@gmail.com (M. Junaid).

https://doi.org/10.1016/j.wroa.2026.100527
Received 22 December 2025; Received in revised form 12 March 2026; Accepted 21 March 2026
Available online 22 March 2026

owing to its potential for large-scale production and multifunctionality (Masud et al., 2023). It is frequently used as an efficient biosorbent for contaminants owing to its abundant surface oxygen-containing functional groups (e.g., $C = O$, -OH, -COOH) and elevated porosity (Zhang et al., 2024). The plentiful biomass in nature offers a substantial and cost-effective supply of biochar, significantly enhancing its practical use. At present, biochar is utilised to remove a range of pollutants from water, including micro(nano)plastics (MNPs) (Cairns et al., 2024), heavy metals (Yi et al., 2019), antibiotics (Cheng et al., 2021), polycyclic aromatic hydrocarbons (Yao et al., 2024), and per- and polyfluoroalkyl substances (Kundu et al., 2021).

In 2023, total global plastic production was estimated at 413.8 million tons (vs. 360 million tons in 2018), of which only 36.5 million tons is recycled, and the rest is dumped into the environment (PlasticEurope 2024). As a result of natural weathering and anthropogenic activities, huge quantities of plastic fragments and particles of polydisperse nature ended up in terrestrial and aquatic environments. Microplastics (MPs) and nanoplastics (NPs), also jointly termed MNPs, are plastic particles ranging in size from <1 μm to 5 mm and are presently known as persistent pollutants (Junaid et al., 2024). MNPs ubiquitously contaminated the global environment, such as rivers (Kiss et al., 2021), oceans (Isobe et al., 2019), soil (Guo et al., 2020) and air (Sridharan et al., 2021). The varying sizes, morphology, and polymers of MNPs affect their environmental behaviour and interaction with biotic and abiotic components. NPs (< 1000 nm) are particularly concerning due to their prevalence and diminutive size, which facilitate ingestion by many aquatic organisms (Pitt et al., 2018; Nanninga et al., 2020). MNPs may exhibit several surface functional groups, including CH_3–, COO–, and $C = C$, enabling them to interact with both inorganic (Ho and Leung, 2021) and organic pollutants (Junaid et al., 2024; Junaid et al., 2023), as well as organic matter (Junaid and Wang, 2021). Plastic particles can undergo trophic transfer in the food chain (Junaid et al., 2024) and were recently identified and measured in human blood for the first time (Leslie et al., 2022). As the size of NPs diminishes, they provide an increased risk to ecological and human health (Liu et al., 2023). Furthermore, NPs were often distributed in freshwater, with contamination levels as high as 10^{14}, rendering their removal challenging (Besseling et al., 2018; Junaid et al., 2024). As the particle size of MNPs decreases, the potential of sewage treatment facilities in eliminating them from water declines, resulting in the persistent release of NPs into the environment (Groppe et al., 2022).

Adsorption is considered a potential solution for mitigating MNP pollution, owing to its low energy consumption, cost-effectiveness, and repeatability (Zhou et al., 2022). To achieve highly effective MNP adsorbent materials, several modifications, such as acid oxidation, metal salt activation, iron modification, and ball milling, have been implemented (Magid et al., 2021; Shi et al., 2023; Xing et al., 2023). Moreover, to tackle the difficulties in biochar recovery, magnetic separation has been extensively studied for its efficiency and speed. Iron-containing particles, including $FeCl_3$ (Singh et al., 2021), Fe_3O_4 (Shi et al., 2023), Fe $(NO_3)_3$ (Wang et al., 2021), and Fe mining waste (Kim et al., 2024) have been employed in the synthesis of magnetic biochar. Magnetic biochar often possesses a larger specific surface area, enhanced homogeneity, and a greater number of oxygen-containing functional groups, resulting in superior adsorption capacity (Magid et al., 2021; Wang et al., 2021). In comparison to pristine biochar, magnetic biochar demonstrates superior adsorptive removal efficacy for MNPs (Shi et al., 2023). MNPs, along with biochar, possess a negative charge and exhibit hydrophobic properties. Consequently, these materials may either engage through hydrophobic interactions or repel one another electrostatically. To enhance removal efficiency, biochar can be modified to possess a net positive charge and increased hydrophobicity, hence improving interactions through electrostatic attraction and hydrophobic forces (Hanif et al., 2024). The use of cationic surfactants enhances the hydrophobicity of magnetic biochar (Shi et al., 2023). Cetyltrimethylammonium bromide (CTAB) is a conventional and cost-effective cationic surfactant utilized for biochar modification and the regulation of its surface characteristics (Xing et al., 2024). CTAB has been employed to alter magnetic biochar for the removal of MNPs in batch tests conducted by multiple previous studies, all of which attained removal efficiencies ranging from 90% to 99%. These investigations revealed that CTAB improved the characteristics of biochar, resulting in increased removal efficacy (Hanif et al., 2024; Parashar and Hait, 2024; Shi et al., 2023; Xing et al., 2024). MNP degradation, biochar regeneration, and reuse remain challenging, and associated methods such as pyrolysis (Duan et al., 2025), ultrasonication (Huang et al., 2024), chemical methods (Mahmoud et al., 2024), and hydrothermal degradation (Zhu et al., 2022) are still in their infancy.

So far, a limited number of reviews have summarized studies on biochar application for MNPs removal, such as the nexus between MNPs and biochar for treatment of aquatic media (Cairns et al., 2024), modified biochar solutions for emerging aquatic contaminants (Zhang et al., 2024), sustainable adsorbents for MNPs' mitigation (Das et al., 2024), and biochar as an adsorbent for MNPs removal (Ji et al., 2024; Kumar et al., 2023). However, these studies lack important aspects of the comparison between pristine and modified biochar in terms of surface area, adsorption capacity, and MNPs removal efficiency, as well as comprehensive data synthesis, bibliometric analysis, statistical analysis, laboratory vs. real-world sample comparison, correlation analysis, influencing factors, removal mechanisms, and regeneration potentials. A recent review by Ji et al. on MNP removal by biochar as adsorbents provides valuable insights into adsorption mechanisms and modification techniques (Ji et al., 2024). However, the present review offers some novel additions that transcend beyond earlier work, especially employing data driven statistical approach to analyse available studies. First, a quantitative comparative analysis was conducted using Mann-Whitney U tests to validate the statistically significant differences between pristine and modified biochar in terms of surface area and adsorption capacity that had not been investigated in prior studies. Second, the correlation analysis was performed to highlight the nexus between key variables including adsorption capacity, surface area, pyrolysis temperature, surface area, MNP size that had not been previously examined. Third, bibliometric mapping and Sankey diagram flow analysis were integrated to visualize research trends and the distribution of principal experimental parameters across core studies. Fourth, a comprehensive comparison of MNP removal across different environmental samples (freshwater, seawater, wastewater, and soil) with location-specific data was presented. Finally, we systematically evaluate adsorption mechanisms (general and polymer specific) and biochar regeneration techniques with cycle-based efficiency data, offering practical insights for sustainable application of biochar for MPN removal. Therefore, the current study aims at highlighting a comprehensive bibliometric analysis of the available literature using multiple approaches, comparing the application of pristine and modified biochar for MNP removal in synthetic laboratory and environmental samples, elucidating factors affecting biochar interaction with MNPs, enlisting removal or adsorption mechanisms of MNPs on biochar, summarizing MNP degradation and biochar regeneration approaches, and identifying research gaps, economic feasibility, and future directions.

2. Literature search and data analysis

2.1. Literature search

A systematic literature search was performed using multiple databases, including Google Scholar, ScienceDirect, and Web of Science, to collect studies on the application of pristine and modified biochar for the removal of environmental MNPs. Multiple keywords were used with different combinations for the literature search, such as "microplastics, nanoplastics, micro(nano)plastics, biochar, pristine biochar, magnetic biochar, removal, remediation, regeneration, reuse, degradation mechanism, pyrolysis, aquatic environment, soil, freshwater, rivers, and

seawater." Preferred Reporting Items for Systematic reviews and Meta-Analyses (PRISMA) method was used for selection and exclusion of studies. The collected studies were then filtered, and the selection criteria comprised original research articles that were published in English. Studies failed to fulfil the selection criteria were removed. The literature search was performed in December 2024, with an additional search in March 2025. A total of 29 research articles highlighting the removal of MNPs from various matrices using biochar were finally selected.

2.2. Data analysis

The data extraction and bibliography management were conducted using Lean Library Workspace (Online Reference Manager, sciwheel.com). Microsoft Power BI Desktop 2025, OriginPro 2022 and BioRender (online image drawing tool, biorender.com) were used for data analysis and development of illustrations. Mann-Whitney U test was applied using IBM SPSS Statistic 20 to evaluate the significance difference between pristine and modified biochar for different parameters. Normality of the collected data was checked using IBM SPSS Statistic 20. Microsoft Power BI Desktop 2025 was used to run the correlation analysis.

3. Results and discussion

3.1. Bibliometric analysis and flow of the field

A thorough bibliometric analysis on the co-occurrence of scientific terms or keywords was carried out using VOSviewer version 1.6.20 (https://www.vosviewer.com/) on 29 core publications. Through this analysis, a total of 786 keywords were identified, with 44 meeting the threshold. The software employs a meticulous process to screen the most pertinent terms from the titles and abstracts of the publications. Subsequently, six irrelevant terms were manually excluded, refining the selection for accuracy. Fig. 1a illustrates the annual number of articles published recently. Fig. 1b shows the distribution of studies using laboratory versus environmental samples, highlighting that significantly fewer studies have utilized real-world or field samples. Fig. 1c-d shows the obtained overlay and network visualization maps that illustrate connections between co-occurring terms through lines connecting circles. These lines signify the level of confidence in the association

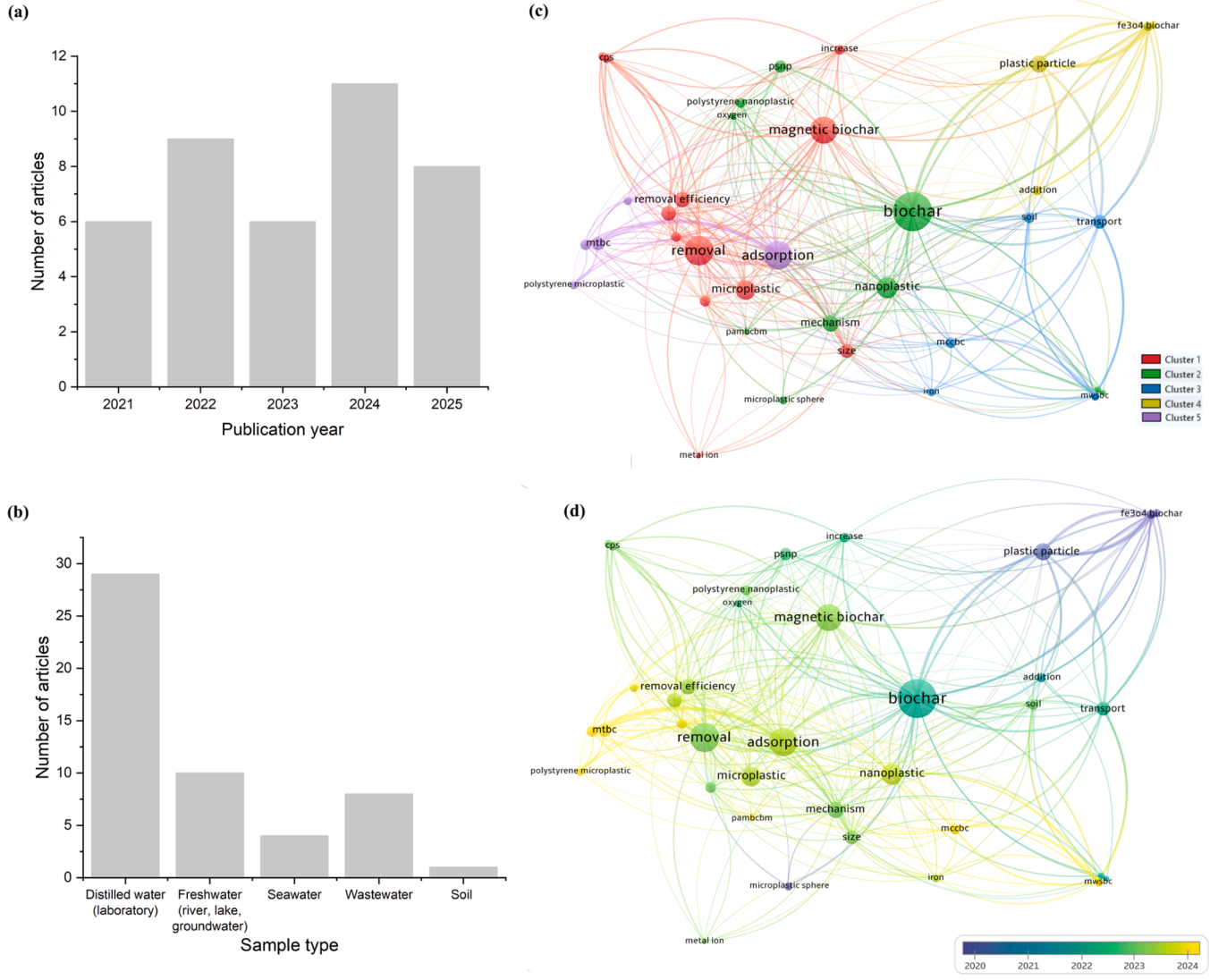

Fig. 1. **(a)** Number of research articles published on application of biochar for removal of MNPs in recent years and **(b)** type of samples employed for treatment in those studies. Bibliometric analysis of co-occurring terms in core research articles ($n = 29$) on removal of MNPs using pristine and modified biochar. **(c)** Network visualization displays co-occurring terms as nodes and co-occurring links as edges and **(d)** overlay visualization shows temporal trend of co-occurring terms. Where node size represents the frequency of the term, edge thickness shows the strength of co-occurrence and cluster color portrays group of closely related terms.

between keywords. The font size variation of terms indicates their frequency of occurrence, while the node curves signify the co-occurrence of terms within the same article. Fig. 1c shows the network visualization map of the terms grouped into various clusters. The data consisted of 38 items, grouped into five distinct clusters, each represented by a unique colour. The links between the clusters exhibited a total link strength of 6708, with 337 links created. Cluster 1 (red) comprises 12 terms, with significant terms including "magnetic biochar, microplastic, removal, size, and cps (carboxyl polystyrene)." Cluster 2 (green) encompasses 10 terms that are dominated by terms such as "biochar, nanoplastic, mechanism, polystyrene nanoplastic, microplastic sphere, and pambcbm (polyaniline-coated magnetic biochar ball-milled)." Cluster 3 (blue) comprises six terms, mainly including "transport, soil, iron, mccbc (magnetic corncob biochar), mwsbc (magnetic walnut shell biochar)." Cluster 4 (yellow) contains 5 terms with significant inclusions: "plastic particle, Fe_3O_4 biochar, and porous medium." Cluster 5 (violet) comprises five terms, such as "adsorption, polystyrene microplastic, and functional group." Fig. 1d overlay visualization map illustrates the evolving research trends in the application of biochar for MNPs removal, which shows that most of the relevant studies have been conducted in the recent past, after 2020. The significant terms from studies published before 2020 and 2022 mainly included general terms such as plastic particles, biochar, transport, addition, soil, increase, microplastic sphere, and Fe_3O_4 biochar. More recently, in 2023 and 2024 onwards, several important and specific terms appeared, mainly including magnetic biochar, polystyrene nanoplastic, cps, iron, mccbc, mwsbc. Some general terms such as adsorption, removal efficiency, microplastic, size, and mechanism have also appeared in recent years to show how this field is evolving over time.

Fig. 2 Sankey diagram was used to show the flow of the field through analysis of extracted data from core research articles ($n = 29$) in terms of biochar type (feedstock/parent material), biochar type (pristine/modified), biochar modification type, pyrolysis temperature for biochar production, type of MNP polymer, and size used. Overall, a total of 82 data records were obtained from the core research articles on the basis selected variable. As for biochar type (pristine/modified), among data points ($n = 82$), modified biochar was evaluated in a higher number of experiments ($n = 58$) for MNP removal, more than twice that of pristine biochar ($n = 24$). Regarding biochar type (origin/parent material), among modified biochar, corncob biochar-CCB ($n = 8$) was the most employed biochar to remove MNPs, followed by mesquite biochar-MSB ($n = 6$), bagasse biochar-BGB ($n = 6$), walnut shell biochar-WSB ($n = 5$), sawdust biochar-SDB ($n = 5$), rapeseed straw biochar-RPB ($n = 4$), pinewood biochar-PWB ($n = 3$), cellulose biochar-CLB ($n = 3$), etc. As for pristine biochar, based on parent material, MSB ($n = 6$) was the commonly used biochar, followed by WSB ($n = 3$), PWB ($n = 3$), CLB ($n = 3$), etc. In the case of biochar modification, $FeCl_3$ magnetized biochar ($n = 13$) was commonly used, followed by $Fe(NO_3)_3$ and $FeSO_4$ magnetized biochar ($n = 8$), acid-modified biochar ($n = 7$), Fe_3O_4 magnetized biochar ($n = 6$), $Na_2S_2O_4$ and $NaBH_4$-$FeCl_3$ magnetized biochar ($n = 5$), iron waste-modified biochar ($n = 5$), $FeCl_3$ and $FeSO_4$ magnetized biochar ($n = 3$), and $FeCl_3$ magnetized biochar ($n = 3$). Commercial sources of iron have been mostly used to magnetize biochar; other sustainable sources, such as mining waste (Magid et al., 2021), red mud waste (Feng et al., 2025), and steelmaking waste, should be explored for their potential use and safety for biochar magnetization. Regarding pyrolysis temperature for biochar production, a pyrolysis temperature >500-≤700 °C was used in most of the experiments ($n = 30$), followed by pyrolysis temperatures of ≤500 °C ($n = 27$) and >700 °C ($n = 24$). Biochar produced at temperatures higher than 500 °C appeared suitable for higher MNP removal that not only kept macropores (10–25 μm) intact but also generated upper-limit mesopore structures (100 nm) (Zhang et al., 2024). As for MNP polymers, PS ($n = 52$) was used in most of the experiments, followed by COOH-PS ($n = 14$), NH_2-PS ($n = 7$), PVC ($n = 4$), PE ($n = 2$), and PA ($n = 2$). PS has been largely used in laboratory studies, which partly represent environmental relevance, owing to widespread contamination of PS in ecosystems. Overall, polymers such as PE and PP are also abundantly present in the

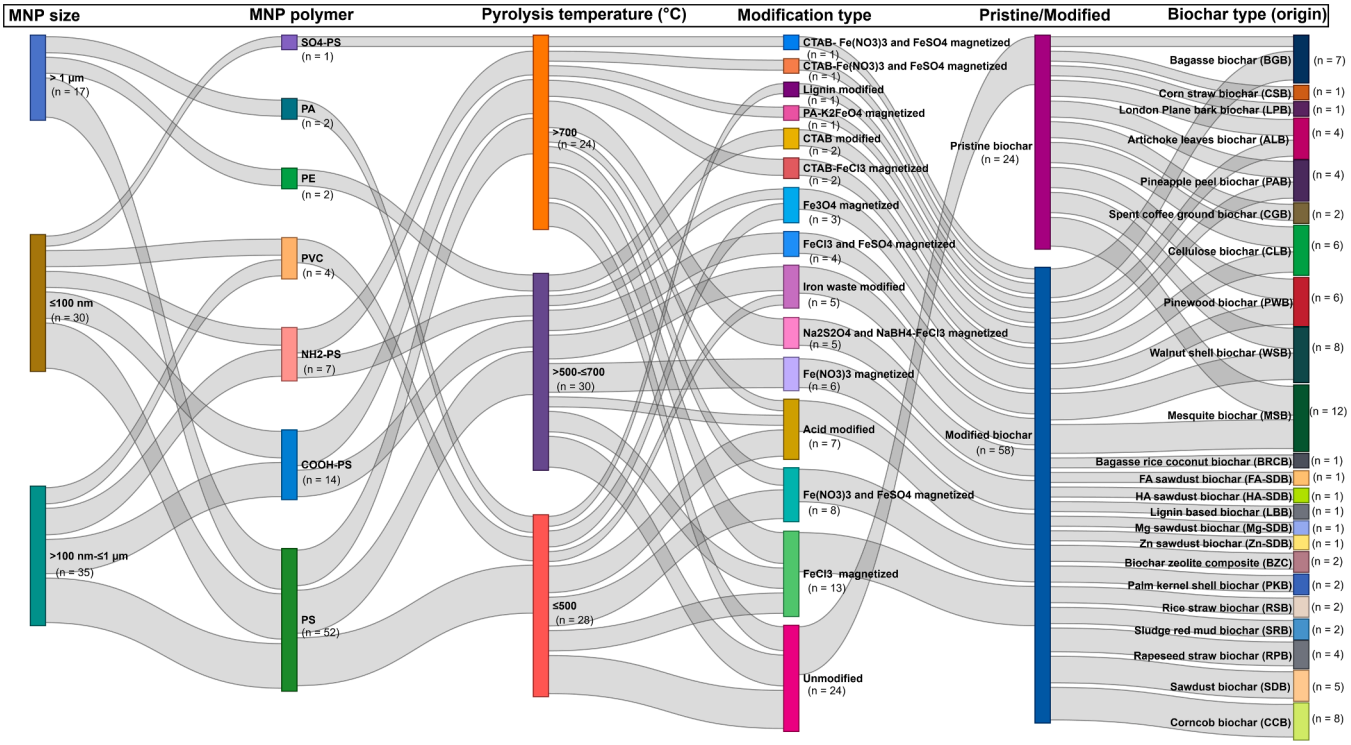

Fig. 2. Sankey diagram highlights summary of research trends in applications of pristine and modified biochar for removal of MNPs. Overlapping variables including biochar type (parent material/origin), biochar type (pristine or modified), biochar modification type, pyrolysis temperature (°C) for biochar production, MNP polymer removed, and MNP size. Data were extracted from published studies and are given in Table 1.

environment, attributed to their huge global consumption and innate property of some polymers to resist natural degradation (Rodrigues et al., 2018). Therefore, common environmentally relevant polymers should also be investigated in future studies for their potential removal using biochar. Regarding MNP size, plastic particles with sizes >100 nm-≤1 μm were mostly used ($n = 35$). followed by ≤100 nm ($n = 30$) and >1 μm ($n = 17$). Interestingly, most of the studies were conducted using NPs (<1000 nm) compared to MPs (>1 μm - 5 mm), which is an environmentally relevant attribute of these studies, as the concentration of NPs was reported to be 10^{14} times higher than that of MPs (Besseling et al., 2018) and they are more hazardous due to their ability to cross biological defence barriers using the Trojan horse effect and developing eco-corona (Junaid and Wang, 2021; Kihara et al., 2021). Spherical-shaped MNPs are mostly used in available studies; other more toxic morphologies, such as fibres, films, foams, and fragments, should also be included in future studies (Junaid et al., 2023).

3.2. Data driven comparison of pristine and modified biochar for MNP removal

Pristine and modified biochar can significantly vary in terms of their surface properties, which can greatly impact the adsorption of MNPs on biochar and their removal from environmental matrices. Biochar modification was mainly based on the addition of Fe from various sources and occasionally in terms of acidifying biochar or coating biochar with CTAB, zeolite, polyaniline, lignin, humic acid (HA), and fulvic acid (FA). Modified biochar enhanced adsorption of MNPs due to improved surface properties. To analyse the difference between surface properties and associated performance of pristine and modified biochar to remove MNPs, data on surface area (m^2/g), adsorption capacity (mg/g), and removal of MNPs (%) were extracted from the available studies. Our results showed that the modified biochar (8.25–897.7 m^2/g) exhibited significantly higher (Mann-Whitney test, $p = 0.035$) surface area than that of pristine biochar (1.30–540.36 m^2/g) (Fig. 3a). Similarly, the adsorption capacity of modified biochar (10.92–1723 mg/g) was significantly higher ($p = 0.030$) than that of the pristine biochar (0.56–80.3 mg/g) (Fig. 3b). The percentage removal of MNPs was also significantly higher ($p = 0.001$) by modified biochar (25–100%), compared to pristine biochar (14–100%) (Fig. 3c). Removal percentages for modified biochar were skewed toward higher values (>80%) compared to pristine biochar (Fig. 3c). Most of the studies reported an increase in surface area and adsorption properties of biochar after modification, albeit a decrease in surface area of iron-modified SDB (9.6 m^2/g) compared to pristine biochar (305.3 m^2/g) was also reported, attributed to the pore blockage of modified biochar by Fe_3O_4. However, the adsorption capacity of modified SDB was still higher than that of the pristine biochar, attributed to the improved structure and surface properties (Duan et al., 2025). This phenomenon implies that for modified biochar, surface properties other than surface area could be the leading factor controlling MNP adsorption. Multiple mechanisms can explain this paradox, e.g., the elevated adsorption of MNPs could be attributed to strong electrostatic interactions between iron oxide mediated positively charged biochar surfaces and negatively charged MNPs (Duan et al., 2025; Shi et al., 2023). Modified biochar exhibits specific sites with higher adsorption energy that exceeds the non-specific van der Waals forces, which mainly dominate on pristine biochar. Therefore, the higher binding energy per site leads to a greater overall adsorption capacity even with fewer total sites, i.e., lower surface area (Kim et al., 2024). As the surface area decreased, the surface of biochar becomes rougher with nanoclusters iron oxide creating hot spots for MNP adsorption (Xing et al., 2024). As shown in Fig. 5C, modified SDB with coated fine particulate Fe_3O_4 provides multiple active sites for MNPs, even within a constricted pore structure (Duan et al., 2025). Moreover, the O/C ratio and surface polarity can significantly change after iron modification. For instance, the magnetic WSB showed increased O/C ratio (0.09) compared to pristine biochar (0.02),

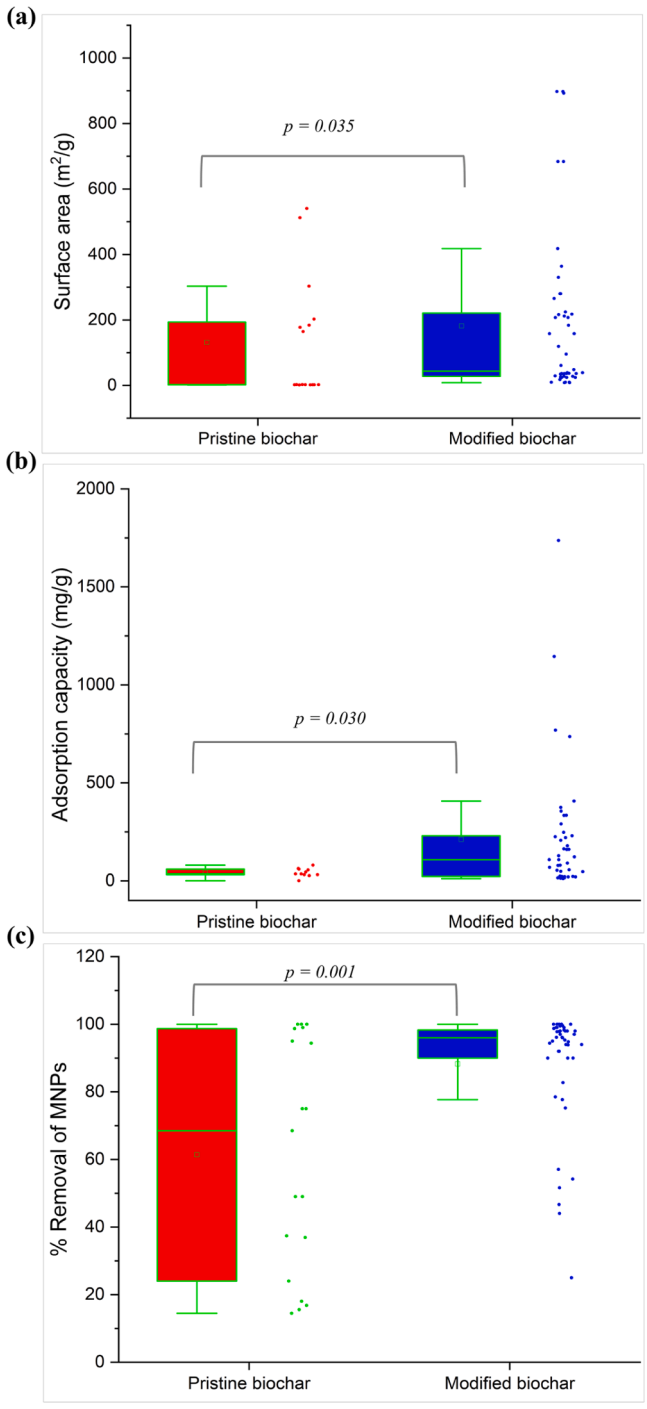

Fig. 3. Mann-Whitney test highlights the significant difference in **(a)** surface area ($p = 0.035$), **(b)** adsorption capacity ($p = 0.030$), and **(c)** percentage removal of MNPs ($p = 0.001$) between pristine biochar and modified biochar. Data were extracted from published studies and are given in Table 1.

suggesting enhanced hydrophilic properties that increased adsorption of anionic PSMPs on modified WSB via hydrogen bonding, despite no significant increase in surface area (Kim et al., 2024). Therefore, iron modification can introduce diverse adsorption mechanisms including ligand exchange, surface complexation, and cation bridging that operate synergistically to improve MNP adsorption independent of surface area (Singh et al., 2021; Zhu et al., 2022).

Pearson correlation analysis showed a significantly positive correlation between surface area and pyrolysis temperature for pristine biochar ($r = 0.81, p < 0.05$); however, for modified biochar this correlation

was positive but not significant ($r = 0.37$) (Fig. 4a, b). The adsorption capacity showed a significantly positive correlation with the size of MNPs ($r = 0.78$, $p < 0.05$) for modified biochar, and for pristine biochar this association was negative ($r = -0.26$), albeit not significant. Spearman correlation analysis showed similar results, but more associations were found among the variables (Fig. 4c, d). For instance, surface area with pyrolysis temperature ($r = 0.54$) and %MNP removal with MNP size ($r = 0.48$) showed a positive relationship for pristine biochar. For modified biochar, %MNP removal with adsorption capacity ($r = 0.51$) and pyrolysis temperature ($r = 0.41$) and surface area with pyrolysis temperature ($r = 0.41$) showed positive correlation. An increase in pyrolysis temperature will increase the surface area of biochar (Shi et al., 2023; Zhang et al., 2024); therefore, a strong correlation has been evidenced between these two parameters for pristine biochar. After modification, the surface area shows a weak correlation with pyrolysis temperature, attributed to the loading of modification entities on the surface of biochar. On the other hand, improved structural properties, surface area, pore volume, and functional groups lead to a positive correlation between biochar adsorption capacity and MNP size, implying a higher removal efficiency for larger MNPs (Babalar et al., 2024; Tong et al., 2020).

Modified biochar often shows higher adsorption capacities for large sized plastic particles (as highlighted by strong positive correlation between adsorption capacities and MNP size in Fig. 4b, $r = 0.78$, $p < 0.05$). This phenomenon can be explained by multiple interrelated factors: firstly, biochar possesses a hierarchical pore structure as defined by International Union of Pure and Applied Chemistry (IUPAC): micropores (<2 nm), mesopores (2–50 nm), and macropores (>50 nm) (Leng et al., 2021). For NPs (<100 nm), pore filling and diffusion into internal pore networks within mesopores and small macropores is the dominant adsorption mechanism (Magid et al., 2021; Zhu et al., 2022). However, for MPs (>1 μm), pore filling is physically limited because MP diameters exceed most biochar pore entrances. As an alternative, physical trapping in terms of interlocking of MPs into pore openings or inter-particle space becomes preferred adsorption mechanism (Wang et al., 2020a). Further, larger MPs exhibits greater cross-sectional area, enabling enhanced

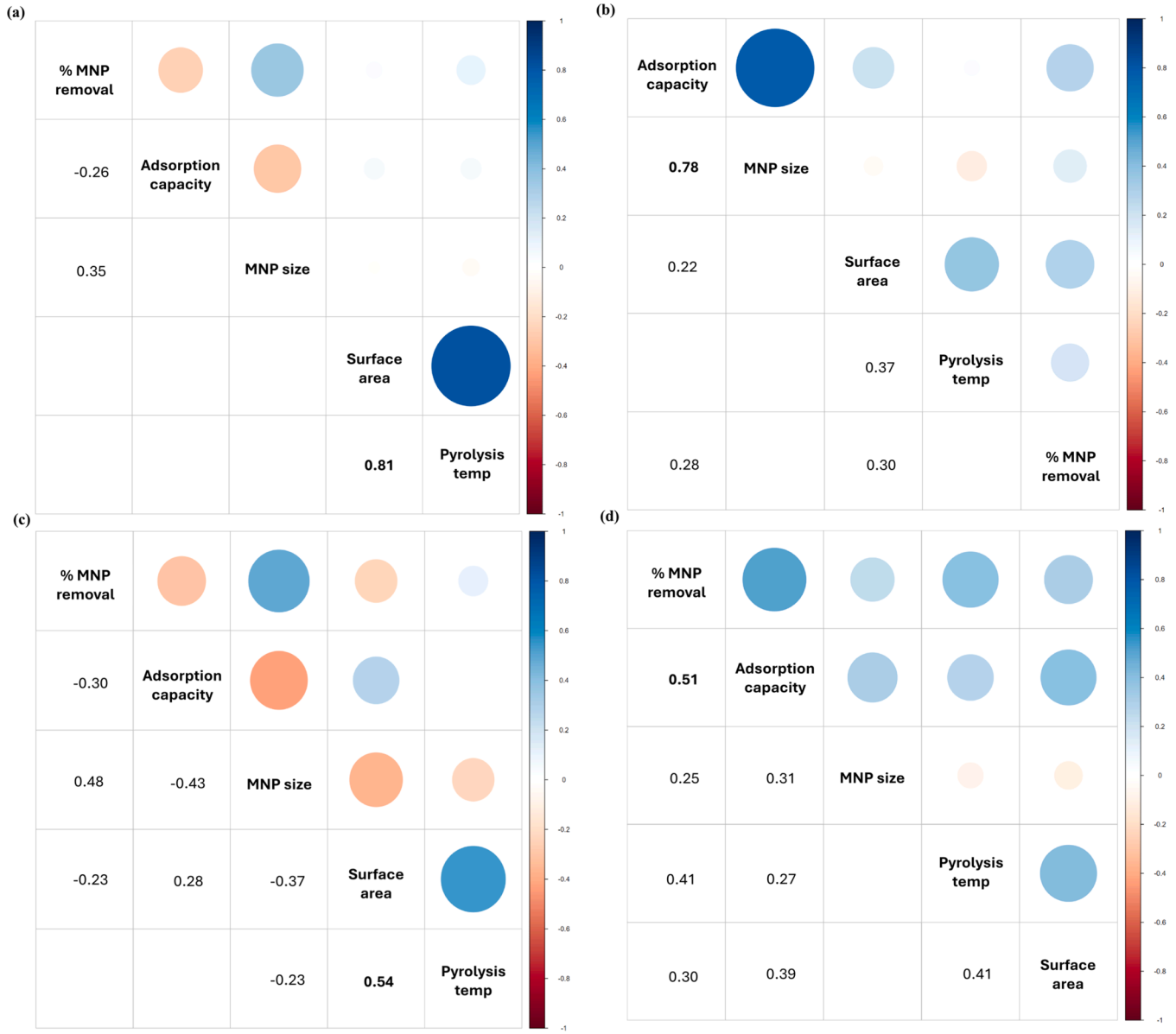

Fig. 4. Pearson correlation analysis among biochar adsorption capacity, surface area, pyrolysis temperature, MNP size, and %MNP removal for **(a)** pristine biochar and **(b)** modified biochar. Spearman correlation analysis among biochar adsorption capacity, surface area, pyrolysis temperature, MNP size, and %MNP removal for **(c)** pristine biochar **(d)** modified biochar. Data were extracted from published studies and are given in Table 1.

adsorption on biochar surface through van der Waals forces (Babalar et al., 2024). Babalar et al. highlighted that 15 μm PSMPs exhibited more rapid adsorption kinetics than 2 μm PSMPs on magnetic biochar zeolite composite (BCZ), attributed to the larger contact area enabling stronger adsorption. However, this correlation is non-linear beyond an optimal size (typically 10–50 μm, depending on biochar porosity), at which point gravitational settling may dominate the removal process rather than adsorptive interactions (Hanif et al., 2024). Furthermore, adsorption capacity (mg/g) accounts for all mass retained by the biochar, encompassing both chemical adsorption (electrostatic bonding, surface complexation, and hydrogen bonding) and physical retention (trapping, sieving, and entanglement). For larger MPs, physical mechanisms contribute disproportionately to the measured capacity, as evidenced by studies showing MP accumulation predominantly at pore entrances rather than within internal pores (Wang et al., 2020a; Zhao et al., 2022a). Although this may be viewed as an inflation of actual adsorption capacity, from a remediation perspective, total mass removal remains the most relevant metric, regardless of the specific retention mechanism.

3.3. MNP removal from laboratory samples using pristine and modified biochar

3.3.1. Pristine biochar

Several recent studies employed pristine biochar to remove MNPs in synthetic laboratory samples (Table 1). The microstructure of biochar includes pores of varying sizes (<1 nm to 50 μm), enabling the removal of both MPs and NPs (Zhang et al., 2024). For instance, Wang et al. used corn straw biochar (CSB) (pyrolysis temperatures 300, 400, and 500 °C) and hardwood biochar (Oxford Charcoal Company, UK) to immobilize PSMPs (10 μm) and reported the removal efficiency of biochar >95%, significantly higher than the sand filter. CSB produced at 500 °C with a surface area of 177.5 m^2/g showed the highest removal efficiency for PSMPs, attributed to the abundance of thin chip and honeycomb structures (Wang et al., 2020). Zhang et al. prepared London Plane bark biochar (LPB) through pyrolysis at 550 °C and documented a relatively higher adsorption capacity of LPB for PSNPs (1000 nm) at 60.05 mg/L, which could be attributed to the large size of PS and higher number of pores (10–25 μm) in LPB as the pyrolysis temperature increased from 350 °C to 550 °C (Zhang et al., 2024). Compared to biochar before PSNPs removal (Fig. 5A-a), PSNPs are massively adsorbed on biochar surface after treatment through pore filling of carbon tubes (Fig. 5A-b) Further, biochar-PS interaction leads to a slight decrease in $(Mg_{0.042}Ca_{0.958})CO_3$ peak and increase in amorphous C peak, highlighting masking effect of PSNPs in XRD diffraction pattern (Fig. 5A-c) (Zhang et al., 2024). Mahmoud et al. produced pineapple peel biochar (PAB) and artichoke leaves biochar (ALB) at 300–350 °C and demonstrated the adsorption capacities of 29.33 and 12.22 mg/g for PSNPs (1000 nm), respectively. A slightly higher adsorption capacity for ALB was attributed to a relatively higher surface area (2.542 m^2/g) compared to PAB (2.168 m^2/g) (Mahmoud et al., 2024). Ganie et al. investigated the influence of pyrolysis temperatures (350, 550, and 750 °C) on BGB, and a peak adsorption capacity of 44.90 mg/g for PSNPs (<500 nm) was observed at 750 °C, having a surface area as high as 540.36 m^2/g (Ganie et al., 2021). Similarly, Shi et al. used PWB generated at 300–700 °C with a surface area of 1.30–202.66 m^2/g to remove PSNPs (100 nm) and reported an elevated adsorption capacity of 55.46–80.30 mg/g (Shi et al., 2023). While Kim et al. reported a very low adsorption capacity of 0.56 mg/g for PSMPs (210–30 K Da) after treatment with WSB prepared at 700 °C, comprising a relatively higher surface area of 512.18 m^2/g (Kim et al., 2024). Tong et al. produced CLB at 400 °C with a relatively low surface area of 2 m^2/g and treated PSMPs (0.02–2 μm) with a removal efficiency of 36.9–68.5%. The size of MNPs showed an inverse relation with the removal efficiency (Tong et al., 2020). In contrast, Torboli et al. showed 100% removal efficiency for PSMPs sized ≥ 2 μm and 49% removal efficiency for PSMPs sized 1 μm using spent coffee ground biochar (CGB) prepared at 300–500 °C (Torboli et al., 2025).

In conclusion, elevated pyrolysis temperatures produce pristine biochar with increased surface area (as indicated by the correlation matrix in Fig. 4a, c) and improved adsorption capability, due to the formation of pore structures resembling honeycomb networks. The type of biochar parent material/feedstock is significant, and lignocellulosic-based biochar (e.g., pinewood, bagasse) demonstrates superior performance compared to agricultural wastes (e.g., walnut shells) at equivalent temperatures, indicating that pore accessibility and surface chemistry are essential factors in addition to surface area.

3.3.2. Modified biochar (oxidized and magnetic)

Modified biochar (magnetic and non-magnetic) has been extensively used in recent studies to enhance interactive properties and subsequent regeneration of biochar (Table 1). For instance, Magid et al. prepared CCB at pyrolysis temperatures of 500–900 °C and oxidized it using 5% of HNO_3/H_2SO_4. The adsorption ability of oxidized biochar for PSNPs (50 nm) was enhanced with elevated pyrolysis temperature, demonstrating an adsorption capacity ranging from 15.22 to 23.98 mg/g, mainly attributed to an increase in specific surface area (17.8–60.8 m^2/g). Adsorption occurred in two phases: an initial fast adsorption onto the surface followed by a slower adsorption likely attributed to the diffusion of PSNPs into the interior of the biochar (Magid et al., 2021). Similarly, Zhu et al. produced mesoporous CCB from contaminated corncobs sourced from a mining region at a pyrolysis temperature of 650 °C that showed a remarkable adsorption capacity of 56.02 mg/g for PSNPs (100 nm) (Zhu et al., 2022), surpassing the oxidized CCB (20.89 mg/g) (Magid et al., 2021). The adsorption rate of contaminated CCB for PSNPs was 100%, which was 34.5% and 6.9% higher than that of pristine CCB and commercial activated carbon under the same conditions (Zhu et al., 2022). This significant difference in adsorption capacities of NPs for biochar could be mainly attributed to differences in NP size (100 nm vs. 50 nm), surface areas (216.01 m^2/g vs. 17.8–60.8 m^2/g), and pore volumes (0.22 cm^3/g vs. 0.04–0.13 cm^3/g) for contaminated and oxidized biochar, respectively (Magid et al., 2021; Zhu et al., 2022). Prior to PSNPs adsorption, the surface of contaminated CCB exhibited irregular cracks and pores at hundred nanometre sizes (Fig. 5B-a), which were filled and covered with plastic particles after adsorption (Fig. 5B-b). Mahmoud et al. modified PAB and ALB using oxalic acid, which significantly increased the surface areas to 29.14 m^2/g and 25.42 m^2/g (pristine PAB 2.16 m^2/g and pristine ALB 2.54 m^2/g); however, the associated adsorption capacities were moderately changed to 12.70 mg/g and 15.26 mg/g (pristine PAB 29.33 mg/g and pristine ALB 12.22 mg/g), respectively (Mahmoud et al., 2025). Feng et al. produced sludge-industrial red mud waste biochar (SRB) at 500 °C and modified it using lignin, and modified SRB showed an elevated adsorption capacity of 406.68 mg/g for PSNPs (100 nm), mainly attributed to the high surface area (217.62 m^2/g) and improved adsorptive properties after the introduction of red mud and lignin (Feng et al., 2025).

More recently, researchers have magnetized biochar using various commercial sources of iron to enhance its surface area, electrostatic properties and regeneration. For instance, Singh et al. synthesised magnetic MSB at 550 °C and 850 °C using $FeCl_3$, exhibiting adsorption capacities of 290.20, 225.11, and 206.46 mg/g for NH_2-PSNPs (1000 nm), COOH-PSNPs (1000 nm), and COOH-PSNPs (30 nm) spheres, respectively. The elevated removal of NH_2-PSNPs was attributed to the complexation and strong electrostatic attraction of the amine group with magnetic biochar (Singh et al., 2021). Shi et al. produced PWB through pyrolysis at 300, 500, and 700 °C and magnetized it using magnetite Fe_3O_4 and reported a 43.67, 82.73, and 57.02% increase in adsorption of PSNPs (100 nm) compared to that with pristine biochar. For pristine PSNPs, UV-aged PSNPs, NH_2-PSNPs, and COOH-PSNPs, the adsorption capacities of magnetic PWB ranged from 07.71 to 229.57 mg/g, compared to that of pristine biochar (55.46 to 80.30 mg/g). Magnetic PWB pyrolyzed at 500 °C exhibited the highest removal efficiency at 95.2%, attributed to its greater specific surface area and abundant

Table 1
Recent studies on the application of pristine and modified biochar for MNPs removal from laboratory samples.

Biochar type (origin/ modification)	Pyrolysis temperature	Surface area/pore size	MNP polymer and size	Adsorption capacity/ Removal efficiency	Reference
Pristine biochar					
Corn straw biochar (CSB)	500 °C	177.5 m^2/g	PSMPs (10 μm)	>95%	(Wang et al., 2020)
London Plane bark biochar (LPB)	550 °C	Higher number of pores (10–25 μm)	PSNPs (1000 nm)	60.05 mg/g	(Zhang et al., 2024)
Pineapple peel biochar (PAB) Artichoke leaves biochar (ALB)	300–350 °C	PAB 2.168 m^2/g ALB 2.542 m^2/g	PSNPs (1000 nm)	PAB 31.1 mg/g ALB 35.2 mg/g	(Mahmoud et al., 2024)
Bagasse biochar (BGB)	350–750 °C	1.44–540.36 m^2/g	PSNPs (<500 nm)	44.9 mg/g	(Ganie et al., 2021)
Pinewood biochar (PWB)	300–700 °C	1.30–202.66 m^2/g	PSNPs (100 nm)	55.46–80.30 mg/g	(Shi et al., 2023)
Walnut shell biochar (WSB)	700 °C	512.18 m^2/g	PSMPs (210–30 K Da)	0.56 mg/g	(Kim et al., 2024)
Cellulose biochar (CLB)	400 °C	2 m^2/g	PSNPs (0.02 μm) PSNPs (0.2 μm) PSMPs (2 μm)	68.5% 37.4% 36.9%	(Tong et al., 2020)
Spent coffee ground biochar (CGB)	300 °C 500 °C	NA	PSMPs (1–5 μm)	100% for MPs ≥ 2 μm 49% for MPs 1 μm	(Torboli et al., 2025)
Mesquite biochar (MSB)	550 °C 850 °C	164.6 m^2/g 302.9 m^2/g	NH_2-PSNPs (1000 nm) COOH-PSNPs (1000 nm) COOH-PSNPs (30 nm)	NA	(Singh et al., 2021)
Modified biochar (magnetic and non-magnetic)					
Corncob biochar (CCB), HNO_3/H_2SO_4 modified	500–900 °C	17.8–60.8 m^2/g	PSNPs (50 nm)	15.22–23.98 mg/g	(Magid et al., 2021)
Contaminated Corncob biochar (CCB), mining area	650 °C	216.01 m^2/g	PSNPs (100 nm)	56.02 mg/g	(Zhu et al., 2022)
Pineapple peel biochar (PAB) Artichoke leaves biochar (ALB), oxalic acid modified	300 °C 350 °C	PAB 29.14 m^2/g ALB 25.42 m^2/g	PSNPs (1000 nm)	PAB 12.70 mg/g ALB 15.26 mg/g	(Mahmoud et al., 2025)
Sludge-industrial red mud waste (SRB), lignin modified	500 °C	217.62 m^2/g	PSNPs (100 nm)	406.68 mg/g	(Feng et al., 2025)
Mesquite biochar (MSB), $FeCl_3$ magnetized	550 °C 850 °C	25.8 m^2/g 34.5 m^2/g	NH_2-PSNPs (1000 nm) COOH-PSNPs (1000 nm) COOH-PSNPs (30 nm)	290.20 mg/g 225.11 mg/g 206.46 mg/g	(Singh et al., 2021)
Pinewood biochar (PWB), Fe_3O_4 magnetized	300–700 °C	8.25–207.33 m^2/g	PSNPs (100 nm)	107.70–229.57 mg/g	(Shi et al., 2023)
Sawdust biochar (SDB) Zn-SDB Mg-SDB, $Fe(NO_3)_3$ magnetized	550 °C	363.80 m^2/g 265.47 m^2/g 329.87 m^2/g	PSNPs (1000 nm)	374.57 mg/g 355.72 mg/g 334.03 mg/g	(Wang et al., 2021)
Biochar zeolite composite (BZC), KOH activated, $FeCl_3$ magnetized	850 °C	897.7 m^2/g	PSMPs (2 μm) (15 μm)	736 mg/g 769 mg/g	(Babalar et al., 2024)
Sawdust biochar (SDB), humic acid (HA), fulvic acid (FA), $Fe(NO_3)_3$ magnetized	550 °C	NA	PSNPs (80 nm)	20.63 mg/g 23.80 mg/g	(Zhao et al., 2024)
Walnut shell biochar (WSB), Fe-mining waste magnetized	700 °C	892.64 m^2/g	PSMPs (210–30 K Da)	19.23 mg/g	(Kim et al., 2024)
Cellulose biochar (CLB), $FeCl_3$ magnetized	400 °C	24.2 m^2/g	PSNPs (0.02 μm) PSNPs (0.2 μm) PSMPs (2 μm)	78.5% 77.7% 75.2%	(Tong et al., 2020)
Corncob biochar (CCB), $Fe(NO_3)_3$ and $FeSO_4$ magnetized	500 °C	27.82 m^2/g	0.5 d aged PAMPs (78 μm) 1.0 d aged PAMPs (44 μm)	1145 mg/g 1737 mg/g	(Li et al., 2023)
Corncob biochar (CCB), Walnut shell biochar (WSB), $Fe(NO_3)_3$ and $FeSO_4$ magnetized	500 °C	38.97 m^2/g 279.9 m^2/g	PVCNPs (0.05–1 μm)	22.59 mg/g 20.10 mg/g	(Li and Chen, 2024)
Bagasse biochar (BGB), K_2FeO_4 magnetized, polyaniline modified	800 °C	224.42 m^2/g	PSNPs (50 nm)	334.45 mg/g	(Wang et al., 2025)
Bagasse biochar (BGB), magnetized with $FeCl_3$, modified with $Na_2S_2O_4$ and $NaBH_4$	750 °C	158 m^2/g	NH_2-PSNPs (100 nm) SO_4^{2-}-PSNPs (100 nm)	NH_2-PS 128.36 mg/g SO_4^{2-}-PS 78.48 mg/g > 90 %	(Ganie et al., 2025)
Bagasse biochar (BGB), magnetized with $FeCl_3$, modified with $Na_2S_2O_4$ and $NaBH_4$	750 °C	36.25 m^2/g	COOH-PSNPs (500 nm) COOH-PSNPs (100 nm) NH_2-PSNPs (100 nm)	90.30 mg/g 79.60 mg/g 46.71 mg/g	(Ganie et al., 2023)
Sawdust biochar (SDB), $FeCl_3$ and $FeSO_4$ magnetized	600 °C	9.6 m^2/g	PSNPs (1000 nm) NH_2-PSNPs (1000 nm) COOH-PSNPs (1000 nm)	48.7 mg/g 220 mg/g 122 mg/g	(Duan et al., 2025)
Lignin based biochar (LBB) $FeCl_3$ magnetized	750 °C	417.81 m^2/g	PSNPs (100 nm)	68.57 mg/g	(Jiao et al., 2025)

(*continued on next page*)

Table 1 (*continued*)

Modified biochar (magnetic and non-magnetic)					
Rice straw biochar (RSB), $FeCl_3$ magnetized, cetyltrimethylammonium bromide (CTAB) modified	750 °C	Magnetic CTAB-RSB 95.69 m^2/g magnetic RSB 119.13 m^2/g	PSNPs (<100 nm)	Magnetic CTAB-RSB 54.07 mg/g magnetic RSB 10.92 mg/g	(Xing et al., 2024)
Rapeseed straw biochar (RPB), $Fe(NO_3)_3$ and $FeSO_4$ magnetized, CTAB modified	800 °C	683.6 m^2/g	PSNPs and COOH-PSNPs (600–1000 nm)	PSNPs 163.4 mg/g COOH-PSNPs 159.6 mg/g	(Shi et al., 2023)
Palm kernel shell biochar (PKB), CTAB modified	600 °C	NA	PEMPs (2–4 μm)	96.12% removal efficiency	(Hanif et al., 2024)
Bagasse, rice husk, coconut shell biochar (BRCB), $FeCl_3$ magnetized, CTAB modified	900 °C	183.67 m^2/g	COOH-PSNPs (1000 nm)	247.52 mg/g	(Parashar and Hait, 2024)

Adsorption capacity (Q_{max}) and removal efficiency were the highest values reported in the studies.

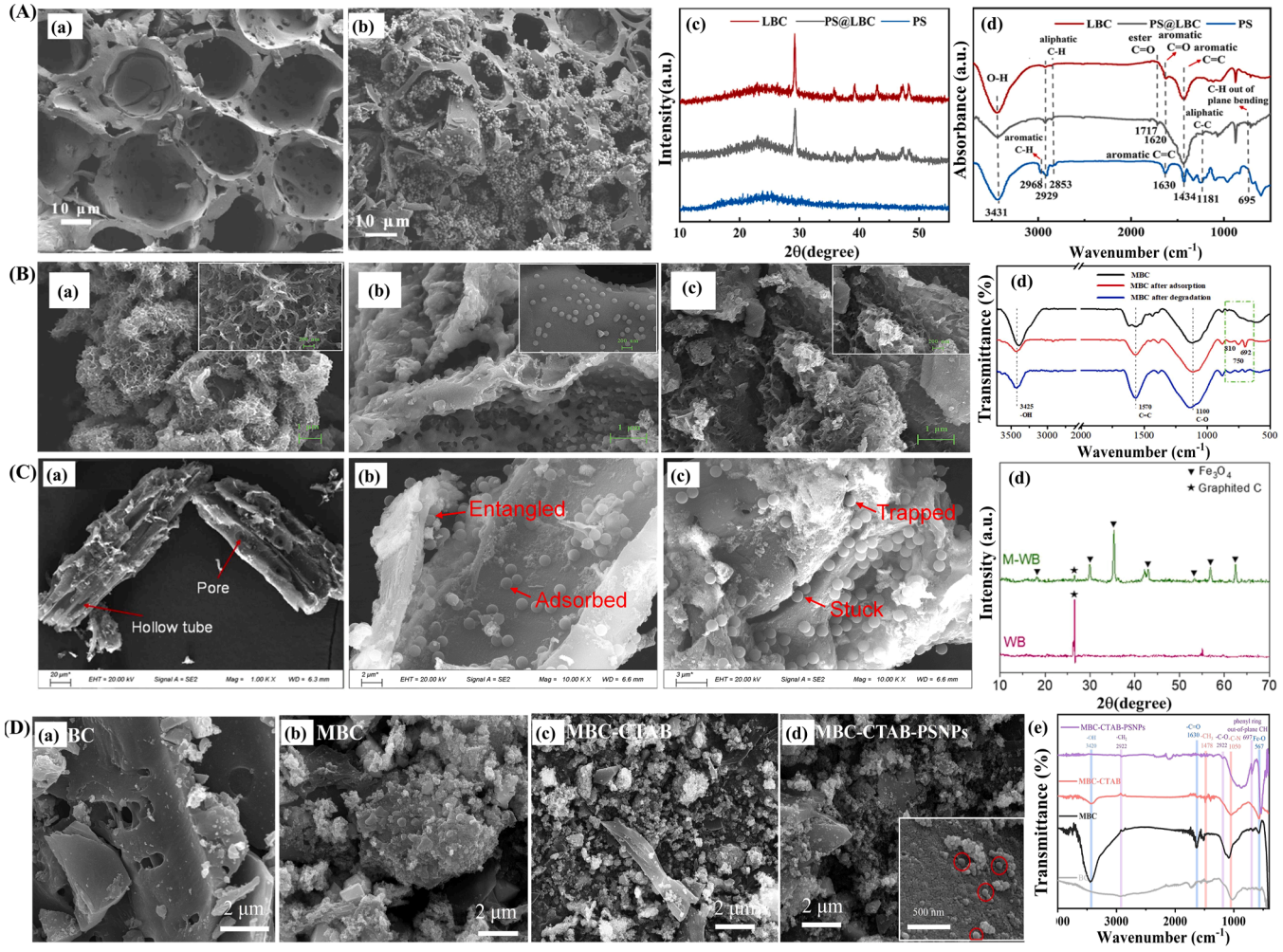

Fig. 5. Surface characterization of pristine and modified biochar before and after MNP removal in selected published studies. **(A)** SEM images of London Plane bark pristine biochar (550 °C): **(a)** before PSNPs removal, **(b)** after PSNPs removal, **(c)** associated XRD pattern, and FTIR spectra **(d)**. Copyright (2024) Elsevier. **(B)** SEM images of mining area contaminated corncob-derived mesoporous biochar (650 °C): **(a)** before PSNPs adsorption, **(b)** after PSNPs adsorption, **(c)** after hydrothermal degradation of PSNPs, and **(d)** associated FTIR spectra. Copyright (2022) Elsevier. **(C)** SEM images of iron modified sawdust biochar (600 °C): **(a)** before PSNPs removal, **(b, c)** after PSNPs removal with adsorption mechanisms and **(d)** XRD spectra of iron modified biochar before PSNPs treatment. Copyright (2025) Elsevier. **(D)** SEM images of rice straw biochar (750 °C): **(a)** pristine biochar before PSNPs removal, **(b)** iron modified biochar before PSNPs removal, **(c)** cetyltrimethylammonium bromide (CTAB) modified biochar before PSNPs removal, **(d)** iron-CTAB modified biochar after PSNPs removal, and associated FTIR spectra. Copyright (2024) Elsevier. (A) Adapted with permission from Zhang et al. (Zhang et al., 2024). (B) Adapted with permission from Zhu et al. (Zhu et al., 2022). (C) Adapted with permission from Duan et al. (Duan et al., 2025). (D) Adapter with permission from Xing et al. (Xing et al., 2024).

oxygen-containing functional groups (Shi et al., 2023).

Wang et al. prepared SDB at 550 °C and magnetized it using Fe $(NO_3)_3$ to obtain magnetic SDB, Zn-SDB, and Mg-SDB, achieving maximum adsorption capacities of 374.57, 355.72, and 334.03 mg/g for PSNPs (1 μm), respectively. Modification of biochar by Fe, Zn, and Mg significantly increased adsorption capacity, attributed to sufficient contact area and active sites (Wang et al., 2021). Babalar et al. synthesised a magnetic BZC using $FeCl_3$, polyethylene glycol, and polyethyleneimine at 850 °C, which augmented adsorption capacities as high as 736 mg/g and 769 mg/g for PSMPs with sizes of 2 μm and 15 μm,

respectively. The elevated adsorption capacity was attributed to the metal oxide on the magnetic BZC surface and the presence of strong electrostatic attractions between the negatively charged MP surface and the positively charged magnetic BZC (Babalar et al., 2024). Zhao et al. prepared SDB at 550 °C and magnetized it using $Fe(NO_3)_3$ and reported an adsorption capacity of 20.63 mg/g and 23.80 mg/g for PSNPs (80 nm) in the presence of HA and FA, respectively. The presence of HA and FA reduced adsorption by 53.2% and 80.3%. Magnetic SDB is predicted to preferentially bind and generate ligands with the aromatic and hydrophobic components of the organic matter, hence limiting the attachment of PSNPs (Zhao et al., 2024). Kim et al. prepared magnetic WSB through co-pyrolysis of walnut shells and Fe-mining waste at 700 °C, reporting a lower adsorption capacity of 0.77–6.75 mg/g for PSMPs, albeit higher than that of pristine biochar (0.27–0.79 mg/g), suggesting that the incorporation of Fe uplifted the adsorption process through electrostatic interactions between magnetic WSB and PSMPs (Kim et al., 2024). Tong et al. produced cellulose CLB at 400 °C and magnetized it using $FeCl_3$ and magnetic CLB significantly reduced the transportation of PSNPs (0.02 μm), PSNPs (0.2 μm), and PSMPs (2 μm) to 0.5, 1.3, and 2.6%, compared to that of pristine biochar-sand mixture (68.5, 37.4, and 36.9%) and pure sand (78.5, 77.7, and 75.2%), respectively (Tong et al., 2020). Li et al. synthesized CCB at 500 °C and magnetized it using Fe $(NO_3)_3$ and $FeSO_4$ to remove pristine PAMPs (120 μm), 0.5-day-aged PAMPs (78 μm), and 1.0-day-aged PAMPs (44 μm). The adsorption amount of PA on magnetic CCB was increased with the increase in aging duration, e.g., PA-0.5 and PA-1.0 showed adsorption amounts of 1145 mg/g and 1737 mg/g, respectively. Aged PA showed a higher removal efficiency (~97%) compared to pristine PAMPs (~25%). Aged PAMPs strongly interacted with magnetic CCB, which can be attributed to reduced particle size, decline in crystallinity, and abundance of oxygen-containing functional groups (Li et al., 2023). Li and Chen prepared CCB and WSB at 500 °C ($Fe(NO_3)_3$ and $FeSO_4$ magnetized), with corresponding surface areas of 38.97 m^2/g and 279.9 m^2/g, and removal capacities of 22.59 mg/g and 20.10 mg/g for PVCNPs (0.05–1 μm) (Li and Chen, 2024). Wang et al. produced BGB at 800 °C, magnetized with K_2FeO_4, and modified with polyaniline, exhibiting a relatively high surface area of 224.42 m^2/g and a high adsorption capacity of 334.45 mg/g for PSNPs (50 nm) (Wang et al., 2025). Similarly, Ganie et al. conducted two studies using BGB (pyrolysis temperature 750 °C), magnetized with $FeCl_3$, and modified with $Na_2S_2O_4$ and $NaBH_4$. BGBs have surface areas of 158 m^2/g and 36.25 m^2/g, the former BGB was used to remove NH_2-PSNPs (100 nm) SO_4^{2-}-PSNPs (100 nm) at adsorption capacities of 128.36 mg/g and 78.48 mg/g (Ganie et al., 2025), and the latter BGB was used to remove COOH-PSNPs (500 nm), COOH-PSNPs (100 nm), and NH_2-PSNPs (100 nm) with adsorption capacities of 90.30 mg/g, 79.60 mg/g, and 46.71 mg/g (Ganie et al., 2023), respectively. Duan et al. produced SDB at a pyrolysis temperature of 750 °C and magnetized it with $FeCl_3$ and $FeSO_4$, and modified SDB exhibited a relatively low surface area (9.6 m^2/g); albeit high adsorption capacities of 48.7 mg/g, 220 mg/g, and 122 mg/g, respectively, for PSNPs (1000 nm), NH_2-PSNPs (1000 nm), and COOH-PSNPs (1000 nm). Elevated adsorption capacity of SDB was attributed to its rough surface with porous tubes, hollow tubes stacked, and abundance of fine particulate Fe_3O_4 coating (Fig. 5C-a, d) (Duan et al., 2025). In contrast, lignin-based biochar (LBB) produced at 750 °C, magnetized with $FeCl_3$, possessed a higher surface area of 417.81 m^2/g and a lower adsorption capacity of 68.57 mg/g for PSNPs (100 nm) (Jiao et al., 2025).

3.3.3. CTAB modified biochar

Multiple studies also used CTAB-modified biochar to remove MNPs (Table 1). For instance, Xing et al. produced rice straw biochar (RSB) at 750 °C, magnetized it using $FeCl_3$ and modified it with CTAB for the adsorption removal of PSNPs (50–100 nm). Magnetic CTAB-RSB demonstrated a maximum adsorption capacity of 54.07 mg/g, significantly higher than magnetic RSB (10.92 mg/g) and black carbon (BC, 11.62 mg/g). Pristine RSB displays an uneven structure and a comparatively smooth exposed surface (Xing et al., 2024). The biochar displays irregular interior pore diameters because of high-temperature pyrolysis (Fig. 5D-a). Following coprecipitation-pyrolysis modification, iron oxide nanoclusters are detected on the surface of RSB (Fig. 5D-b). Following CTAB modification, the included iron oxide nanoclusters undergo erosion and fragmentation, leading to an enhanced dispersion and reduced particle size (Fig. 5D-c) (Xing et al., 2024). Shi et al. prepared RPB at 800 °C and magnetized it using $FeCl_3$ and $FeSO_4$ and further modified it using CTAB to remove PSNPs and COOH-PSNPs (600–1000 nm). The removal capacities of magnetic CTAB-RPB for PSNPs and COOH-PSNPs were 163.4 and 159.6 mg/g, respectively. Following modification by CTAB, the removal efficiency was improved by 29% for PSNPs and 14% for COOH-PSNPs (Shi et al., 2023). Hanif et al. prepared palm kernel shell biochar (PKB) at 600 °C and modified it using CTAB to remove polyethylene (PE) MPs (2–4 μm) at removal efficiencies of 95.71% and 96.12%, respectively, measured by turbidity and gravimetric techniques (Hanif et al., 2024). Parashar and Hait produced bagasse, rice husk, and coconut shell biochar (BRCB) at 900 °C, magnetized it using $FeCl_3$, and modified it further using CTAB that enhanced the adsorption capacity, i.e., 247.52 mg/g for COOH-PSNPs (1000 nm) (Parashar and Hait, 2024).

In summary, acid-, iron-, and CTAB-modified biochar demonstrates improved MNP removal potential, with adsorption capabilities influenced by pyrolysis temperature, biochar type, and modification type. Elevated pyrolysis temperatures typically enhance surface area and adsorption capacity; however, a relatively weak association was seen between pyrolysis temperature and surface area for modified biochar due to post-pyrolysis modifications (Fig. 4d). Modifications enhance biochar performance through electrostatic interactions and an increase in active sites. Nonetheless, adsorption efficiency is also affected by the MNP size, functional groups, and presence of organic matter. Modified biochar, especially magnetic versions, presents a promising and adjustable method for the removal of MNPs. Overall, the removal efficiency of biochar is contingent upon plastic size: bigger particles such as MPs (≥1–10 μm) are often removed with over 95% efficiency, whereas NPs (<500 nm) demonstrate reduced adsorption owing to size limitations and increased mobility.

3.4. MNP removal using pristine and modified biochar from environmental samples

To our knowledge, no study has yet been conducted on the removal of environmental MNPs from real-world samples. However, multiple studies revealed the application of biochar for the removal of manufactured or pristine standard MNPs using environmental samples, including freshwater (river, lake, tap water, and groundwater), seawater, wastewater, and soil samples globally. Most of the studies using environmental samples have been conducted in China, India, the USA, and Canada (Table 2).

3.4.1. Freshwater

Multiple freshwater studies have been conducted in China that showed efficient removal of MNPs from freshwater samples using various types of pristine and modified biochar. For instance, the adsorption capacities of pristine LPB for PSNPs (1 μm) were respectively reported at 46.5 mg/g and 51.0 mg/g in the Yellow River water and tap water samples from China, comparatively lower than that of the pure water (60.05 mg/g), mainly attributed to the presence of impurities in environmental water samples (Zhang et al., 2024). Similarly, magnetic CTAB-RSB successfully removed PSNPs (50–100 nm) from the Yangtze River water samples with a removal efficiency of up to 60%; however, the removal efficiency of magnetic biochar in river water was reduced compared to that in pure water. The reduced adsorption under natural conditions was mainly attributed to competitive adsorption of DOM or interfering ions (Xing et al., 2024). Moreover, magnetic CTAB-RPB removed PSNPs and COOH-PSNPs (600–1000 nm) from Ximi Lake,

Table 2
Application of pristine and modified biochar for MNPs removal from real environmental samples.

Sample location or characteristics	Biochar type	MNP polymer and size	Adsorption capacity/ removal efficiency	References
Freshwater				
Yellow River, China	London Plane bark biochar (LPB), pristine	PSNPs (1 μm)	46.5 mg/g 51.0 mg/g	(Zhang et al., 2024)
Tap water, China				
Yangtze River, China	Rice straw biochar (RSB), $FeCl_3$ magnetized, CTAB modified	PSNPs (50–100 nm)	60%	(Xing et al., 2024)
Ximi Lake, China	Rapeseed straw biochar (RPB), Fe $(NO_3)_3$ and $FeSO_4$ magnetized, CTAB modified	PSNPs, COOH-PSNPs (600–1000 nm)	95.3% 97.8%	(Shi et al., 2023)
Jing River, China	Sawdust biochar (SDB), Fe $(NO_3)_3$ magnetized	PSNPs (80 nm)	25.6 mg/g	(Zhao et al., 2024)
Lake Pucheng, China	Sawdust biochar (SDB), Fe $(NO_3)_3$ magnetized	PSNPs (80 nm)	9.3 mg/g	(Zhao et al., 2024)
Tap water Groundwater Lake water, China	Bagasse biochar (BGB), K_2FeO_4 magnetized, polyaniline (PA) modified	PSNPs (50 nm)	97% for tap water 96% for groundwater 94% for lake water	(Wang et al., 2025)
Tap water, China	Sawdust biochar (SDB), $FeCl_3$ and $FeSO_4$ magnetized	NP1, PSNPs (1000 nm) NP2, NH_2-PSNPs (1000 nm) NP3, COOH-PSNPs (1000 nm)	37.11 mg/g for NP1 37.45 mg/g for NP2 66.49 mg/g for NP3	(Duan et al., 2025)
River water, China			55.0 mg/g for NP1 46.0 mg/g for NP2 80.0 mg/g for NP3	
Lake water, China			52.0 mg/g for NP1 43.0 mg/g for NP2 91.0 mg/g for NP3	
Groundwater, China			21.4 mg/g for NP1 5.32 mg/g for NP2 69.4 mg/g for NP3	
Freshwater, India	Mesquite biochar (MSB), $FeCl_3$ magnetized	NP1, NH_2-PSNPs (1000 nm) NP2, COOH-PSNPs (1000 nm) NP3,	NP1, 12.8 mg/g NP2, 18.3 mg/g NP3, 12.6 mg/g	(Singh et al., 2021)
Groundwater, India		COOH-	NP1, 15.6 mg/g	

Table 2 (*continued*)

Sample location or characteristics	Biochar type	MNP polymer and size	Adsorption capacity/ removal efficiency	References
		PSNPs (30 nm)	NP2, 18.8 mg/g NP3, 12.7 mg/g	
Tap water, India			NP1, 5.0 mg/g NP2, 15.4 mg/g NP3, 16.6 mg/g	
River water Tap water, India	Bagasse biochar (BGB), magnetized with $FeCl_3$, modified with $Na_2S_2O_4$ and $NaBH_4$	NH_2-PSNPs (100 nm) SO_4^{2-}-PSNPs (100 nm)	River water 90% for NH_2-PS 89% for SO_4^{2-}-PS Tap water 96% for NH_2-PS 94% for SO_4^{2-}-PS	(Ganie et al., 2025)
River water, India	Bagasse biochar (BGB), magnetized with $FeCl_3$, modified with $Na_2S_2O_4$ and $NaBH_4$	NP1, COOH-PSNPs (500 nm) NP2, COOH-PSNPs (100 nm) NP3, NH_2-PSNPs (100 nm)	99% for NP1 82% for NP2 95% for NP3	(Ganie et al., 2023)
Tap water, Canada	Biochar zeolite composite (BZC), KOH activated, $FeCl_3$ magnetized	PSMPs (2 μm) PSMPs (15 μm)	95.0% 97.5%	(Babalar et al., 2024)
Seawater				
Yorktown Beach, USA	Pineapple peel biochar (PAB) Artichoke leaves biochar (ALB)	PSNPs (1000 nm)	61.8% for PAB 80.9% for ALB	(Mahmoud et al., 2024)
Yorktown Beach, USA	Pineapple peel biochar (PAB) Artichoke leaves biochar (ALB), oxalic acid modified	PSNPs (1000 nm)	65.9% for PAB 83.1% for ALB	(Mahmoud et al., 2025)
Xiamen, China	Sawdust biochar (SDB), Fe $(NO_3)_3$ magnetized	PSNPs (80 nm)	27.4 mg/g	(Zhao et al., 2024)
Seawater, China	Sawdust biochar (SDB), $FeCl_3$ and $FeSO_4$ magnetized	NP1, PSNPs (1000 nm) NP2, NH_2-PSNPs (1000 nm) NP3, COOH-PSNPs (1000 nm)	66.15 mg/g for NP1 67.35 mg/g for NP2 71.0 mg/g for NP3	(Duan et al., 2025)
Wastewater and soil				
Synthetic wastewater, China	Pristine sludge biochar (PSB), Waste activated sludge biochar (WASB)	PENPs (50–500 nm)	14.10 mg/g for PSB, 15.20 mg/g for WASB	(Wang et al., 2022)

(*continued on next page*)

Table 2 (*continued*)

Sample location or characteristics	Biochar type	MNP polymer and size	Adsorption capacity/ removal efficiency	References
Wastewater, Yangling, China	Sawdust biochar (SDB), $Fe(NO_3)_3$ magnetized	PSNPs (80 nm)	12.2 mg/g	(Zhao et al., 2024)
Automotive industry wastewater, China	Bagasse biochar (BGB), K_2FeO_4 magnetized, polyaniline modified	PSNPs (50 nm)	95%	(Wang et al., 2025)
WWTP effluents, China	Sawdust biochar (SDB), $FeCl_3$ and $FeSO_4$ magnetized	NP1, PSNPs (1000 nm) NP2, NH_2-PSNPs (1000 nm) NP3, COOH-PSNPs (1000 nm)	21.64% 27.49% 61.0%	(Duan et al., 2025)
Wastewater, India	Bagasse biochar (BGB), magnetized with $FeCl_3$, modified with $Na_2S_2O_4$ and $NaBH_4$	NH_2-PSNPs (100 nm) SO_4^{2-}-PSNPs (100 nm)	80% for NH_2-PS 74% for SO_4^{2-}-PS	(Ganie et al., 2025)
Synthetic wastewater, India	Bagasse biochar (BGB), magnetized with $FeCl_3$, modified with $Na_2S_2O_4$ and $NaBH_4$	NP1, COOH-PSNPs (500 nm) NP2, COOH-PSNPs (100 nm) NP3, NH_2-PSNPs (100 nm)	98% for NP1 94% for NP2 94% for NP3	(Ganie et al., 2023)
Sewage effluent, WWTP, India	Bagasse, rice husk, coconut shell biochar (BRCB), $FeCl_3$ magnetized, CTAB modified	COOH-PSNPs (1000 nm)	94–96%	(Parashar and Hait, 2024)
Wastewater, Kelowna WWTPs, Canada	Biochar zeolite composite (BZC), KOH activated, $FeCl_3$ magnetized	PSMPs (2 μm) PSMPs (15 μm)	75–85% 81–90%	(Babalar et al., 2024)
River sandy soil, China	CCB and WSB, Fe $(NO_3)_3$ and $FeSO_4$ magnetized	(PVC—NPs, 0.33 μm)	Reduce PVC transfer by 31.08% by CCB, 37.46% by WSB, compare to pristine sandy soil (85.10%)	(Ni et al., 2024)

China, water samples with removal efficiencies of 95.3% and 97.8%, respectively (Shi et al., 2023). Zhao et al. used magnetic SDB to remove PSNPs (80 nm) from water samples collected from the Jing River and Lake Pucheng, China. The adsorption capacity of SDB for PSNPs in the river water samples (25.6 mg/g) was higher than that of lake water samples (9.3 mg/g) (Zhao et al., 2024). Wang et al. used magnetic polyaniline-modified BGB to remove PSNPs (50 nm) from tap water, groundwater, and lake water in China at removal efficiencies of 97, 96, and 94%, respectively (Wang et al., 2025). Another study from China used magnetic SDB to remove PSNPs (1000 nm), NH_2-PSNPs (1000 nm), and COOH-PSNPs (1000 nm) at adsorption capacities of 37, 37, and 66 mg/g in tap water; 55, 46, and 80 mg/g in river water; 52, 43, and 91 mg/g in lake water; and 21, 5, and 69 mg/g in groundwater, respectively (Duan et al., 2025).

Multiple studies have also been conducted in India. For instance, magnetic MSB showed the removal of NH_2-PSNPs (1000 nm), COOH-PSNPs (1000 nm), and COOH-PSNPs (30 nm) in groundwater, higher than that of freshwater and tap water from India. This was attributed to the higher ionic strength of groundwater (18.97×10^{-3} M), compared to tap water (14.78×10^{-3} M) and freshwater (1.28×10^{-3} M) (Singh et al., 2021). Another study from India used magnetic BGB to remove NH_2-PSNPs (100 nm) and SO_4^{2-}-PSNPs (100 nm) and showed higher removal efficiencies of 90 and 89% in river water and 96 and 94% in tap water, respectively (Ganie et al., 2025). Ganie et al. conducted another study with the magnetic BGB to remove COOH-PSNPs (500 nm), COOH-PSNPs (100 nm), and NH_2-PSNPs (100 nm) from river water and showed removal efficiencies of 99, 82, and 95%, respectively (Ganie et al., 2023). The magnetic BZC successfully removed PSMPs (2 μm) and PSMPs (15 μm) at removal efficiencies of 95% and 97.5% from Canadian tap water, respectively (Babalar et al., 2024).

3.4.2. Seawater

Relatively fewer studies have been conducted on the removal of MNPs from seawater using biochar. For instance, pristine PAB and ALB, respectively, removed 61.8% and 80.9% of PSNPs (1000 nm) from seawater samples collected from Yorktown Beach, USA (Mahmoud et al., 2024). Mahmoud et al. conducted another study using oxalic acid-modified PAB and ALB and showed slightly higher removal efficiencies of 65.9% and 83.1% for PSNPs (1000 nm) in seawater from Yorktown Beach, USA (Mahmoud et al., 2025). Magnetic SDB showed the highest removal efficiencies for PSNPs (80 nm) in seawater (27.4 mg/g), followed by surface water (25.6 mg/g), municipal wastewater (12.2 mg/g), and lake water (9.3 mg/g) samples from China (Zhao et al., 2024). The higher removal of PSNPs from seawater and surface water was attributed to the relatively lower DOM levels of 0.37 mg/L and 1.36 mg/L, in comparison to wastewater (25.3 mg/L) and lake water (7.48 mg/L). Moreover, the adsorption of PSNPs in seawater was enhanced by a higher ionic strength and the presence of coexisting cations. Therefore, the magnetic SDB-PSNP interaction in the natural environment is affected by not only DOM but also other environmental factors (Zhao et al., 2024). Another study from China used magnetic SDB to remove PSNPs (1000 nm), NH_2-PSNPs (1000 nm), and COOH-PSNPs (1000 nm) from seawater samples from China at adsorption capacities of 66.15 mg/g, 67.35 mg/g, and 71.0 mg/g, respectively (Duan et al., 2025).

3.4.3. Wastewater and soil

Multiple studies also used pristine and modified biochar to remove MNPs from wastewater. Most of the studies were conducted in China. For instance, waste-activated sludge biochar showed the adsorption capacity of 15.20 mg/g for PENPs (50–500 nm) from synthetic wastewater, compared to pristine activated sludge (14.10 mg/g), mainly attributed to the presence of extracellular polymeric substance (EPS) in pristine sludge (Wang et al., 2022). Zhao et al. used magnetic SDB to remove PSNPs (80 nm) from wastewater samples from Yangling, China, at an adsorption capacity of 12.2 mg/g (Zhao et al., 2024). Polyaniline-modified magnetic BGB was used to treat PSNPs (50 nm) at a removal efficiency of 95% from automotive industry wastewater, China (Wang et al., 2025). Magnetic SDB showed relatively lower removal efficiencies of 21, 27, and 61% for PSNPs (1000 nm), NH_2-PSNPs (1000 nm), and COOH-PSNPs (1000 nm) in WWTP effluents from China, respectively (Duan et al., 2025). Multiple studies from India also used biochar to remove MNPs from wastewater. For instance, Ganie et al. used magnetic BGB to remove NH_2-PSNPs (100 nm) and SO_4^{2-}-PSNPs (100 nm) from wastewater samples from India with removal percentages of 80% and 74%, respectively (Ganie et al., 2025). Another study by Ganie et al. also used magnetic BGB to remove

COOH-PSNPs (500 nm), COOH-PSNPs (100 nm), and NH_2-PSNPs (100 nm) from synthetic wastewater at removal percentages of 98, 94, and 94%, respectively (Ganie et al., 2023). CTAB-modified magnetic BRCB was used to remove COOH-PSNPs (1000 nm) at the efficiency of 94–96% in sewage WWTP effluents from India (Parashar and Hait, 2024). Magnetic BZC showed the maximum adsorption capacity of 75–85% and 81–90% for 2 μm and 15 μm PSMPs in wastewater samples from the Kelowna wastewater treatment facility, Canada. The reduced adsorption in wastewater may result from the positive charges on the magnetic BZC attracting and binding with anionic species (nitrate, phosphorus) rather than PSMPs, hence decreasing total adsorption efficacy. Elevated ionic strength in the wastewater, resulting from the presence of these ions, can diminish the electrostatic attraction between the positively charged magnetic BZC and the negatively charged PSMPs (Babalar et al., 2024).

Only one study is available so far on the removal of MNPs from soil using biochar. Magnetic CCB and WSB were used to PVCNPs from river sandy soil collected from Xinyang, China. Magnetic CCB and WSB significantly reduced the transportation rate of PVCNPs, respectively, to 31.08% and 37.46%, compared to that in pristine sandy soil (85.10%). Significant retention of PVCNPs in the rainwater-biochar-soil system is attributable to the presence of coexisting ions (Ni et al., 2024).

In summary, studies employing environmental samples demonstrated inconsistent MNP removal efficiencies across different water types. Notable gaps include a lack of geographic diversity in studies, which were mostly conducted in China, India, the USA, and Canada; inadequate research on seawater and soil; and insufficient comprehension of competitive adsorption mechanisms within complex natural matrices. Reduced removal efficiency of MNPs in real-world samples, influenced by parameters such as dissolved organic matter (DOM) and ionic strength, highlights the necessity for further optimisation of biochar for practical use.

3.4.4. Environmental relevance of laboratory studies

A major limitation of the available studies on MNPs removal using biochar is the overwhelming reliance on commercially available spherical polystyrene (PS) MP/NPs as model plastic particles. Among available 29 core studies, 52 of 82 experiments (63%) used PS-MPs/NPs, with 30 experiments (37%) employing aminated or carboxylated PS derivatives to investigate removal efficiency of biochar (Fig. 2). This PS dominant approach raises uncertainties about the validity of reported removal efficiencies for polydisperse real-world environmental MNPs. Environmental plastic pollution encompasses an intricate mixture of polymers including PE, PP, PVC, PET, and PA with diverse sizes, morphologies, and weathering status (Junaid et al., 2024; Junaid et al., 2024; Junaid and Wang, 2022). PE and PP are predominant polymers that account for >50% of global plastic production and environmental pollution (Rodrigues et al., 2018). These polymers differ fundamentally from PS in aromaticity, density and surface chemistry (Hanif et al., 2024; Kim et al., 2024; Li et al., 2023). Characterised removal mechanisms for PS (π-π interactions, pore filling, and electrostatic attraction) exhibit limited transferability to PE/PP. In the case of non-aromatic polymers such as PE, PP, PVC, hydrophobic partitioning and physical entanglement within the biochar's organic structure become the dominant removal mechanism (Hanif et al., 2024; Li et al., 2023). Hanif et al. demonstrated 96% removal efficiency for PE-MPs by CTAB modified PKB, and major removal mechanism was electrostatic and hydrophobic interactions rather than π-π bonding (Hanif et al., 2024). Li et al. reported that weathered PA-MPs showed enhanced adsorption (1737 mg/g) compared to pristine PA for magnetic CCB after developing oxygen-containing groups during weathering, and associated removal mechanism was hydrophobic interactions (Li et al., 2023). In natural aquatic and terrestrial systems, MNPs rarely exist in a pristine state, and they undergo surface modification through the adsorption of natural organic matter (NOM), extracellular polymeric substances (EPS), and the formation of microbial biofilms, resulting in a complex coating known as an eco-corona (Junaid and Wang, 2021). This eco-corona essentially alters MNP-biochar interface through competitive site adsorption, charge reversal, bridging or blocking effect, and biofilm formation (Junaid and Wang, 2021; Xing et al., 2024; Zhao et al., 2024). Therefore, laboratory studies using pristine MNPs mainly PS likely overestimate removal efficiencies for two reasons: (i) they neglect the eco-corona that reduces MNP-biochar affinity in real word samples, and (ii) they over-represent polymers amenable to π-π interactions. Studies using environmental samples (Section 3.4) confirm this that the removal efficiencies in river water, wastewater, and seawater were consistently lower than in pure water systems (e.g., 60% vs. >95% for PS-NPs (Xing et al., 2024) and 60 mg/g vs. 46 mg/g for PS-NPs (Zhang et al., 2024)). To improve the ecological relevance of plastic remediation studies, future research should investigate complex MNP mixtures (e.g., PE, PP, PS, and PVC) that possess environmentally representative properties. Formation of eco-corona on MNPs and associated impacts on treatment should also be investigated, ensuring that laboratory-derived biochar removal efficiencies are scalable and applicable to complex real-world matrices.

3.5. Biochar comparison with other adsorbents for MNP removal

Activated carbon (AC) is a well-known material commonly used for removal of MNPs. Commercial AC possesses high surface areas (500–1500 m^2/g) and well-developed micropores, attaining removal efficiency >95% for MPs >10 μm (Wang et al., 2020). However, due to pore size constraints, it is less effective for treatment of NPs (<1 μm) with removal efficiencies reported to be lower than 50% for NPs <100 nm (Zhu et al., 2022). As for economic feasibility, the production cost of AC, typically ranging from USD 1500 to 2000 per tonne, is substantially higher than that of biochar, which is estimated at approximately USD 246 per tonne (Amalina et al., 2024). Conversely, modified biochar offers comparable or superior removal performance for MNPs at approximately one-sixth the cost (Li et al., 2023). In addition, AC regeneration is a costly process and significantly add to the overall maintenance cost of the treatment system. For biochar regeneration, the conventional regeneration techniques are applicable for MNP treatment (i.e. adsorbate desorption and adsorbate decomposition). The thermal regeneration has been recommended for adsorbate decomposition and commonly used industrial scale, which is considered as a cost-effective process (Román et al., 2013; Wang et al., 2020).

Carbon nanotubes (CNTs) exhibit remarkable MNP adsorption ability (up to 1650 mg/g) attributed to their defined mesoporous structure and high aspect ratio, with magnetic CNTs achieving complete removal of PE, PET, and PA from aqueous solutions (Tang et al., 2021). However, practical applications for MNP removal are limited by: (i) high production costs of CNTs (approximately USD 114,000 per tonne) (Zhu, 2023), (ii) challenging separation from treated water (Tang et al., 2021), and (iii) potential toxicity implications from nanoparticle leaching, as carbon nanotubes have demonstrated toxic effects on aquatic organisms correlated with heavy metal impurities and hydrophobic surface properties (Pikula et al., 2020). In comparison, biochar presents a more sustainable and safer alternative with convenient regeneration (especially magnetic biochar) and lower ecotoxicological risks, while carbon-based adsorbents including CNTs face challenges such as high regeneration costs and lack of standardized testing methods (Anuwa-Amarh et al., 2024).

Graphene-based materials are also used as adsorbents for the removal of MNPs. Graphene oxide and reduced graphene oxide present strong π-π interactions with aromatic polymers like PS, attaining high removal efficiencies >90% (Anuwa-Amarh et al., 2024). However, production of graphene-based nanomaterials for large-scale water treatment is as high as USD 50,000–200,000 per tonne. Moreover, their production has significant environmental footprint owing to involvement of harsh chemical oxidation process (Hummer's method) (Asghar et al., 2022). On the other hand, modified biochar, particularly CTAB-functionalized biochar, achieves comparable MNP removal

efficiency (95–99%) at comparatively negligible cost (Hanif et al., 2024).

In summary, application of biochar for MNP treatment has several practical advantages over other adsorbents including (i) feedstock flexibility: municipal sludge, agricultural wastes, domestic waste and industrial byproducts can be pyrolysed to produce relatively cost-effective biochar; (ii) tuneable surface properties: modification can target treatment for specific polymers (e.g., Fe-oxides for functional PS/PE; CTAB for PS/PE/PP); (iii) magnetic separability: overcomes the recovery challenge plaguing powdered adsorbents; (iv) regenerability: multiple cycles (5–7) achievable through combined pyrolysis, hydrothermal, ultrasonication and chemical methods; (v) scalability: existing pyrolysis setup can be adapted for biochar production at regional scales.

4. Factors affecting MNPs' interaction with biochar

Multiple factors such as characteristics of MNPs (polymer type, functional group, size, shape, aging, and concentration), biochar properties (surface area, pore size, pore volume, concentration, zeta potential, charge, functional group, and modification), and environmental conditions (pH, temperature, organic matter, interfering ions, reaction time, and agitation) can influence the adsorption of MNPs on biochar and their removal from the environment (Fig. 6).

4.1. MNP properties

4.1.1. Polymer type and functional group

Plastic polymer type and functional groups can significantly influence their interaction with biochar. For instance, PEMPs exhibited superior removal efficiency with CTAB-PKB compared to PAMPs. While polymer type can considerably influence the retention of suspended particles, mostly owing to variations in density (Hanif et al., 2024). Both polymers possess densities that closely approximate that of water (PE = 0.91–0.94 g/cm^3, PA = 1.01 g/cm^3), hence reducing the impact of gravitational forces on the removal process (Gao et al., 2021). PSNPs with different functional groups, such as NH_2-PSNPs, COOH-PSNPs, and UV-aged PSNPs, showed higher removal rates with magnetic PWB compared to pristine PSNPs (Shi et al., 2023). NH_2-PSNPs revealed higher adsorption rates compared to other plastic types, likely due to the positive charge on its surface, which aggressively attracted the negatively charged biochar (Zhao et al., 2022; Singh et al., 2021). This underscores the need to comprehend the physical and chemical characteristics of plastic particles, in addition to polymer type, in affecting their interaction with biochar.

4.1.2. Size, shape, and aging

Size, shape, and aging of MNPs can also alter their adsorption on biochar. Regarding the size of MNPs, for instance, the rate constant for 15 μm PSMPs in the pseudo-second-order model exceeds that of 2 μm PSMPs, indicating a more rapid adsorption of larger MP particles on magnetic BZC (Babalar et al., 2024). Larger MPs often possess a greater cross-sectional area than smaller MPs (Na et al., 2021). An increase in cross-sectional area facilitates enhanced Van der Waals forces (Winterton, 1970) and additional attractive forces between the bigger MPs and the inside surfaces of the AC pores (Zheng et al., 2007). Moreover, larger MPs are usually denser, causing them to descend more rapidly through the water column and make contact with surfaces more readily (Babalar et al., 2024). The removal efficiency of various MPs by CTAB-modified PKB was in the following order: PEMPs (40–48 μm) > PENPs (159–756 nm) ≈ PEMPs (2–4 μm) > PA microfibers (<5 mm) ≈ PAMPs (6–9 μm) > mix MPs. A removal efficiency of 99% is attained for PEMPs (40–48 μm), even with pristine biochar, as the filter media effectively captures these larger MPs inside its pores, while smaller MPs and NPs showed enhanced mobility inside the filter medium. Further, when the particle size of MPs is sufficiently diminutive (<10 μm), their adsorption may significantly escalate, as the small MPs may be directly adsorbed onto the biochar surface and enmeshed inside the pores of biochar (Wang et al., 2021; Wang et al., 2020). The magnetic CLB and quartz mixture was able to remove all three sizes of COOH-MNPs (0.02 μm, 0.2 μm, and 2 μm), and the breakthrough percentage was in the order of 68%, 36%, and 34%, implying that larger MNPs showed relatively higher adsorption capacity than smaller ones (Tong et al., 2020). This size range of MNPs (0.02 μm-2 μm) is near colloid sizes (0.001 μm-1 μm), where the polarity and magnitude of surface charge can be crucial in controlling how the particles interact with surfaces while the effects of the pore system become less noticeable (Bhattacharjee, 2016). Contrary to expectations, PENPs exhibit superior removal efficiency compared to numerous larger-sized MP samples, ascribed to NP agglomeration (Hanif

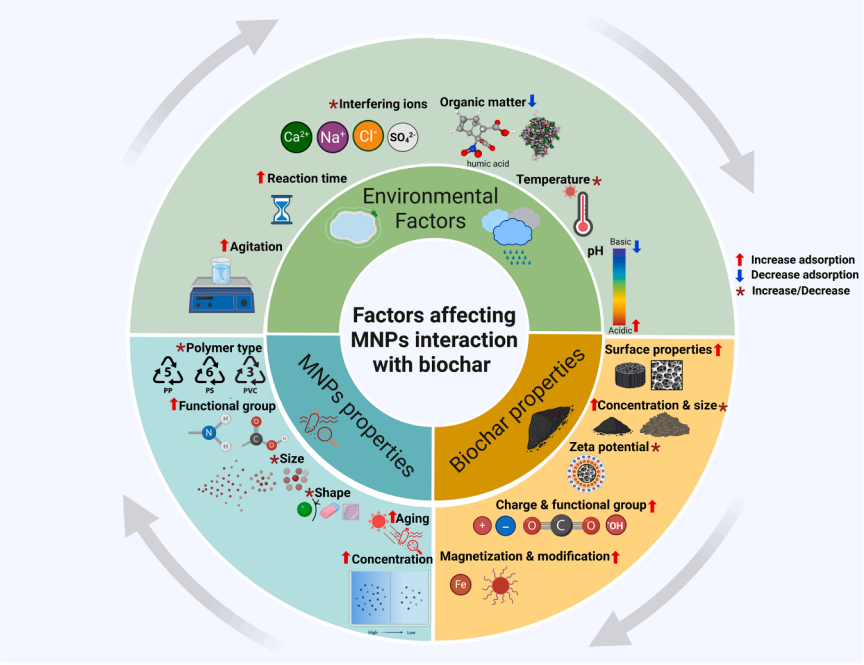

Fig. 6. Factors affecting the adsorption or interaction of MNPs with pristine and modified biochar.

et al., 2024). Similarly, the adsorption of PSMP-210 (molecular weight, 210 Da) on magnetic WSB was much greater than that of PSMP-10 K (10, 000 Da) and PSMP-32 K (32,000 Da) at the same starting concentrations, indicating the viability for the removal of low molecular weight MPs (Kim et al., 2024).

Regarding the shapes of plastic particles, Hanif et al. reported the removal efficiency of various shaped MNPs for CTAB-PKB exhibits the following trend: irregular > spherical > fibre. Nonetheless, the overall removal efficiency of PA microfibers was lowest compared to that of other MNPs, potentially attributable to the morphology and smoothness of the fibres. These properties diminish the probability of efficient filtering, since fibres may demonstrate less adherence to the filter medium surface despite their substantial size and restricted mobility. (Hanif et al., 2024). The superior removal efficiencies demonstrated by irregularly shaped MNPs can be attributed to their reduced mobility within the filter medium. These particles are more prone to entanglement with the biochar, and their textured surfaces facilitate immobilisation by conforming to the grooves and pores of the biochar. The polished surfaces enhance movement inside the filter bed, decreasing the likelihood of being hindered by the filter medium (Hanif et al., 2024). Other studies have also indicated that spherical MNPs demonstrate significant mobility and may readily traverse filter media (Dong et al., 2021; Tumwet et al., 2022; Waldschläger and Schüttrumpf, 2020)

The removal efficiency of pristine PAMPs by using magnetic CCB was unaffected by particle size. However, the removal of aged PAMPs was significantly influenced by particle size. The removal efficiencies of PAMPs-0.5 day and PAMPs-1 day aged considerably increased with a decrease in particle size within the range of 75–180 μm. Nonetheless, when the aged PAMPs were <75 μm, the particle size did not influence their adsorption (Li et al., 2023). Similarly, UV-aged PSNPs showed higher removal rates with magnetic PWB compared to pristine PSNPs, mainly attributed to an increase in functional groups with aging (Shi et al., 2023).

4.1.3. Concentration

Concentration of MNPs showed a direct relationship with adsorption of plastic particles on biochar. With the rise in PSNP concentration (20–200 mg/L), the adsorption isotherms demonstrated an ascending trend with a maximum adsorption capacity of 54.09 mg/g on magnetic CTAB-RSB, reflecting an almost 500% increase relative to BC (11.62 mg/g) and magnetic RSB (10.92 mg/g) (Xing et al., 2024). Similarly, the removal efficiencies of PSMPs with PAB and ALB were recorded at 1.4 mg/g and 7.64 mg/g, respectively, at a concentration of 10 mg/L PSMPs. And with an increase in PSMP concentration (50 mg/L), the adsorption capacities were also increased to 2.5 mg/g and 12.5 mg/g for PAB and ALB, respectively (Mahmoud et al., 2024). Similarly, increasing the PSNPs/COOH-PSNPs concentration from 2 to 8 mg/L enhanced the removal efficiencies of magnetic CTAB-RPB from 88.8% to 95.2% for PSNPs and from 85.3% to 91.2% for COOH-PSNPs (Shi et al., 2023). This direct nexus between increasing MNP concentration and associated adsorption on biochar could be attributed to the greater quantity of contaminants relative to the accessible sites on the biochar surface (Mahmoud and Ibrahim, 2023).

4.2. Biochar properties

4.2.1. Surface characteristics

Biochar surface characteristics such as surface area, pore volume, and pore number play a critical role in the adsorption of plastic particles. Pristine biochar greatly varies in surface properties, largely attributed to parent biomass and pyrolysis conditions. For instance, ALB demonstrated a marginally greater surface area, reduced pore size, and total pore volume compared to PAB. The surface area, average pore size, and total pore volume for ALB were 2.542 m^2/g, 0.5776 nm, and 7.3×10^{-4} cm^2/g, whereas for PAB they were 2.168 m^2/g, 2.242 nm, and 2.4×10^{-3} cm^2/g, respectively (Mahmoud et al., 2024). Concerning the impact of pyrolysis temperature, ranging from 300 °C to 400 °C, the microstructural surface and layer thickness of CSB increased, and between 400 °C and 500 °C, the comparatively weaker components were eliminated, leading to an enhanced pore structure. The surface area of CSB diminishes to 808.3 ± 81.9 m^2/g, 609.0 ± 83.5 m^2/g, and 177.5 ± 16.3 m^2/g at pyrolysis temperatures of 300, 400, and 500 °C, respectively (Wang et al., 2020). However, Magid et al. revealed that the increase in pyrolysis temperature enhanced the surface area, pore volume, and pore size of CCB. Notable increases were detected between biochar pyrolyzed at 500 °C and those pyrolyzed at 700 °C or 900 °C (Magid et al., 2021). The surface area of PWB at 300 °C was 1.301 m^2/g (Shi et al., 2023), indicative of a low surface area typical of low-temperature biochar (Guo and Chen, 2014). With the temperature rising to 500 °C and 700 °C, the surface area of PWB expanded to 183.851 m^2/g and 202.667 m^2/g, respectively (Shi et al., 2023). This phenomenon may be ascribed to the emission of volatiles at elevated temperatures, leading to an increase in pore formation and internal surface area (Guo and Chen, 2014). The oxidised biochar (treated with HNO_3/H_2SO_4) exhibited significantly greater specific surface area and small pore (<100 nm) volume compared to the pristine biochar, with increases of 39.6–107% and 83.3–125%, respectively; however, the average size of small pores (<100 nm) diminished during oxidation (Magid et al., 2021). The enlargement of pores is likely attributable to the degradation and consumption of organic materials during chemical oxidation. The reduction in average pore size during oxidation may be attributed to the formation of comparatively smaller pores. Similarly, a decrease in average pore size was seen in peanut shell biochar treated with HNO_3/H_2SO_4 (Ghaffar and Abbas, 2016).

Surface properties of biochar can also significantly change by magnetization. For instance, in comparison to the pristine PWB, the surface area of magnetic PWB exhibited a rise to 8.25 m^2/g, 211.77 m^2/g, and 207.33 m^2/g, respectively, at 300, 500, and 700 °C, likely owing to biochar modification and particle size reduction from micron to submicron scale as a result of ball milling (Shi et al., 2023). A decrease in the size of biochar particles following ball milling with Fe_3O_4 led to an increase in the surface area. Fe_3O_4 may obstruct the mesopores and macropores (Wang et al., 2021). Similarly, the surface area of pristine CLB was determined to be 2.0 m^2/g at around 400 °C (Tong et al., 2020), which was significantly increased to 24.2 m^2/g after modification with Fe_3O_4, indicating that magnetic CLB may possess more adsorption sites and exhibit enhanced adsorption capacity compared to biochar (Tong et al., 2020). A comparable surface area of magnetic CCB was reported at 27.82 m^2/g, much bigger than that of PAMPs (3.01–6.59 m^2/g), sufficient for their subsequent adsorption (Li et al., 2023). The surface area and total pore volume of the magnetic CCB were 216.01 m^2/g and 0.22 cm^3/g, respectively. Following the adsorption of PSNPs, the specific surface area (145.51 m^2/g) and pore volume (0.14 cm^3/g) were decreased. However, the surface area and total pore volume of magnetic CCB were increased to 200.19 m^2/g and 0.19 cm^3/g during hydrothermal degradation of PSNPs and regeneration of biochar (Zhu et al., 2022). The increased surface area and pore volume may provide more active sites for the entrapment and immobilisation of PSNPs (Wang et al., 2020). The pore volume of mesopores and macropores constituted 80–90% of the overall pore volume, indicating that larger pores significantly contributed to the adsorption of PSNPs (Zhu et al., 2022). In contrast, a reduction in the surface area of magnetic MSB was noted in comparison to the pristine biochar (Singh et al., 2021), which substantiates the iron loading on the surface (Zhu et al., 2017). The surface area of magnetic MSB was measured as 25.8 m^2/g and 34.5 m^2/g, respectively, at 550 °C and 850 °C (Singh et al., 2021), which is comparable to the surface area of magnetic CLB (Tong et al., 2020) and magnetic CCB (J. Li et al., 2023).

Surface characteristics of biochar also significantly change by CTAB. For instance, CTAB diminishes the surface area of magnetic RSB from 119.13 m^2/g to 95.69 m^2/g, but the total pore volume escalates from 0.18 cm^3/g to 0.19 cm^3/g. The results indicate that the magnetic CTAB-

RSB experiences erosion in micropores, leading to a substantial decrease in micropore quantity and an increase in mesopore quantity (Xing et al., 2024). Similarly, the pore size of CTAB-PKB (993–1018 nm) was reduced after CTAB addition compared to pristine PKB (760-2192 nm). The decrease in pore size indicates that CTAB was effectively deposited onto the biochar surface, resulting in pore reconstruction (Hanif et al., 2024). Moreover, the surface area of magnetic CTAB-RPB (683.6 m^2/g) was decreased after CTAB modification compared to magnetic RPB (828.2 m^2/g). Despite the reduced specific surface area of magnetic CTAB-RPB, it demonstrated superior removal efficiency for PSNPs and COOH-PSNPs compared to magnetic RPB (Shi et al., 2023).

4.2.2. Concentration and size

Biochar concentration and particle size can also impact the adsorption of MNPs. For instance, the adsorption of PSMPs increased with increasing adsorbent dosage of magnetic BZC (0.1–2 g/L), with the highest adsorption of 100 mg/L PSMPs at 1 g/L magnetic BZC (Babalar et al., 2024). However, there is an optimum biochar concentration, and when equilibrium is reached, there is no further active adsorption surface available, attributed to the aggregate formation (Gupta, 2023). For example, Kim et al. observed no significant improvement in PSMP adsorption on magnetic WSB at concentrations above 0.6 g/L (Kim et al., 2024). At the minimal adsorbent quantity of 5.0 mg for PAB and ALB, the maximum adsorption capacity of PSNPs was achieved at 31.1 and 35.2 mg/g, respectively, while a large dose (100 mg) resulted in lower adsorption of PSNPs (2.1 and 2.7 mg/g) (Mahmoud et al., 2024). Under this circumstance, an elevated biochar mass to plastic particles ratio was observed, resulting in decreased adsorption (Wan et al., 2022). The removal efficiencies improved from 18.3 to 72.4% for PSNPs and from 0.9 to 78.3% for COOH-PSNPs when the dose of CTAB-RPB was elevated from 0.3 to 3 g/L. Regarding the size of biochar particles, the ball-milled CTAB-RPB exhibited superior removal efficiency compared to the 40–60 mesh CTAB-RPB at a dose of 0.3 g/L. The removal efficiencies of PSNPs reduced as the particle size of CTAB-RPB increased (Shi et al., 2023).

4.2.3. Zeta potential

Zeta potential also plays a critical role in the adsorption of MNPs on biochar. Change in temperature and pH can significantly impact the zeta potential of both biochar and MNPs. For instance, in a very acidic pH (2–4), the zeta potential of PSMPs and magnetic BZC tends to be positive, signifying that the dispersed particles in the acidic solution possess positive charges that can favour the interaction between biochar and MNPs (Babalar et al., 2024). Kumar et al. assert that a positive zeta potential results from the presence of positively charged groups on the particle (Ravi Kumar et al., 2004). When the pH rises above 4, the zeta potential of magnetic BZC and PSMPs transitions from positive to negative. The magnetic BZC exhibits a positive charge within the pH range of 2 to 10 and becomes slightly negative beyond a pH of 10. The elevated positive zeta potential of magnetic BZC indicates that the polymer coating influenced the surface charge (Babalar et al., 2024). However, at elevated pH levels, deprotonation induces a repulsive attraction between magnetic BZC and PSMPs, hence diminishing the adsorption of PSMPs (Babalar et al., 2024). Similarly, the pH climbed from 3 to 11, and the zeta potentials of CTAB-RPB, PSNPs, and COOH-PSNPs fell progressively to −55.7, −41.7, and −69.0 mV, respectively (Shi et al., 2023). The concentration of OH ions rose with the elevation of pH, neutralising positively charged surfaces and generating a negative zeta potential (Wang et al., 2021). Consequently, MNPs exhibited considerable stability under alkaline conditions owing to the robust electrostatic repulsion among the particles, leading to a marked reduction in removal efficiency (Shi et al., 2023). Biochar typically exhibits a negative zeta potential due to its negative surface charge (Wang et al., 2020). Further, the zeta potential of the biochar becomes less negative if it is produced at high pyrolysis temperatures, which can also favour MNP sorption (Ganie et al., 2021; Magid et al., 2021).

4.2.4. Charge and functional group

Charge and functional groups on biochar can substantially impact the adsorption of MNPs. For instance, the elevated positive charge on the magnetic WSB (7.26 at pH 5) compared to the pristine WSB (−5.85 at pH 5) influenced the PSMP removal (Kim et al., 2024). At the same biochar concentration (0.2–1.0 g/L), magnetic WSB exhibited superior removal efficiency (77.0–100.0%) for PSMPs compared to pristine WSB (14.5–16.8%). This difference in adsorption capacity is ascribed to the significant positive charge and enhanced hydrophilic properties of magnetic WSB, as indicated by the O/C ratios: WSB = 0.02 compared to magnetic WSB = 0.09 (Kim et al., 2024). The increased presence of metal oxide groups on magnetic WSB is considered crucial for the effective adsorption of anionic PSMPs (Liu et al., 2019). Following the adsorption of PSNPs on CCB, the bands at 3429 c/m (-OH) and 1102 c/m (C—O-C) exhibited a considerable reduction, indicating that the OH group may be crucial in the adsorption of PSNPs onto CCB via hydrogen bonds (Magid et al., 2021). The reduction of the ether group (C—O-C) following the adsorption of PSNPs may be attributed to hydrophobic interactions between biochar and PSNPs, as C—O-C groups are nonpolar (Magid et al., 2021).

4.2.5. Magnetization and modificationz

Magnetization of biochar can be done using various iron sources such as Fe_3O_4, $Fe(NO_3)_3$, $FeCl_3$, $FeSO_4$, Fe mining waste, red mud waste, and steelmaking waste. The adsorption capacity of biochar significantly increases after magnetisation (Zhang et al., 2024). RSB was successfully magnetized using Fe_3O_4, revealing the saturation magnetisation at 21.5 emu/g of the modified biochar, validating its superior magnetic separation efficacy. The adsorbent sample exhibits magnetic attraction, indicating effective separation and recovery capabilities, hence mitigating the challenges of biochar recovery in aquatic systems (Xing et al., 2024). To enhance removal effectiveness, biochar can be changed to possess a net positive charge and increased hydrophobicity using cationic surfactant such as CTAB, hence augmenting interactions through electrostatic attraction and heightened hydrophobic forces. CTAB has been employed to alter magnetic biochar for the removal of MNPs by many researchers (N. Parashar and Hait, 2024; Y. Shi et al., 2023; Xing et al., 2024), all of whom attained removal efficiencies ranging from 90% to 99%. An elevated concentration of CTAB enhances the production of additional admicelles on the biochar surface, hence augmenting MP retention. Magnetic biochar with CTAB modification also attains higher MNP removal efficiencies both in laboratory and environmental samples (Xing et al., 2024). Biochar has also been subjected to oxidation by using HNO_3/H_2SO_4, exhibiting significantly greater specific surface area and improving the adsorption of MNPs (Magid et al., 2021).

4.3. Environmental factors

4.3.1. Interfering ions and ionic strength

The adsorption of MNPs on biochar is influenced by the presence of coexisting ions and the ionic strength of the matrix (Singh et al., 2021; Ganie et al., 2021). The presence of coexisting ions can alter the electrochemical characteristics of the adsorbent surface and lead to competitive adsorption (Heo et al., 2022). Moreover, ionic strength influences MNP aggregation (Bian et al., 2011), thus impacting their adsorption and transport inside porous media (Ni et al., 2024). Ionic strength influences adsorption capacity both positively and negatively (Wadhawan et al., 2020; Sun et al., 2022). The squeezing-out action and competing adsorption can diminish the adsorption of MPs on biochar. Conversely, the electrostatic screening effect and "salting-out" effect enhance the adsorption of MPs on biochar (Zhang et al., 2024).

Cations usually improve the adsorption of MNPs on biochar through bridging, while anions reduce adsorption due to the overall negative charge on biochar and MNPs. For instance, the cations (Ca^{2+}) improved *Ulva prolifera* derived biochar (UPB) mediated PSNPs removal by

86.59%, but the anions (HPO_4^{2-}) reduced it by 28.91% (Huang et al., 2024). The introduction of cations has been seen to diminish the negative repulsion among PSNPs, hence promoting aggregation (Gong et al., 2022). The adsorption of PVCNPs on CCB and WSB exhibited the following order of ionic strength: $Ca^{2+} > SO_4^- > Cl^- > NO_3^-$. Ca^{2+} exhibits a robust retention capacity for PVCNPs in sandy soil columns (Ni et al., 2024). Ca^{2+} can facilitate the bridging effect, hence enhancing the adsorption of negatively charged plastic particles on anionic biochar (Ganie et al., 2021; Ramirez Arenas et al., 2021). Similarly, Cheng et al. also reported that the adsorption of PSNPs in saturated porous media was increased in the presence of Ca^{2+} (Heo et al., 2022). Babalar et al. found the highest adsorption of PSMPs on magnetic BZC at 97.5% in the presence of $CaCl_2$ (Babalar et al., 2024). Conversely, studies have also shown that the presence of cations reduced the adsorption of MNPs on biochar. For instance, the removal of PAMPs using CCB diminished as $CaCl_2$ concentrations increased, attributed to competitive adsorption induced by Ca^{2+}. The adsorption of Ca^{2+} diminishes the available sorption sites and electrostatic attraction between PAMPs and CCB, resulting in a decreased PA adsorption (J. Li et al., 2023). Similarly, the COOH-PSNPs removal diminished in the presence of K^+, Mg^{2+}, and Ca^{2+}; specifically, the efficiency declined from 91.2% to 80.5% as the Ca^{2+} concentration increased from 0 to 5 mM (Y. Shi et al., 2023).

In the presence of sodium salts, a significant increase in the adsorption of PSNPs on LPB was noted in the order of $NaH_2PO_4 > Na_2SO_4 > NaCl > NaNO_3$ when the concentrations rose from 0 mM to 10 mM, implying that the electrostatic shielding effect and the "salting-out" effect are pivotal for PSNPs adsorption (Zhang et al., 2024). The presence of anions such as HPO_4^{2-} and CO_3^{2-}, together with HA, generates substantial competition among PSNPs, thereby impeding the adsorption of PSNPs on magnetic CTAB-RSB. Interfering ions predominantly obscure the surface charge of PSNPs, leading to less electrostatic attraction and a subsequent reduction in adsorption capacity (Xing et al., 2024). The removal efficiencies were 73.3% for PSNPS and 59.1% for COOH-PSNPs in the presence of 5 mM $H_2PO_4^-$. The inhibitory effects of anions on the removal efficiencies were reduced in the following order: $Cl^- < HCO_3^- < SO_4^{2-} < H_2PO_4^-$ for PSNPs and $Cl^- < SO_4^{2-} < HCO_3^- < H_2PO_4^-$ for COOH-PSNPs (Y. Shi et al., 2023). The inhibitory effects of HCO_3^- on the removal efficiencies were attributed to HCO_3^- functioning as a buffer and altering the solution pH to a basic level (Ganie et al., 2021). The significant inhibitory effects caused by SO_4^{2-} and $H_2PO_4^-$ may be ascribed to their elevated charge density (Maia et al., 2021; J. Wang et al., 2021). The adsorption of PSNPs on MSB decreased somewhat to 86% in the presence of PO_4^{3-} (Singh et al., 2021). At extremely low ionic strength and rapid flow, a minimal quantity of MNPs released from biochar in columns, simulating a sudden rainfall. However, a modest quantity of MNPs was released from biochar at high ionic strength (Tong et al., 2020).

Similarly, the presence of NaCl can increase or decrease the adsorption of MNPs on biochar. For instance, the lowest adsorption of PSMPs on magnetic BZC was found in the presence of NaCl, attributed to the competition between negative ions and PSMPs for adsorption on biochar (Babalar et al., 2024). Under conditions of elevated NaCl concentration, chloride ions may establish a double layer at the surface, resulting in electrostatic repulsion between the positively charged biochar and the negatively charged MPs (Babalar et al., 2024). Conversely, with the ionic strength rising from 0 to 1 mol/L, the qe of the PSNPs on magnetic SDB increased 17.4–36.4 mg/kg for HA and 24.1–37.3 mg/kg for FA, respectively. NaCl enhances the accessibility of active sites on magnetic SDB in solutions with various forms of DOM, hence stabilizing the PSNPs (Zhao et al., 2024). The removal efficiency of PSMPs using WSB increased progressively as the ionic strength rose from 0–0.1 M NaCl, attributed to a reduction in the repulsive forces, reduced charge shielding, and a compacted electric double-layer effect that promotes the adsorption of PSMPs on biochar as the ionic strength rises (Kim et al., 2024; Liu et al., 2018; Li et al., 2022). Similarly, the adsorption of PSMPs on PAB increased from 7.9 to 11.1 mg/g with the addition of 10–30 mg NaCl, where NaCl facilitates surface charge neutralisation (Tong et al., 2020; W. Zhao et al., 2022). The percentage removal of PSMPs onto ALB increased from 9.6–10.8 mg/g with the addition of 10–30 mg NaCl. Elevating the concentration of NaCl to 40–100 mg reduced the removal of PSMPs (Mahmoud et al., 2024). This behaviour indicates that Na^+ and Cl^- vigorously battled for the active surface sites (Li et al., 2022).

4.3.2. Organic matter

Adsorption of MNPs on biochar mostly decreases in the presence of organic matter. For instance, Wang et al. posited that the elevated concentration of NOM in river water obstructed PSNP adsorption by competing for adsorption sites on magnetic SDB (J. Wang et al., 2021). Singh et al. indicated that the adsorption of PSNPs onto magnetic MSB diminished as DOM concentration increased (Singh et al., 2021). PSNPs adsorption decreased by 80.2% and 53.2% in the presence of FA and HA, respectively. The decrease is ascribed to magnetic SDB-FA or magnetic SDB-HA complex formation, which obstructs the adsorption of PSNPs (Zhao et al., 2024). FA possesses a greater quantity of oxygen-containing functional groups compared to HA. FA significantly interacts with both SDB and PSNPs in multisolute environments, diminishing the adhesion of PSNPs to SDB surfaces (Zhao et al., 2024). Xing et al. also revealed that the adsorption ability of biochar is considerably diminished with the incorporation of HA, and the effect on the removal efficiency of PSNPs escalates with higher HA concentrations (Xing et al., 2024). The reduction in adsorption capacity may be ascribed to the complexation or π-π stacking interactions between HA and the adsorbate and PSNPs (Aiken et al., 2011; Singh et al., 2021). Similarly, a significant drop in COOH-PSNP adsorption was seen at DOM levels of 5 mg/L or above. The NH_2-PSNPs possessing lone pairs will readily conjugate with HA, resulting in impaired adsorption. (Singh et al., 2021). Contrarily, DOM can facilitate the removal of MNPs in the presence of heavy metals, especially during the phase of heterogeneous aggregation. Biochar-released heavy metals facilitated the aggregation of MNPs by forming bridge connections between DOM and metal ions (Singh et al., 2019).

4.3.3. Reaction time and agitation

An increase in reaction time and shaking speed may enhance the adsorption of MNPs on biochar. For instance, PSNPs' removal by UPB was reported at 55.8% and 86.59% after 8 h and 12 h of reaction time, respectively, indicating an increase in the adsorption with longer reaction time (Huang et al., 2024). The removal of PSMPs by PAB (1.02–4.1 mg/g) surpassed that by ALB (4.1–2.48 mg/g) throughout a response time of 5–25 min. After 30–60 min, the trend shifted to favour greater removal by ALB (5.36–8.3 mg/g) in comparison to PAB (4.36–4.62 mg/g) (Mahmoud et al., 2024). The removal of PSNPs and COOH-PSNPs escalated swiftly over the initial 10 min and thereafter plateaued. At a contact duration of 60 min, the removal efficiencies for PSNPs and COOH-PSNPs attained 95.2% and 91.2%, respectively (Y. Shi et al., 2023). A reduced shaking rate enhanced electrostatic interaction by 63.97% but impeded heterogeneous aggregation, leading to a slight decrease of 1.68% in total removal efficiency (Huang et al., 2024).

4.3.4. Temperature

Temperature can significantly change the properties of both biochar and MNPs; therefore, it can increase or decrease or remain insignificant towards the adsorption of MNPs on biochar. For instance, the adsorption of PSMPs (2 μm) on magnetic BZC increased with an increase in temperature. As temperature rises, the kinetic energy of the molecules escalates. Increased kinetic energy results in more frequent collisions between smaller MPs and the adsorbent surface, hence enhancing adsorption (Babalar et al., 2024). For large-sized PSMPs (15 μm), the highest adsorption was observed at 24 °C (Babalar et al., 2024). The larger surface area of 15 μm PSMPs results in a greater influence of temperature on the Van der Waals forces, leading to a reduction in adsorption at elevated temperatures (Babalar et al., 2024). Similarly, a

significant reduction in adsorption of PSMPs on magnetic WSB was observed with the increase in temperature (99.58% at 288 K to 98.08% at 308 K) (Kim et al., 2024). This pattern indicates an exothermic adsorption process, where increased temperatures reduce Van der Waals forces, hence diminishing adsorption (Kameda et al., 2020). A steady decline in PSMP adsorption on ALB and PAB was observed as the reaction temperature increased from 25 to 50 °C. The maximum removal efficiency of PSMPs occurred at 25 °C, yielding 6.0 mg/g and 3.28 mg/g with ALB and PAB, respectively, while the minimum was observed at 50 °C, indicating an exothermic reaction (Chen et al., 2021; Mahmoud et al., 2024). Similarly, the adsorption of PENPs diminished as the temperature rose from 25 °C to 45 °C, regardless of whether AGS or biochar were utilised as adsorbents. (Wang et al., 2022).

The minimal impact of temperature on the removal efficiency of biochar was also reported. The calculated Gibbs free energy (ΔG) for magnetic PWB interacting with various PSNPs was negative (Shi et al., 2023), signifying that the adsorption process was spontaneous (Sheha and El-Zahhar, 2008). A decrease in ΔG was seen with rising temperature, leading to accelerated interaction (Singh et al., 2021). The enthalpy (ΔH) values for PSNPs, UV-PSNPs, NH_2-PSNPs, and COOH-PSNPs adsorbed by magnetic PWB were 2.45, 3.65, 4.32, and 2.28 kJ/mol, respectively (Shi et al., 2023). The positive ΔH indicated that the adsorption process is endothermic (Sun et al., 2021). Similarly, Gibbs free energy for the interaction of MSB with various PSNPs was significantly negative, indicating the spontaneity of the adsorption process. An increase in temperature resulted in a fall in Gibbs energy (more negative), facilitating accelerated contact and improved removal (Singh et al., 2021).

4.3.5. pH

pH influences the adsorption of MNPs by directly affecting the charge density and ionic strength on the surfaces of both adsorbents and plastic particles (Sun et al., 2020). Most of the studies revealed that acidic conditions favoured MNP adsorption on biochar. For instance, the adsorption of PSMPs on magnetic BZC increased from pH 2.0 to 4.0 and achieved the maximum removal (99%) at pH 4.0, thereafter declining at elevated pH. Under reduced pH, an increased number of amine groups will undergo protonation, resulting in an elevated positive surface charge (Babalar et al., 2024). In contrast, under elevated pH, a diminished number of amine groups will be protonated, leading to a decreased positive surface charge. Under alkaline conditions, OH^- ions might compete with negatively charged MPs for active sites on biochar, hence diminishing adsorption (Babalar et al., 2024). Similarly, at pH 1.0, ALB and PAB showed removal efficiencies of 100% and 99.4% for PSMPs, which were reduced to 94.4% and 98.7% at pH 2.0 (Mahmoud et al., 2024). An increase in pH results in a reduction of free hydrogen ions, thereby impairing the capacity of PSMPs to adhere to biochar, reducing removal efficiencies to 12.5–20.0% and 8.1–29.9% at pH levels ranging from 4.0 to 9.0 (Mahmoud et al., 2024). The negative charges on biochar were entirely neutralised by the available hydrogen ions, promoting the creation of a neutral surface to facilitate direct contact with PSMPs (Oliveira et al., 2023). Similarly, the peak adsorption of PSNPs on pristine CCB occurred at around pH 5.0, whereas the lowest adsorption was seen at pH values around 10.0 (Magid et al., 2021). For oxidised CCB, a greater quantity of PSNPs was adsorbed at lower pH, with the adsorbed amount progressively diminishing as pH increased. At lowered pH, the protonation of the adsorbent surface diminished the negative charges on the surfaces of both biochar and PNSPs, resulting in a comparatively lesser electrostatic repulsion between biochar and PSNPs (Magid et al., 2021). The removal efficiencies of PSMPs on magnetic MSB declined from 99.76% at pH 3.0 to 89.79% at pH 11.0. This pattern may be explained by the tendency of WSB surface charges to become positively charged when the solution pH decreases, hence enhancing the electrostatic attraction to the negatively charged PSMPs (Kim et al., 2024). The zeta potential of PWB and PSNPs reduced with increasing solution pH and remained consistently negative. Notably, as the pH increased, adsorption of PSNPs was still evident (Shi et al., 2023), potentially attributable to the synergistic impact of electrostatic attraction arising from the heterogeneous charge distribution on the biochar surface (Zhu et al., 2018). Nevertheless, as the solution pH surpassed 7.0, the adsorption capacity of PWB reduced somewhat due to the intensified electrostatic repulsion within the pH range of 9–11 (Singh et al., 2021). The highest removal of PSNPs by PWB was found in mildly acidic or neutral pH solutions. (Shi et al., 2023).

Some studies also highlighted that the neutral pH (7.0) is also suitable for the adsorption of MNPs on biochar. For instance, at pH 7.0, both the aged PAMPs and CCB exhibited a negative charge; however, the adsorption capacity of aged PAMPs reached its maximum, attributed to the significant role of hydrophobic interactions (J. Li et al., 2023). The formation of a carboxyl group on the surface of aged PAMPs resulted in a negative charge with the rise in pH (Liu et al., 2022; J. Li et al., 2023). As pH increased, the removal efficiency improved, peaking at pH 7.0, but the zeta potential of CTAB-RSB consistently decreased from 43.77 mV to −46.10 mV, and that for PSNPs varied from −27 mV to −57.43 mV, signifying a negative charge. As pH increased further, the removal efficiency progressively reduced, attributed to electrostatic repulsion between the negatively charged magnetic RSB and PSNPs (Xing et al., 2024). The optimal removal of PSNPs and COOH-PSNPs by RSB was at pH 7.0. As the solution pH increased from 3.0 to 7.0, the removal efficiency improved from 82.0% to 95.2% for PSNPs and from 67.0% to 91.2% for COOH-PSNPs. As the solution pH increased from 7.0 to 11.0, the removal efficiency diminished to 67.4% for PSNPs and 40.7% for COOH-PSNPs. The electrostatic repulsion between RSB and NPs intensified with rising pH. Consequently, NPs exhibited considerable stability under alkaline circumstances owing to the robust electrostatic repulsion, leading to a significant reduction in removal efficiency (Y. Shi et al., 2023).

Studies have also reported the insignificant impact of pH on the adsorption of MNPs on biochar. Despite MSB exhibiting a negative zeta potential across a broad pH range, the effect of pH on COOH-PSNPs removal was minimal, and adsorption can be attributed to the synergistic effects of electrostatic attraction resulting from heterogeneous charge distribution on the composite surface and surface complexation (Singh et al., 2021). Similarly, the zeta potentials of both PSNPs and LPB were negative over a pH range of 1.0 to 11.0, with a notable drop in zeta potentials as the pH increased. This indicates that the electrostatic force between the PSNPs and LPB surface is repulsive, with the repulsion intensifying as pH increases, hence elucidating the reduction in the adsorption capacity in alkaline conditions. Nonetheless, the adsorption of PSNPs was as high as 47.4 mg/L at pH 11, indicating the involvement of other processes in the adsorption process (Zhang et al., 2024).

5. Removal or adsorption mechanisms of MNPs on biochar

5.1. General mechanisms involved in MNP removal

A summary of MNPs' removal or adsorption mechanisms is given in Fig. 7. MNPs' interaction with biochar can occur via many processes, including pore-filling, physical trapping, surface complexation, electrostatic interactions, hydrogen bonding, hydrophobic interactions, and π-π interactions (J. Wang et al., 2021). Some studies have revealed multiple adsorption mechanisms existing at once between biochar and MNPs. For instance, PSMPs interacted with magnetic WSB through multiple adsorption mechanisms, including electrostatic interactions, pore-filling, π-π interactions, and hydrogen bonding. PSMPs were adsorbed exothermically, with adsorption efficiency diminishing as Van der Waals forces weakened at elevated temperatures (Kim et al., 2024). Similarly, Zhang et al. showed multiple adsorption mechanisms between PSNPs and pristine LBP (Zhang et al., 2024). The adsorption took place in terms of pore filling of agglomerated PSNPs within the macropores of LPB. The volume of pores measuring 10–25 μm dramatically diminished owing to PSNP adsorption, so confirming that the trapping effect

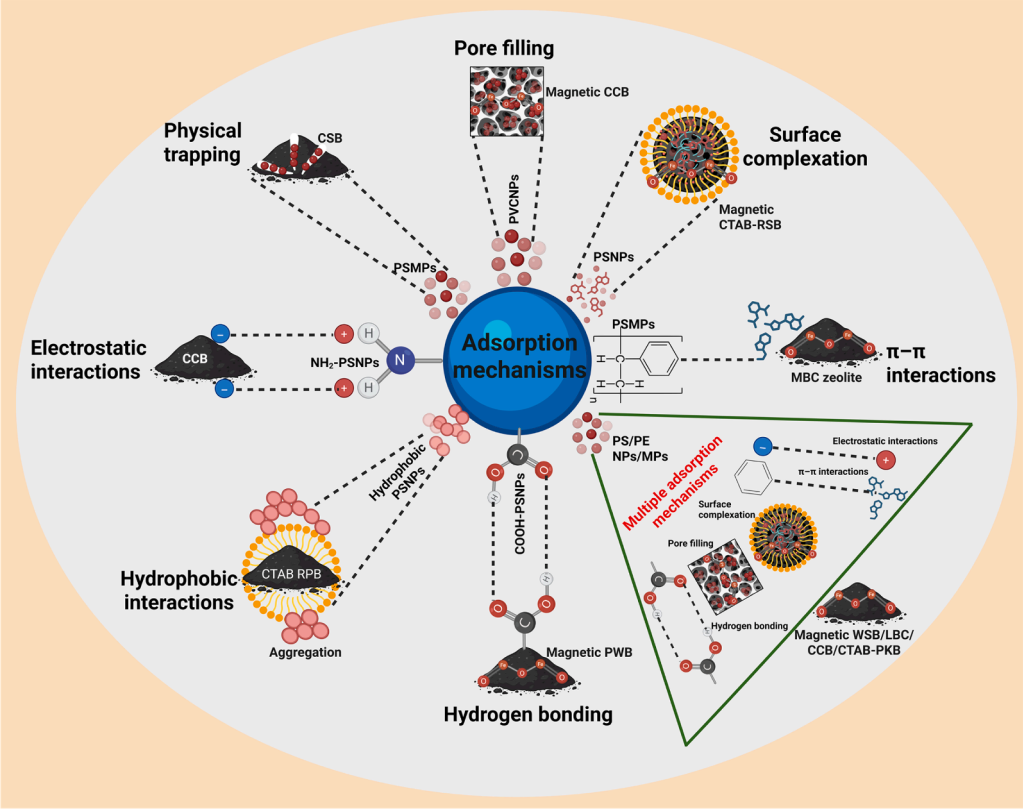

Fig. 7. Removal or adsorption mechanisms of MNPs on pristine and modified biochar.

(physical attachment) was a crucial adsorption mechanism (Zhang et al., 2024) (Fig. 5A-b). As shown in FTIR analysis (Fig. 5A-d), multiple new bands appeared at 695 cm^{-1} and 1181 cm^{-1} after PSNP adsorption on LPB, associated with aliphatic C—H and C—C out-of-plane bending in plastic particles. A new ester C = O bond at 1717 cm^{-1} and reduced signals of aromatic C = O bond at 1620 cm^{-1} showed complex surface interactions between biochar and plastic particles. Moreover, PSNPs' interaction with LPB resulted in a considerable reduction in the -OH band at 3431 cm^{-1}, suggesting the presence of hydrogen bonding (Zhang et al., 2024). PSNPs interacted with contaminated CCB via multiple complex mechanisms (Zhu et al., 2022). Metal oxides and hydroxides on biochar exhibited a positive charge, hence augmenting the adsorption of PSNPs by magnetic CCB via electrostatic interactions (Zhu et al., 2022). After adsorption of CCB on PSNPs, a decrease in peak intensities at 3425 cm^{-1} (-OH) and 1100 cm^{-1} (C—O), respectively, indicated the presence of hydrogen bonding and hydrophobic interactions (Fig. 5B-d) (Zhu et al., 2022). Multiple interaction mechanisms were found between magnetic PWB and functional PSNPs. Electrostatic attraction was confirmed using zeta potential measurement between negatively charged PWB and positively charged NH_2-PSNPs (Shi et al., 2023). In addition to electrostatic adsorption, C–C/C–H, –COOH, and C = O functional groups are also crucial in the adsorption process, indicating the presence of hydrogen bonding. The decreased intensity of C = C and C–O bonds suggests that PWB may interact with PSNPs through π-π stacking due to the presence of a benzene ring (Shi et al., 2023). Hydrophobic interactions likely played a more significant role in the adsorption of PSNPs to pristine CCB, while oxygen-containing surface groups may have been more engaged in the adsorption of PSNPs to oxidised CCB. The pore filling may have contributed to the adsorption of PSNPs onto CCB. In addition to these attractive forces, electrostatic repulsion significantly influences the adsorption between biochar surfaces and PSNPs, as evidenced by the pH dependency of PSNP adsorption (Magid et al., 2021). The negative zeta potential of MSB shifted to +7 mV after interacting with COOH-PSNPs, indicating significant electrostatic attraction. The COO^- stretching associated with acetate functionality has vanished upon adsorption, substantiating the surface complexation of NPs with OH and COO^- groups (Singh et al., 2021). PEMPs' adsorption to CTAB-PKB occurred through various processes, including entanglement with small biochar particles, adherence to biochar grooves, electrostatic interactions, hydrophobic interactions, hydrogen bonding, and filter cake formation. Filter cake forms when particles accumulate, resulting in enhanced retention by obstructing the media pores and capturing more particles (Hanif et al., 2024). Pristine PKB and MPs both possessed a negative surface charge, causing electrostatic repulsion that reduced adsorption (X. Li et al., 2023). Nevertheless, the biochar treated with CTAB acquires a positive surface charge, facilitating electrostatic attraction to the negatively charged plastic particles, hence markedly improving removal efficiency (Shen et al., 2021). The mechanism of magnetic CTAB-RSB for the adsorption of NPs is ascribed to electrostatic interactions, hydrophobic interactions, pore filling, and surface complexation. Electrostatic interaction between positively charged magnetic CTAB-RSB and negatively charged PSNPs is anticipated at the acidic pH range of 3 to 6 (Xing et al., 2024).

Studies have also reported single adsorption mechanisms such as physical trapping, pore filling, or surface adsorption. For instance, Duan et al. reported stuck, trap, adsorption, and entanglement as physical interaction mechanisms between iron-modified SDB and PSNPs (Fig. 5C-b,c) (Duan et al., 2025). Xing et al. also revealed entrapment of PSNPs in magnetic CTAB-RSB as the principal adsorption mechanism (Fig. 5D-d) (Xing et al., 2024). Following adsorption, a prominent characteristic peak of PSNPs is seen at 697 cm^{-1}, corresponding to the out-of-plane vibration of C–H in the PS benzene ring, hence verifying the adsorption of PSNPs on CTAB-RSB (Fig. 5D-e) (Xing et al., 2024). Similarly, CCB enhanced the adsorption of PVCNPs in sandy soil through pore filling or physical trapping. Due to the much smaller particle size of magnetic CCB relative to sandy soil, CCB may impede the pores of the sandy soil column, thereby hindering the transport of PVC—NPs (Ni et al., 2024). PSMP adsorption on CSB was characterised by the

phenomena of stuck, trap, and entangle (Wang et al., 2020; H. Zhao et al., 2022). Similarly, the augmented surface roughness and diminished zeta potentials of the magnetic CLB and quartz mixture might result in surface deposition of plastic particles (Tong et al., 2020; Zhu et al., 2022). PSMPs of small sizes (1.0 and 10 μm) may adhere to the surface of biochar and become entrapped within its pores (J. Wang et al., 2021; Wang et al., 2020). Nonetheless, these methods appear to be ineffective for big MPs, since they are unable to penetrate the small pores of biochar. Two pathways were implicated in the elimination of PAMPs by magnetic CCB. Tiny magnetic CCB particles adhered to the surface of big PAMPs conversely, small PAMPs were adsorbed onto the surface of large biochar particles (J. Li et al., 2023). PAMPs might also engage in hydrogen bonding with CCB owing to the nitrogen and oxygen atoms in its PA structure (J. Li et al., 2023).

Babalar et al. found a notable disparity in zeta potential at the surfaces of magnetic BZC and PSMPs, resulting in a substantial electrostatic attraction due to the variation in surface charges, i.e., the negatively charged PSMP surface and the positively charged magnetic BZC (Babalar et al., 2024). Moreover, the biochar aromatic ring structure may promote π-π interactions between PSMPs and the magnetic BZC surface, resulting in accelerated adsorption (Babalar et al., 2024). PSNPs, being a hydrophobic polymer, prefer to aggregate into colloidal clusters via hydrophobic interactions in aqueous conditions (Shi et al., 2024). Nevertheless, DOM modifies the surface potential and chemical characteristics of PSNPs, enhancing their electronegativity and augmenting the electrostatic repulsion between DOM-PSNPs and magnetic SDB (Zhao et al., 2024). PSNPs and COOH-PSNPs were primarily eliminated from water by aggregation rather than adsorption. The quantities of PSNPs and COOH-PSNPs adsorbed onto CTAB-RPB were only 1.2% and 3.1% of biochar's removal capacity, respectively, whereas most NPs were eliminated from the water by aggregation. When hydrophobic NPs interacted with the CTAB layer, they might be trapped by the cetyl tail of CTAB, resulting in aggregation into a cluster. Upon reaching a sufficient size, NPs cluster detached from the surface of the biochar and ascended to the liquid surface (Y. Shi et al., 2023).

5.2. Polymer specific removal mechanisms

The predominant use of PS as a standard polymer in most of the studies generated a mechanistic framework heavily biased toward biochar adsorption requiring aromatic structures, yet this mechanism has limited applicability for non-aromatic environmentally abundant polymers such as PE, PP, PVC, PA, and PET (Kim et al., 2024; Shi et al., 2023). PS-specific adsorption mechanisms mainly include π-π bonds, which depend on benzene rings to enable electron donor-acceptor interactions with biochar's aromatic domains, but these are inapplicable for aliphatic polymers like PE and PP and only partially operative for polymers with limited aromatic content (Hanif et al., 2024; Kim et al., 2024; Shi et al., 2023). Similarly, electrostatic interactions as adsorption mechanisms are polymer-dependent, especially for aminated or carboxylated PS. In contrast, pristine PE and PP exhibit a near-neutral surface due to a lack of charged functional groups, making electrostatic attraction a negligible factor compared to hydrophobic interactions. Natural weathering introduces oxygen-containing functional groups ($C=O$, -OH, -COOH) to polymers (PE and PP) through photo-oxidation, facilitating stronger electrostatic interaction with charged biochar surfaces (Li et al., 2023; Liu et al., 2022; Singh et al., 2021). Similarly, hydrogen bonding is also ascribed as a limited adsorption route for pristine polyolefins due to lack of hydrogen bond donors or acceptors, though weathering introduces hydroxyl and carbonyl groups that facilitate bonding with biochar's oxygen rich surface, as demonstrated by aged PA showing significantly higher adsorption than their pristine counterparts. Conversely, hydrophobic interaction is a universal mechanism, though its strength depends on the specific hydrophobicity of the polymer (following the order: PE > PP > PS > PET > PA). Hydrogen bonding can further enhance by increasing the aliphatic carbon content of the biochar, such as through CTAB modification, where the surfactant's alkyl chains provide more effective binding sites (Hanif et al., 2024; Xing et al., 2024; Wang et al., 2020). On the other hand, physical adsorption mechanisms including entanglement, trapping, and pore filling are size-dependent, and polymer-independent mechanisms that function through inter-particle wedging, pore trapping, fiber entanglement, and diffusion into mesopores regardless of polymer chemical properties (Duan et al., 2025; Magid et al., 2021; Zhu et al., 2022; Wang et al., 2020). Modified biochar provides broad-spectrum efficiency to interact with MNPs by combining electrostatic attraction (via quaternary ammonium groups) with hydrophobic partitioning (via alkyl chains), allowing it to engage both aromatic and aliphatic polymers (Hanif et al., 2024; Xing et al., 2024). Despite the urgent need, mixed-polymer studies remain scarce; only two studies in our dataset evaluate PE and PA alongside PS, uncovering polymer-specific behaviours that PS-only models fail to predict (Hanif et al., 2024; Li et al., 2023). Consequently, future research must adopt a polymer-specific framework that distinguishes chemistry-dependent mechanisms (e.g., π-π bonds, hydrogen bonding, electrostatics), which vary with functionality, from physical mechanisms (e.g., pore filling, hydrophobic partitioning) that can be applied universally across plastic types.

6. Biochar regeneration and MNP degradation

For the regeneration of MNPs-laden biochar, conventional biochar regeneration techniques are suitable, which include adsorbate breakdown and desorption (Wang et al., 2020). For biochar recovery after MNPs treatment, various biochar regeneration methods have been reported in literature, such as single pyrolysis, pyrolysis in combination with ultrasonication/chemical method, single ultrasonication, ultrasonication in combination with chemical method, single chemical method, chemical method in combination with shaking and centrifugation, and hydrothermal degradation (Fig. 8, Table 3).

Pyrolysis is a prevalent biochar recycling technique due to its capacity to entirely decompose MNPs. The thermal breakdown of MNPs exceeds that of magnetic biochar, signifying enhanced stability in the latter (J. Wang et al., 2021). Multiple studies used individual pyrolysis or pyrolysis in combination with other methods to recover biochar or degrade MNPs. For instance, Wang et al. performed catalytic pyrolysis in a micro-pyrolizer at 500 °C for 10 min to degrade PSNPs (1000 nm) adsorbed on magnetic SDB. The degradation efficiency of PSNPs was 99% in the first cycle that was reduced to 94% in the fifth cycle. Fe-based catalysts with Lewis and Brønsted acid sites facilitated hydrogenation processes for NP degradation (J. Wang et al., 2021). ROS can interact with hydrocarbons, resulting in their cleavage into low molecular weight molecules that ultimately mineralize into CO_2 and H_2O (Zhu et al., 2022). Jiao et al. subjected PSNPs (100 nm) laden LBB to pyrolysis in a tube furnace at 550 °C under N_2 flow for 10 min to regenerate biochar. Biochar reuse efficiency to remove PSNPs was 88% in the first cycle, and it was significantly reduced to 28% in the third cycle (Jiao et al., 2025). Duan et al. also used pyrolysis (tube furnace, 600 °C N_2 flow 2 h) to regenerate SDB, and biochar reuse efficiencies to remove pristine PSNPs (1000 nm), NH_2-PSNPs (1000 nm), and COOH-PSNPs (1000 nm) were respectively 93, 94, and 99% in the first cycle, which were reduced to 72, 80, and 83% in the sixth cycle (Duan et al., 2025).

Some studies also used pyrolysis in combination with ultrasonication to regenerate biochar. For instance, Babalar et al. used pyrolysis (850 °C) in combination with ultrasonication for BZC regeneration to remove PSMPs, and the reuse efficiency of pristine BZC diminished from 96% to 94% after four cycles, while the reduction in efficiency for modified magnetic BZC was minimal, decreasing from 99.3% to 97% (Babalar et al., 2024). Ultrasonication of magnetic BZC reduced Fe_3O_4 at an average drop of 2.5% each regeneration cycle; however, the rate of Fe_3O_4 reduction may be alleviated with an increasing number of cycles (Babalar et al., 2024). Huang et al. also used pyrolysis (450 °C) in

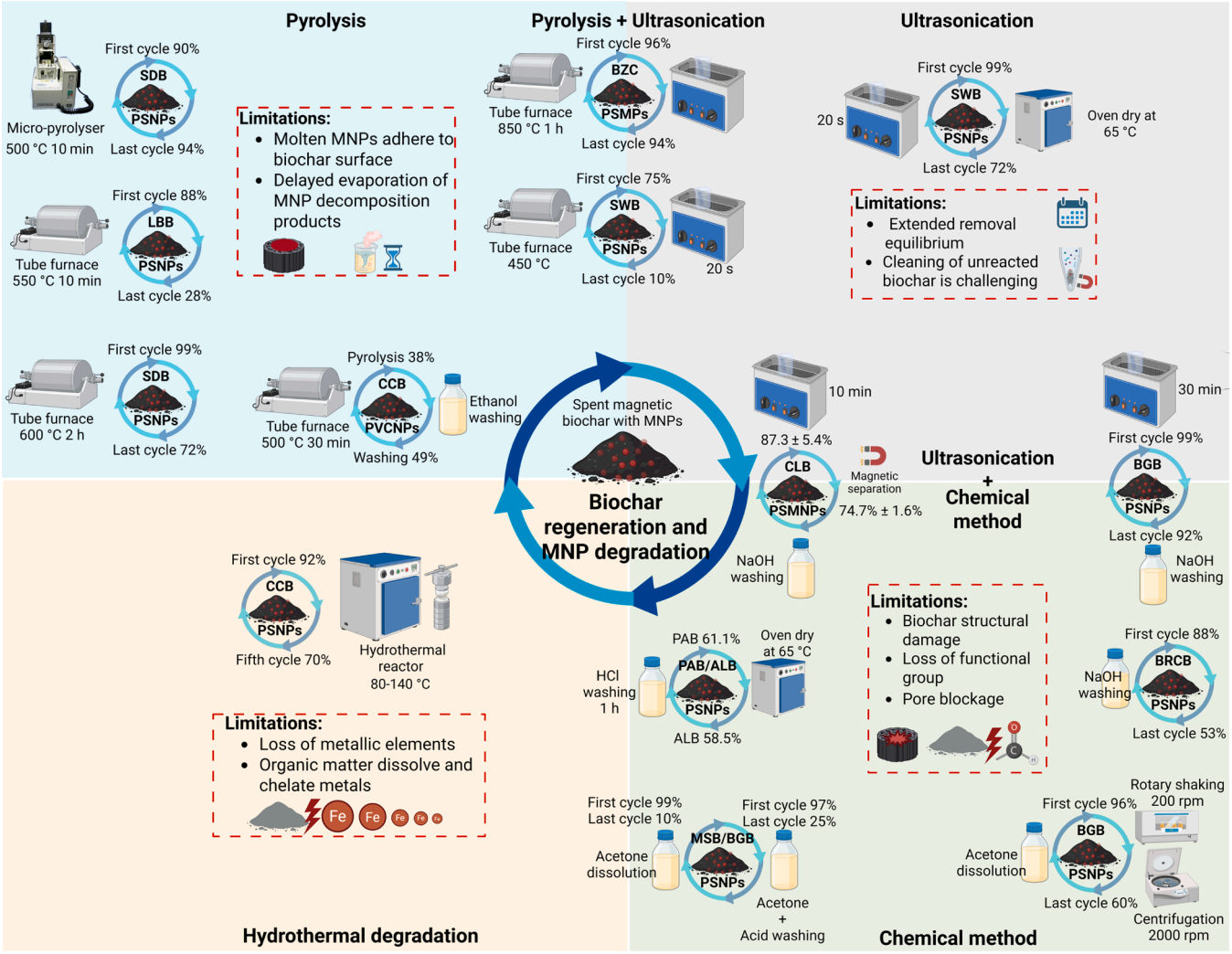

Fig. 8. Biochar regeneration approaches, reuse efficiency or MNPs degradation after treatment.

combination with ultrasonication (20 s) to regenerate SWB and found relatively low reuse efficiency to remove PSNPs (100 nm) at 75% in the first cycle and only 10% in the third cycle. Both adsorption and aggregation diminished, likely owing to NPs obstructing the adsorption sites and the repeated pyrolysis enhancing the stability of magnetic biochar characteristics (Huang et al., 2024). Although co-pyrolysis exhibited limited reusability for SWB, it effectively destroyed NPs and regenerated biochar that can be utilised in applications such as carbon sequestration (Huang et al., 2024). Similarly, lower reuse efficiency of CCB and WSB for PVCNPs removal was observed after regenerating biochar with pyrolysis (500 °C) and ethanol washing. Pyrolysis and ethanol washing showed biochar reuse efficiencies of only 38% and 49% for PVCNP removal, respectively (Li and Chen, 2024). Wang et al. assert that the regeneration of biochar composites through pyrolysis results in the collapse of micropores and the development of a mesoporous structure; however, this exerts minimal influence on adsorption, as the Langmuir model indicates that the adsorption process primarily relies on the availability of adsorption sites, which remain unaffected by pyrolysis (J. Wang et al., 2021).

Some studies used single ultrasonication or ultrasonication in combination with a chemical method/magnetic separation to regenerate biochar. For instance, Tong et al. showed that 74.7% ± 1.6% of PSMPs laden with CLB can be recovered by magnetic separation, while 87.3% ± 5.4% of CLB can be recovered after dispersing it in a 10 mM NaOH solution and ultrasonication for 10 min (Tong et al., 2020). Wang et al. regenerated PSNPs laden with BGB through ultrasonication in a 0.1 M NaOH solution for 30 min, and the regenerated BGB showed a reuse efficiency of 99% in the first cycle and 92% in the seventh cycle (Wang et al., 2025). Huang et al. regenerated PSNPs laden with SWB using ultrasonication (20 s) and then oven-dried (65 °C), and regenerated SWB showed 99% reuse efficiency in the first cycle and 72% in the third cycle (Huang et al., 2024). The ultrasonicated biochar demonstrated reliable reuse performance, sustaining an efficiency exceeding 72% after multiple cycles, likely because ultrasound treatment alters the biochar's structure (Huang et al., 2024), leading to the release of biochar colloids in subsequent recycling processes (Cao et al., 2023). The prolonged removal equilibrium time, extending from 10 h to 14 days, can be ascribed to the elimination of unreacted biochar colloids and other constituents in the solution following each recycling (Huang et al., 2024), suggesting that the release dynamics of biochar substances may influence reuse frequency and efficacy (Huang et al., 2023). Consequently, an approach involving the first desorbing MNPs through ultrasonic recycling for a minimum of three cycles, succeeded by carbon stabilization of the system through co-pyrolysis, can augment reusability (Huang et al., 2024).

Multiple studies also used chemical methods to regenerate biochar. For instance, PSNP-laden PAB and ALB were regenerated using a 0.1 mol/L HCl solution for 1 h, which were subsequently rinsed with distilled water to achieve a neutral pH state. The two recycled PAB and ALB were used to eliminate PSMPs pollutants at pH 7.0, yielding

Table 3
Biochar regeneration and MNP degradation approaches used in the available studies.

Biochar type and adsorbed MNPs	Regeneration method	Regeneration conditions	Biochar reuse efficiency/MNP degradation efficiency	Reference
Sawdust biochar (SDB), PSNPs (1000 nm)	Pyrolysis (micro-pyrolizer)	500 °C for 10 min	First cycle 99% Fifth cycle 94%	(Wang et al., 2021)
Lignin based biochar (LBB), PSNPs (100 nm)	Pyrolysis (tube furnace)	550 °C under N_2 for 10 min	First cycle 88% Third cycle 28%	(Jiao et al., 2025)
Sawdust biochar (SDB), PSNPs (1000 nm) NH_2-PSNPs (1000 nm) COOH-PSNPs (1000 nm)	Pyrolysis (tube furnace)	600 °C under N_2 for 2 h	PS First cycle 93% Sixth cycle 72% NH_2-PS First cycle 94% Sixth cycle 80% COOH-PS First cycle 99% Sixth cycle 83%	(Duan et al., 2025)
Biochar zeolite composite (BZC), PSMPs (2 μm) (15 μm)	Pyrolysis (tube furnace) + Ultrasonication	850 °C under N_2 for 1 h	First cycle 96% Fourth cycle 94%	(Babalar et al., 2024)
Seaweed biochar (SWB), PSNPs (100 nm)	Pyrolysis (tube furnace) + Ultrasonication	Pyrolysis at 450 °C, Ultrasonication for 20s	First cycle 75% Third cycle 10%	(Huang et al., 2024)
Corncob biochar (CCB), Walnut shell biochar (WSB), PVCNPs (0.05–1 μm)	Pyrolysis (tube furnace) + Chemical method	Pyrolysis at 500 °C for 30 min, 50 mL of ethanol	Treated with ethanol 49% After pyrolysis 38%	(Li and Chen, 2024)
Cellulose biochar (CLB), PS-MNPs (0.02–2 μm)	Ultrasonication + Chemical method, Magnetic separation	Ultrasonication for 10 min, 10 mM NaOH solution	87.3% ± 5.4% 74.7% ± 1.6%	(Tong et al., 2020)
Bagasse biochar (BGB), PSNPs (50 nm)	Ultrasonication + Chemical method	Ultrasonication for 30 min, 0.1 M NaOH solution	First cycle 99% Seventh cycle 92%	(Wang et al., 2025)
Seaweed biochar (SWB), PSNPs (100 nm)	Ultrasonication	Ultrasonication for 20 s, oven dry at 65 °C	First cycle 99% Third cycle 72%	(Huang et al., 2024)
Pineapple peel biochar (PAB) Artichoke leaves biochar (ALB), PSNPs (1000 nm)	Chemical method	50 mL HCl for 1h Washed with DW and oven dried at 70 °C	61.1% 58.5%	(Mahmoud et al., 2025)
Mesquite biochar (MSB), NH_2-PSNPs (1000 nm) COOH-PSNPs (1000 nm), COOH-PSNPs (30 nm)	Chemical method	Acetone dissolution	NH_2-PS First cycle 99% Fourth cycle 95% COOH-PS First cycle 99% Fourth cycle 95% COOH-PS First cycle 48% Fourth cycle 10%	(Singh et al., 2021)
Bagasse biochar (BGB), COOH-PSNPs (500 nm) COOH-PSNPs (100 nm) NH_2-PSNPs (100 nm)	Chemical method	Acetone dissolution Acid washing	COOH-PS First cycle 97% Third cycle 91% COOH-PS First cycle 95% Third cycle 70% NH_2-PS First cycle 80% Third cycle 25%	(Ganie et al., 2023)
Bagasse biochar (BGB), NH_2-PSNPs (100 nm) SO_4^{2-}-PSNPs (100 nm)	Chemical method + Shaking + Centrifugation	Aceton rotary shaker at 200 rpm for 1 hr centrifuged at 2000 rpm 5 mL 98 % acetone	NH_2-PS First cycle 96% Sixth cycle 60% SO_4^{2-}-PS First cycle 95% Seventh cycle 65%	(Ganie et al., 2025)
Bagasse, rice husk, coconut shell biochar (BRCB), COOH-PSNPs (1000 nm)	Chemical method	0.1 M NaOH	First cycle 88% Fourth cycle 53%	(Parashar and Hait, 2024)
Contaminated Corncob biochar (CCB), mining area, PSNPs (100 nm)	Hydrothermal degradation	NPs + DW (20:50) 80–140 °C	First cycle 92.2% Fifth cycle 70.2%	(Zhu et al., 2022)

removal efficiencies of 61.1% and 58.5%, respectively (Mahmoud et al., 2024). Singh et al. used acetone dissolution to regenerate PSNP-laden magnetic MSBs, showing reuse efficiency of 99% in the first cycle and 95% in the fourth cycle for both NH_2-PSNPs (1000 nm) and COOH-PSNPs (1000 nm), while 48% in the first cycle and 10% in the fourth cycle for COOH-PSNPs (30 nm) (Singh et al., 2021). Acetone dissolution led to the release of Fe from the composite following adsorption with PSNPs, and it was found to be below the acceptable limits for iron in drinking water (<0.3 mg/L). The separation of sorbed PSNPs and the regeneration of the adsorbent for reuse have potential for industrial-scale applications (Singh et al., 2021). Ganie et al. used acetone dissolution and acid washing to regenerate PSNPs laden with BGB and found the removal efficiencies of 97% in the first cycle and 91% in the third cycle for COOH-PSNPs (500 nm), 95% in the first cycle and 70% in the third cycle for COOH-PSNPs (100 nm), and 80% in the first cycle and 53% in the third cycle for NH_2-PSNPs (100 nm), respectively (Ganie et al., 2023). Ganie et al. in another study, regenerated BGB using 95% acetone in a rotary shaker (200 rpm, 1 hr) and centrifugation (2000 rpm) and found the removal efficiencies to be 96% in the first cycle and 60% in the sixth cycle for NH_2-PSNPs and 95% in the first cycle and 65% in the sixth cycle for SO_4^{2-}-PSNPs (Ganie et al., 2025). Parahshar and Hait regenerated PSNPs loaded BRCB using 0.1 M NaOH and found 88%

reuse efficiency in the first cycle and 25% in the fourth cycle (N. Parashar and Hait, 2024).

Zhu et al. used hydrothermal degradation to regenerate PSNPs laden with magnetic CCB (Zhu et al., 2022). The reusability of CCB was assessed during five successive regeneration cycles, and the adsorption capacity of CCB reached 45 mg/g after five cycles. The degradation efficiency of PSNPs decreased from 92.2% in the first cycle to 70.2% after five cycles, attributed to the loss of metallic constituents. During hydrothermal degradation, DOM can solubilize and chelate metal ions (Zhu et al., 2022). Plastic particles disappeared from the CCB surface after degradation, and surface properties were partly restored (Fig. 5B-c). The intensity of peaks associated with the vibration of PSNP aromatic rings at 810, 750, and 692 cm^{-1} largely decreased after hydrothermal degradation, showing the effective removal of PSNPs (Fig. 5B-c) (Zhu et al., 2022). However, the residual compounds are not readily and thoroughly eliminated from the active areas with basic hydrothermal treatment (Jonidi Jafari et al., 2017).

In summary, biochar regeneration methods exhibit inherent trade-offs: pyrolysis is effective yet energy-demanding and may modify biochar porosity, whereas ultrasonication paired with chemicals is less invasive but has challenges regarding long-term stability. The chemical method provides ease of use but is ineffective for small or functionalized MNPs, whereas hydrothermal degradation demonstrates potential yet encounters scalability issues related to metal leaching. Therefore, combined approaches, such as ultrasonication, chemical washing, and moderate pyrolysis, may achieve a compromise between biochar efficiency and reusability, although they necessitate additional optimisation for practical implementation.

7. Limitations, economic feasibility, research gaps and future directions

7.1. Limitations and methodological challenges

- Quantification of actual adsorption efficiency of MNP on biochar is challenging by the lack of standardized analytical procedures (Koelmans et al., 2019). Most studies rely on indirect quantification (e.g., fluorescence intensity, UV–Vis spectrophotometry) that may not accurately distinguish between aggregated versus adsorbed MNPs (Y. Shi et al., 2023). Analysis using UV–Vis spectrophotometry can yield high adsorption concentrations due to the release of fine biochar colloids or changes in light scattering caused by MNP-biochar complexes (J. Wang et al., 2021). Previous studies suggested that apparent negative adsorption may be attributed to analytical interference rather than true desorption (Zhang et al., 2024). Advanced analytical techniques such as pyrolysis GC/MS or Nile Red staining are relatively more accurate, which are not routinely applied in quantification of adsorbed concentration of MNPs (M. Junaid et al., 2024; Primpke et al., 2020).
- Post-adsorption quantitative recovery of MNPs from biochar remains challenging. Desorption can be inefficient due to strong interactions (e.g., π-π bonding, hydrophobic interactions), leading to underestimation of adsorbed amounts (Duan et al., 2025). For magnetic biochar, while recovery is facilitated by magnetic separation, complete separation of MNP-laden biochar from media is rarely 100% efficient, with residual biochar colloids remaining suspended (Tong et al., 2020). In terrestrial samples, distinguishing between biochar-retained MNPs and soil particles is also analytically challenging (Ni et al., 2024).
- DOM, inorganic ions, and colloidal particles in natural water and soil samples can interfere with MNP-biochar interactions. Active sites on biochar surfaces can be blocked by DOM through competitive adsorption, which can reduce MNP removal efficiency by up to 80% (Zhao et al., 2024). Similarly, cations such as Ca^{2+} may either compete or bridge with MNPs depending on concentration, creating non-linear effects that can complicate adsorption process (Li et al., 2023). In wastewater, organic matter and surfactants can alter aggregation behaviour and surface charges, making laboratory-based adsorption capacities poorly representing real-world treatment performance (Babalar et al., 2024).
- A critical limitation in available studies is the inability to distinguish between actual adsorption (bonded on biochar surfaces) versus heteroaggregation (MNP-biochar or MNP-MNP clustering) followed by sedimentation (Shi et al., 2023). Shi et al. highlighted that 97% of apparent removal capacities for some biochar systems may result from aggregation rather than adsorption, with implications for biochar regeneration and reusability (Shi et al., 2023). Studies that report removal efficiencies without taking account of aggregation may overestimate actual adsorption capacity.

7.2. Comparative economic feasibility of biochar application

- The estimated biochar production cost ranges from USD 150–600 per tonne depending on scale, feedstock, and pyrolysis technology. Biochar produced from agricultural waste (corncob, rice straw, bagasse) represents the lower cost (USD 150–250/tonne) compared to engineered modified biochar (USD 300–600/tonne), including the modification reagents and energy costs (Tang et al., 2026; Samsudin et al., 2025). This compares favourably with commercial CNTs (USD 1000–120,000/tonne) (Chenarani et al., 2025; Zhu, 2023), AC (USD 1500–2000/tonne) (Lee and He, 2025), and graphene (USD 50, 000–200,000/tonne) (Gkika et al., 2025).
- Biochar production becomes cheaper and more cost-effective at scales >1000 tonnes/year. Pyrolysis facilities processing agricultural waste at regional scale can achieve production costs below USD 200/tonne (Kadam et al., 2025). Magnetic biochar can be regenerated for 4–7 cycles with an efficiency loss <30% (Duan et al., 2025; Wang et al., 2025). Thermal degradation of adsorbed MNPs on spent biochar during pyrolysis generates recoverable energy (approximately 25–40 MJ/kg for PS), improving life-cycle economics (Grigiante et al., 2010; Javed et al., 2022). Moreover, biochar production from agricultural waste prevents emissions (CO_2, $PM_{2.5}$) from open-field burning, providing additional benefits in carbon credits and lowering health costs (Kadam et al., 2025).

In conclusion, while adsorption technologies face immense challenges for high-flow applications (e.g., major wastewater treatment plants), biochar-based adsorption of MNPs is economically viable for (i) stormwater bioretention systems, (ii) decentralized water treatment, (iii) polishing steps post-conventional treatment, and (iv) industrial wastewater with high MNP loads. Hence, the combination of low cost, regeneration potential, and waste pyrolysis makes modified biochar a rational, and often superior alternative to both conventional and advanced MNP removal methods.

7.3. Research gaps and future directions

- Most of the research on biochar-based MNP removal was performed in controlled laboratory settings utilizing batch or column experiments. Subsequent investigations ought to concentrate on extensive field studies to assess the biochar MNP removal potential in real environmental matrices (e.g., rivers, lakes, and oceans). Furthermore, there is currently no study that has emphasized the removal of environmental MNPs (which are naturally polydisperse) from real-world samples. The examined MNPs are predominantly commercially available spherical polystyrene, which might be less abundant in the environment compared to other MNP shapes such as films, foams, fragments, fibres, and MNP polymers including PP, PE, PA, polymethyl methacrylate (PMMA), PVC, and PET have been inadequately studied. Moreover, NPs posed more challenges for their removal through biochar owing to their diminutive size and enhanced mobility. Numerous studies demonstrated reduced

adsorption of NPs on biochar in comparison to MPs. Research should concentrate on the development of biochar with improved NP retention and removal capabilities.

- The long-term efficiency and aging impacts of biochar in laboratory and natural environments remain little comprehended. Studies are required to evaluate the temporal alterations in biochar characteristics and their effect on removal efficiency. The impact of biochar on the removal of artificially aged MNPs has been studied; however, the natural aging of biochar and MNPs requires additional investigation.
- The impact of diverse environmental factors, including competitive ions, pH, temperature, salinity, and organic matter on biochar's performance, has been examined in laboratory settings; however, these factors necessitate investigation in natural aquatic and terrestrial environments where conditions are more intricate.
- Although adsorption and filtration mechanisms are frequently reported, the precise interactions (e.g., electrostatic forces, hydrophobic contacts, hydrogen bonding) between biochar and various types of MNPs require more investigation to elucidate any biochar-MNP polymer/shape/size-specific interaction mechanisms.
- The impact of various modification techniques (e.g., magnetic coating, chemical activation, organic matter treatment) on the removal efficiency of biochar remains suboptimally addressed. Future research ought to systematically evaluate modification strategies. Magnetisation of biochar was mainly achieved using iron from several commercially accessible sources. Research seldom employed sustainable iron sources, such as red mud waste or iron mining byproducts, to magnetize biochar. Moreover, the alteration of biochar with iron may result in either an enhancement or reduction of its surface area and adsorption capacity. Consequently, this necessitated additional research to elucidate the definitive effects of biochar magnetisation.
- Most research concentrates on individual MNP polymers and seldom examines mixtures of several polymers, sizes, or shapes for biochar treatment. Investigation is required to ascertain the performance of biochar in the presence of a polydisperse mixture of plastic particles and to determine if competitive adsorption takes place.
- Although certain studies address biochar regeneration by pyrolysis, ultrasonication, and chemical techniques, the practical reusability of biochar in continuous systems and the effects of regeneration cycles on its efficiency are still inadequately researched. The optimisation of biochar regeneration methods, their economic viability, and the degradation of MNPs from spent biochar require further investigation.
- The economic viability of large-scale biochar production and deployment for the removal of MNPs requires assessment, including comparisons with current technologies. Further research is required on sustainable feedstocks for biochar manufacturing. The influence of various biomass feedstocks (e.g., agricultural waste, municipal sludge) on the efficacy of biochar for the removal of MNPs remains inadequately investigated.
- The fate of biochar-MNP complexes in the environment, including sedimentation, degradation, or re-release, remains ambiguous and necessitates additional research. Moreover, the modification of biochar using mining waste or other sources should be evaluated for its ecological safety.
- The integration of biochar into existing water and wastewater treatment infrastructures, such as filtration facilities and stormwater systems, necessitates empirical studies. Most experiments are performed in static systems. Investigation is required to assess biochar's efficacy under dynamic situations (e.g., flowing water, tidal influences). The absence of standardized methodologies for assessing the removal effectiveness of MNPs by biochar impedes comparative analysis. Establishing standardized testing techniques is crucial for advancement in the discipline.

The identified limitations and future research directions underscore the necessity for interdisciplinary studies that integrate materials science, environmental engineering, and toxicology to enhance the safe and sustainable use of biochar in the remediation of MNPs.

8. Conclusion

This review emphasizes the effective removal of MNPs employing both pristine and modified biochar. Feedstock, pyrolysis temperature, and modification are essential primary factors for optimizing biochar. Corncob biochar, mesquite biochar, bagasse biochar, walnut shell biochar, and sawdust biochar were the predominant biochars utilized for MNP removal. Laboratory studies using environmental samples from freshwater, seawater, and wastewater for the removal of typical MNPs have been done; however, research on the removal of real-world MNPs from aquatic and terrestrial remains scarce. Increased pyrolysis temperatures ($>500\ ^{\circ}C$) yield high-quality biochar with enhanced surface area and superior adsorption capacity, attributed to the development of pore structures akin to a honeycomb configuration. Modified biochar, particularly with magnetic properties, offers a promising and adaptable approach for the removal of MNPs and high biochar regeneration. MNP removal potential of biochar is dependent on plastic size: larger particles like MPs are often removed with over 95% efficiency, whereas NPs exhibit decreased adsorption due to size constraints and enhanced mobility. The adsorption of MNPs on biochar can be influenced by the characteristics of MNPs (polymer type, functional group, size, shape, aging, and concentration), the properties of biochar (surface area, pore size, pore volume, concentration, zeta potential, charge, functional group, and modification), and environmental conditions (pH, temperature, organic matter, interfering ions, reaction time, and agitation). The interaction of MNPs with biochar can transpire through several mechanisms, including pore-filling, physical entrapment, surface complexation, electrostatic interactions, hydrogen bonding, hydrophobic interactions, and π-π interactions. Integrated methods, including ultrasonication, chemical washing, and moderate pyrolysis, can increase biochar regeneration; however, they require further optimization for practical application. A multidisciplinary method integrating materials science, environmental engineering, and ecotoxicology is required to optimize and enhance the application of biochar in the remediation of environmental plastics.

Funding

The authors would like to acknowledge the funding support from the Leverhulme Trust (Grant Reference No RPG-2024–221).

CRediT authorship contribution statement

Muhammad Junaid: Writing – review & editing, Writing – original draft, Visualization, Software, Formal analysis, Data curation, Conceptualization. **Stuart Cairns:** Writing – review & editing, Validation, Supervision, Resources, Funding acquisition. **Iain Robertson:** Writing – review & editing, Validation, Supervision, Resources, Funding acquisition. **Peter J. Holliman:** Writing – review & editing, Validation, Supervision, Resources, Funding acquisition.

Declaration of competing interest

The authors declare that they have no known competing financial interests or personal relationships that could have appeared to influence the work reported in this paper.

Data availability

Data will be made available on request

References

Afraz, M., Muhammad, F., Nisar, J., Shah, A., Munir, S., Ali, G., Ahmad, A., 2024. Production of value added products from biomass waste by pyrolysis: an updated review. Waste Manag. Bull. 1, 30–40. https://doi.org/10.1016/j.wmb.2023.08.004.

Aiken, G.R., Hsu-Kim, H., Ryan, J.N., 2011. Influence of dissolved organic matter on the environmental fate of metals, nanoparticles, and colloids. Env., Sci, Technol 45, 3196–3201. https://doi.org/10.1021/es103992s.

Amalina, F., Abd Razak, A.S., Zularisam, A.W., Aziz, M.A.A., Krishnan, S., Nasrullah, M., 2023. Comprehensive assessment of biochar integration in agricultural soil conditioning: advantages, drawbacks, and future prospects. Phys. Chem. Earth 132, 103508. https://doi.org/10.1016/j.pce.2023.103508. Parts A/B/C.

Amalina, F., Krishnan, S., Zularisam, A.W., Nasrullah, M., 2024. Pristine and modified biochar applications as multifunctional component towards sustainable future: recent advances and new insights. Sci. Total Env. 914, 169608. https://doi.org/10.1016/j.scitotenv.2023.169608.

Anuwa-Amarh, N.A., Dizbay-Onat, M., Venkiteshwaran, K., Wu, S., 2024. Carbon-based adsorbents for microplastic removal from wastewater. Mater. (Basel) 17. https://doi.org/10.3390/ma17225428.

Asghar, F., Shakoor, B., Fatima, S., Munir, S., Razzaq, H., Naheed, S., Butler, I.S., 2022. Fabrication and prospective applications of graphene oxide-modified nanocomposites for wastewater remediation. RSC Adv 12, 11750–11768. https://doi.org/10.1039/d2ra00271j.

Babalar, M., Siddiqua, S., Sakr, M.A., 2024. A novel polymer coated magnetic activated biochar-zeolite composite for adsorption of polystyrene microplastics: synthesis, characterization, adsorption and regeneration performance. Sep Purif Technol 331, 125582. https://doi.org/10.1016/j.seppur.2023.125582.

Besseling, E., Redondo-Hasselerharm, P., Foekema, E.M., Koelmans, A.A., 2018. Quantifying ecological risks of aquatic micro- and nanoplastic. Crit. Rev. Env. Sci. Technol. 1–49. https://doi.org/10.1080/10643389.2018.1531688.

Bhattacharjee, S., 2016. DLS and zeta potential - what they are and what they are not? J. Control, Release 235, 337–351. https://doi.org/10.1016/j.jconrel.2016.06.017.

Bian, S.-W., Mudunkotuwa, I.A., Rupasinghe, T., Grassian, V.H., 2011. Aggregation and dissolution of 4 nm ZnO nanoparticles in aqueous environments: influence of pH, ionic strength, size, and adsorption of humic acid. Langmuir 27, 6059–6068. https://doi.org/10.1021/la200570n.

Cairns, S., Meza-Rojas, D., Holliman, P.J., Robertson, I., 2024. Interactions between biochar and nano(micro)plastics in the remediation of aqueous media. Int. J. Env. Res. 18, 87. https://doi.org/10.1007/s41742-024-00635-0.

Cao, W., Xu, H., Zhang, X., Xiang, W., Qi, G., Wan, L., Gao, B., 2023. Novel post-treatment of ultrasound assisting with acid washing enhance lignin-based biochar for CO2 capture: adsorption performance and mechanism. Chem. Eng. J. 471, 144523. https://doi.org/10.1016/j.cej.2023.144523.

Chen, T., Da, T., Ma, Y., 2021. Reasonable calculation of the thermodynamic parameters from adsorption equilibrium constant. J. Mol, Liq 322, 114980. https://doi.org/10.1016/j.molliq.2020.114980.

Chenarani, Bentolhoda, Ghaemi, Ahad, Hemmati, Alireza, 2025. A review on the conversion of carbon dioxide into solid carbon materials, Iranian. Chem. Eng. J.

Cheng, N., Wang, B., Wu, P., Lee, X., Xing, Y., Chen, M., Gao, B., 2021. Adsorption of emerging contaminants from water and wastewater by modified biochar: a review. Env. Pollut. 273, 116448. https://doi.org/10.1016/j.envpol.2021.116448.

Das, K.P., Chauhan, P., Staudinger, U., Satapathy, B.K., 2024. Exploring sustainable adsorbents to mitigate micro-/nano-plastic contamination: perspectives on electrospun fibrous constructs, biochar, and aerogels. Env., Sci,: Adv 3, 1217–1243. https://doi.org/10.1039/D4VA00039K.

Dong, S., Xia, J., Sheng, L., Wang, W., Liu, H., Gao, B., 2021. Transport characteristics of fragmental polyethylene glycol terephthalate (PET) microplastics in porous media under various chemical conditions. Chemosphere 276, 130214. https://doi.org/10.1016/j.chemosphere.2021.130214.

Duan, X., Chen, X., Shi, L., Cao, Y., Liang, Y., wang, T., Huang, C., Cao, Y., 2025. Functionality-dependent removal efficiency and mechanisms of polystyrene microplastics by a robust magnetic biochar. J. Environ. Chem. Eng. 13, 115509. https://doi.org/10.1016/j.jece.2025.115509.

Feng, D., Yi, J., Liu, Y., Fu, J., Gong, R., Li, H., 2025. Efficiency of adsorption ofPSNPs using spontaneous magnetic biochar prepared from pyrolysis of municipal sludge and industrial red mud solid waste. J. Chem, Technol, Biotechnol. https://doi.org/10.1002/jctb.7819.

Ganie, Z.A., Khandelwal, N., Tiwari, E., Singh, N., Darbha, G.K., 2021. Biochar-facilitated remediation of nanoplastic contaminated water: effect of pyrolysis temperature induced surface modifications. J. Hazard, Mater 417, 126096. https://doi.org/10.1016/j.jhazmat.2021.126096.

Ganie, Z.A., Khandelwal, N., Choudhary, A., Darbha, G.K., 2023. Clean water production from plastic and heavy metal contaminated waters using redox-sensitive iron nanoparticle-loaded biochar. Env., Res 235, 116605. https://doi.org/10.1016/j.envres.2023.116605.

Ganie, Z.A., Choudhary, A., Darbha, G.K., 2025. Agro-waste biochar embedded sulfidised nZVI for removal of microplastics and synthetic dyes from wastewater: a continuous filtration approach with effective removal in complex aqueous matrices. Colloids Surf. A: Physicochem. Eng. Asp. 710, 136233. https://doi.org/10.1016/j.colsurfa.2025.136233.

Gao, J., Pan, S., Li, P., Wang, L., Hou, R., Wu, W.-M., Luo, J., Hou, D., 2021. Vertical migration of microplastics in porous media: multiple controlling factors under wet-dry cycling. J. Hazard, Mater 419, 126413. https://doi.org/10.1016/j.jhazmat.2021.126413.

Ghaffar, A., Abbas, G., 2016. Adsorption of phthalic acid esters (PAEs) on chemically aged biochars. Green Process. Synth. 5. https://doi.org/10.1515/gps-2016-0014.

Gkika, D.A., Maroulas, K.N., Kyzas, G.Z., 2025. Various reduced graphene oxide green synthetic routes: comparing the cost procedures. ACS Omega 10, 36221–36237. https://doi.org/10.1021/acsomega.5c04090.

Gong, Y., Bai, Y., Zhao, D., Wang, Q., 2022. Aggregation of carboxyl-modified polystyrene nanoplastics in water with aluminum chloride: structural characterization and theoretical calculation. Water Res. 208, 117884. https://doi.org/10.1016/j.watres.2021.117884.

Grigiante, M., Ischia, M., Baratieri, M., Dal Maschio, R., Ragazzi, M., 2010. Pyrolysis analysis and solid residue stabilization of polymers, waste tyres, spruce sawdust and sewage sludge. Waste Biomass Valor 1, 381–393. https://doi.org/10.1007/s12649-010-9038-2.

Groppe, P., Wintzheimer, S., Eigen, A., Gaß, H., Halik, M., Mandel, K., 2022. Real-time monitoring of magnetic nanoparticle-assisted nanoplastic agglomeration and separation from water. Env. Sci.: Nano 9, 2427–2439. https://doi.org/10.1039/D2EN00131D.

Guo, J., Chen, B., 2014. Insights on the molecular mechanism for the recalcitrance of biochars: interactive effects of carbon and silicon components. Env., Sci, Technol 48, 9103–9112. https://doi.org/10.1021/es405647e.

Guo, J.-J., Huang, X.-P., Xiang, L., Wang, Y.-Z., Li, Y.-W., Li, H., Cai, Q.-Y., Mo, C.-H., Wong, M.-H., 2020. Source, migration and toxicology of microplastics in soil. Env. Int. 137, 105263. https://doi.org/10.1016/j.envint.2019.105263.

Gupta, P., 2023. Mechanisms involved in the removal of contaminants by biochar from an aqueous medium. Integrative Strategies for Bioremediation of Environmental Contaminants. Elsevier, pp. 199–223. https://doi.org/10.1016/B978-0-443-14013-6.00015-9. Volume Two.

Hanif, M.A., Ibrahim, N., Hayazi, N.A., Dahalan, F.A., Md. Ali, U.F., Jalil, A.A., Syafiuddin, A., 2024. Enhancement of microplastics and nanoplastics removal via filtration method using surface-engineered palm kernel shell biochar. Sep Purif Technol, 130596. https://doi.org/10.1016/j.seppur.2024.130596.

Haziq, J.M., Amalina, I.F., Syukor, A.R.A., 2020. Peat Swamp Groundwater treatment: Efficiency of Mixed Citrus Peel and Kernel Activated Carbon Layer. IOP Conference ….

Heo, Y., Lee, E.-H., Lee, S.-W., 2022. Adsorptive removal of micron-sized polystyrene particles using magnetic iron oxide nanoparticles. Chemosphere 307, 135672. https://doi.org/10.1016/j.chemosphere.2022.135672.

Ho, W.-K., Leung, K.S.-Y., 2021. The crucial role of heavy metals on the interaction of engineered nanoparticles with polystyrene microplastics. Water Res. 201, 117317. https://doi.org/10.1016/j.watres.2021.117317.

Huang, J., Tan, X., Ali, I., Duan, Z., Naz, I., Cao, J., Ruan, Y., Wang, Y., 2023. More effective application of biochar-based immobilization technology in the environment: understanding the role of biochar. Sci, Total Env. 872, 162021. https://doi.org/10.1016/j.scitotenv.2023.162021.

Huang, J., Tan, X., Ali, I., Ok, Y.S., Duan, Z., Liang, J., Zhu, R., 2024. Efficient removal of nanoplastics by iron-modified biochar: understanding the removal mechanisms. Env. Pollut 363, 125121. https://doi.org/10.1016/j.envpol.2024.125121.

Isobe, A., Iwasaki, S., Uchida, K., Tokai, T., 2019. Abundance of non-conservative microplastics in the upper ocean from 1957 to 2066. Nat. Commun. 10, 417. https://doi.org/10.1038/s41467-019-08316-9.

Javed, N., Muhammad, S., Iram, S., Ramay, M.W., Jaffri, S.B., Damak, M., Fekete, G., Varga, Z., Székács, A., Aleksza, L., 2022. Analysis of fuel alternative products obtained by the pyrolysis of diverse types of plastic materials isolated from a dumpsite origin in Pakistan. Polymer 15. https://doi.org/10.3390/polym15010024.

Ji, G., Xing, Y., You, T., 2024. Biochar as adsorbents for environmental microplastics and nanoplastics removal. J. Environ. Chem. Eng. 12, 113377. https://doi.org/10.1016/j.jece.2024.113377.

Jiao, Y., Wang, S., Sun, B., Han, Y., Zhang, Z., Shen, X., Li, Z., 2025. Adsorption efficiency and in-situ catalytic thermal degradation behaviour of microplastics from water over Fe-modified lignin-based magnetic biochar. Sep Purif Technol 353, 128468. https://doi.org/10.1016/j.seppur.2024.128468.

Jonidi Jafari, A., Kakavandi, B., Jaafarzadeh, N., Rezaei Kalantary, R., Ahmadi, M., Akbar Babaei, A., 2017. Fenton-like catalytic oxidation of tetracycline by AC@Fe3O4 as a heterogeneous persulfate activator: adsorption and degradation studies. J. Ind. Eng. Chem. 45, 323–333. https://doi.org/10.1016/j.jiec.2016.09.044.

Junaid, M., Wang, J., 2021a. Interaction of micro(nano)plastics with extracellular and intracellular biomolecules in the freshwater environment. Crit. Rev. Env. Sci. Technol. 1–25. https://doi.org/10.1080/10643389.2021.2002078.

Junaid, M., Wang, J., 2021b. Interaction of nanoplastics with extracellular polymeric substances (EPS) in the aquatic environment: a special reference to eco-corona formation and associated impacts. Water Res. 201, 117319. https://doi.org/10.1016/j.watres.2021.117319.

Junaid, M., Wang, J., 2022. Microplastics contamination in receiving water systems. In: Ni, B., Xu, Q., Wei, W. (Eds.), Microplastics in Urban Water Management. Wiley, pp. 243–286. https://doi.org/10.1002/9781119759379.ch8.

Junaid, M., Abbas, Z., Siddiqui, J.A., Liu, S., Tabraiz, S., Yue, Q., Wang, J., 2023a. Ecotoxicological impacts associated with the interplay between micro(nano)plastics and pesticides in aquatic and terrestrial environments. TrAC Trends Anal. Chem., 117133 https://doi.org/10.1016/j.trac.2023.117133.

Junaid, M., Liu, S., Chen, G., Liao, H., Wang, J., 2023b. Transgenerational impacts of micro(nano)plastics in the aquatic and terrestrial environment. J. Hazard, Mater 443, 130274. https://doi.org/10.1016/j.jhazmat.2022.130274.

Junaid, M., Hamid, N., Liu, S., Abbas, Z., Imran, M., Haider, M.R., Wang, B., Chen, G., Khan, H.K., Yue, Q., Xu, N., Wang, J., 2024a. Interactive impacts of photoaged micro (nano)plastics and co-occurring chemicals in the environment. Sci. Total Env. 927, 172213. https://doi.org/10.1016/j.scitotenv.2024.172213.

Junaid, M., Liu, S., Yue, Q., Wei, M., Wang, J., 2024b. Trophic transfer and interfacial impacts of micro(nano)plastics and per-and polyfluoroalkyl substances in the

environment. J. Hazard. Mater. 465, 133243. https://doi.org/10.1016/j.jhazmat.2023.133243.
Junaid, M., Liu, S., Liao, H., Yue, Q., Wang, J., 2024c. Environmental nanoplastics quantification by pyrolysis-gas chromatography-mass spectrometry in the Pearl River, China: first insights into spatiotemporal distributions, compositions, sources and risks. J. Hazard. Mater 476, 135055. https://doi.org/10.1016/j.jhazmat.2024.135055.
Kadam, P., Dwivedi, P., Marrero, T.W., 2025. Biochar economics for private landowners with payments from carbon markets and federal incentives. Glob., Change Biol., Bioenergy 17. https://doi.org/10.1111/gcbb.70065.
Kameda, T., Horikoshi, K., Kumagai, S., Saito, Y., Yoshioka, T., 2020. Adsorption of urea, creatinine, and uric acid onto spherical activated carbon. Sep Purif Technol 237, 116367. https://doi.org/10.1016/j.seppur.2019.116367.
Kihara, S., Köper, I., Mata, J.P., McGillivray, D.J., 2021. Reviewing nanoplastic toxicology: it's an interface problem. Adv, Colloid Interface Sci 288, 102337. https://doi.org/10.1016/j.cis.2020.102337.
Kim, J., Lee, Y.-G., Kim, H., Chon, K., Phae, C., 2024. One-step synthesis of magnetic biochar via co-pyrolysis of walnut shells and Fe-rich mine tails for adsorption capacity improvement of polystyrene sulfonate microplastics: role of microplastic size. Environ. Technol. Innov. 34, 103624. https://doi.org/10.1016/j.eti.2024.103624.
Kiss, T., Fórián, S., Szatmári, G., Sipos, G., 2021. Spatial distribution of microplastics in the fluvial sediments of a transboundary river - a case study of the Tisza River in Central Europe. Sci. Total Env. 785, 147306. https://doi.org/10.1016/j.scitotenv.2021.147306.
Koelmans, A.A., Mohamed Nor, N.H., Hermsen, E., Kooi, M., Mintenig, S.M., De France, J., 2019. Microplastics in freshwaters and drinking water: critical review and assessment of data quality. Water Res. 155, 410–422. https://doi.org/10.1016/j.watres.2019.02.054.
Kumar, R., Verma, A., Rakib, M.R.J., Gupta, P.K., Sharma, P., Garg, A., Girard, P., Aminabhavi, T.M., 2023. Adsorptive behavior of micro(nano)plastics through biochar: co-existence, consequences, and challenges in contaminated ecosystems. Sci, Total Env. 856, 159097. https://doi.org/10.1016/j.scitotenv.2022.159097.
Kundu, S., Patel, S., Halder, P., Patel, T., Hedayati Marzbali, M., Pramanik, B.K., Paz-Ferreiro, J., de Figueiredo, C.C., Bergmann, D., Surapaneni, A., Megharaj, M., Shah, K., 2021. Removal of PFASs from biosolids using a semi-pilot scale pyrolysis reactor and the application of biosolids derived biochar for the removal of PFASs from contaminated water. Env. Sci.: Water Res. Technol. 7, 638–649. https://doi.org/10.1039/D0EW00763C.
Lee, B., He, J., 2025. Circular carbon capture: comparative life cycle and techno-economic assessment of waste-derived activated carbons. Env., Sci, Technol 59, 25791–25802. https://doi.org/10.1021/acs.est.5c09338.
Leng, L., Xiong, Q., Yang, L., Li, H., Zhou, Y., Zhang, W., Jiang, S., Li, H., Huang, H., 2021. An overview on engineering the surface area and porosity of biochar. Sci, Total Env. 763, 144204. https://doi.org/10.1016/j.scitotenv.2020.144204.
Leslie, H.A., van Velzen, M.J.M., Brandsma, S.H., Vethaak, A.D., Garcia-Vallejo, J.J., Lamoree, M.H., 2022. Discovery and quantification of plastic particle pollution in human blood. Env. Int 163, 107199. https://doi.org/10.1016/j.envint.2022.107199.
Li, J., Chen, X., 2024. A turbidity-based study of removing polyvinyl chloride nanoplastics using magnetic biochar. J. Environ. Chem. Eng. 12, 113067. https://doi.org/10.1016/j.jece.2024.113067.
Li, S., Yang, M., Wang, H., Jiang, Y., 2022. Adsorption of microplastics on aquifer media: effects of the action time, initial concentration, ionic strength, ionic types and dissolved organic matter. Env., Pollut 308, 119482. https://doi.org/10.1016/j.envpol.2022.119482.
Li, J., Chen, X., Yu, S., Cui, M., 2023a. Removal of pristine and aged microplastics from water by magnetic biochar: adsorption and magnetization. Sci, Total Env. 875, 162647. https://doi.org/10.1016/j.scitotenv.2023.162647.
Li, J., Yu, S., Chen, X., Cai, Y., Cui, M., 2023b. Highly enhanced adsorption of antibiotics on aged polyamide microplastics. Colloids Surf. A: Physicochem. Eng. Asp. 658, 130690. https://doi.org/10.1016/j.colsurfa.2022.130690.
Li, X., Zhang, Y., Xu, H., Sun, Y., Gao, B., Wu, J., 2023c. Granular limestone amended sand filters for enhanced removal of nanoplastics from water: performance and mechanisms. Water Res. 229, 119443. https://doi.org/10.1016/j.watres.2022.119443.
Liu, J., Ma, Y., Zhu, D., Xia, T., Qi, Y., Yao, Y., Guo, X., Ji, R., Chen, W., 2018. Polystyrene nanoplastics-enhanced contaminant transport: role of irreversible adsorption in glassy polymeric domain. Env., Sci, Technol 52, 2677–2685. https://doi.org/10.1021/acs.est.7b05211.
Liu, G., Zhu, Z., Yang, Y., Sun, Y., Yu, F., Ma, J., 2019. Sorption behavior and mechanism of hydrophilic organic chemicals to virgin and aged microplastics in freshwater and seawater. Env., Pollut 246, 26–33. https://doi.org/10.1016/j.envpol.2018.11.100.
Liu, N., Yu, F., Wang, Y., Ma, J., 2022. Effects of environmental aging on the adsorption behavior of antibiotics from aqueous solutions in microplastic-graphene coexisting systems. Sci, Total Env. 806, 150956. https://doi.org/10.1016/j.scitotenv.2021.150956.
Liu, S., Junaid, M., Sadaf, M., Ai, W., Lan, X., Wang, J., 2023. A novel framework-based meta-analysis for in-depth characterization of microplastic pollution and associated ecological risks in Chinese Bays. J. Hazard. Mater 444, 130423. https://doi.org/10.1016/j.jhazmat.2022.130423.
Magid, A.S.I., Islam, M.S., Chen, Y., Weng, L., Li, J., Ma, J., Li, Y., 2021. Enhanced adsorption of polystyrene nanoplastics (PSNPs) onto oxidized corncob biochar with high pyrolysis temperature. Sci. Total Env. 784, 147115. https://doi.org/10.1016/j.scitotenv.2021.147115.
Mahmoud, M.E., Ibrahim, G.A.A., 2023. Cr(VI) and doxorubicin adsorptive capture by a novel bionanocomposite of Ti-MOF@TiO2 incorporated with watermelon biochar and chitosan hydrogel. Int, J. Biol, Macromol 253, 126489. https://doi.org/10.1016/j.ijbiomac.2023.126489.
Mahmoud, S.El.M.E., Abdel-Fattah, T.M., Mahmoud, M.E., Díaz, E., 2024. Assessing the removal efficiency of microplastics: a comparative study using nanosized biochars derived from sustainable sources. Environ. Nanotechnol. Monit. Manag. 22, 100977. https://doi.org/10.1016/j.enmm.2024.100977.
Mahmoud, S.El.M.E., Abdel-Fattah, T.M., Mahmoud, M.E., Díaz, E., 2025. Efficient removal performance of polystyrene microplastics from strongly acidic solutions by two functionalized nanosized biochars derived from low-cost sustainable sources. Sci, Total Env. 969, 178892. https://doi.org/10.1016/j.scitotenv.2025.178892.
Maia, L.C., Soares, L.C., Alves Gurgel, L.V., 2021. A review on the use of lignocellulosic materials for arsenic adsorption. J. Env., Manage 288, 112397. https://doi.org/10.1016/j.jenvman.2021.112397.
Masud, M.A.A., Shin, W.S., Sarker, A., Septian, A., Das, K., Deepo, D.M., Iqbal, M.A., Islam, A.R.M.T., Malafaia, G., 2023. A critical review of sustainable application of biochar for green remediation: research uncertainty and future directions. Sci. Total Env. 904, 166813. https://doi.org/10.1016/j.scitotenv.2023.166813.
Na, S.-H., Kim, M.-J., Kim, J.-T., Jeong, S., Lee, S., Chung, J., Kim, E.-J., 2021. Microplastic removal in conventional drinking water treatment processes: performance, mechanism, and potential risk. Water Res. 202, 117417. https://doi.org/10.1016/j.watres.2021.117417.
Nanninga, G.B., Horswill, C., Lane, S.M., Manica, A., Briffa, M., 2020. Microplastic exposure increases predictability of predator avoidance strategies in hermit crabs. J. Hazard. Mater. Lett., 100005 https://doi.org/10.1016/j.hazl.2020.100005.
Ni, Z., Chen, X., Cui, M., Li, J., 2024. Polyvinyl chloride nanoplastics transport inhibited in natural sandy soil by iron-modified biochar. Env., Monit, Assess 196, 830. https://doi.org/10.1007/s10661-024-13000-7.
Oliveira, A.C., Dantas Neto, A.A., Moura, M.C.P.A., Castro Dantas, T.N., 2023. Use of surfactant-modified adsorbents in the removal of microplastics from wastewater. J. Environ. Chem. Eng. 11, 110827. https://doi.org/10.1016/j.jece.2023.110827.
Parashar, N., Hait, S., 2024a. Cetyl trimethyl ammonium bromide-modified magnetic biochar-integrated sand filter for microplastics removal from secondary-treated sewage effluents: performance evaluation and mechanistic insights. J. Water Process Eng. 59, 105035.
Parashar, N., Hait, S., 2024b. Enhanced microplastics removal from sewage effluents via CTAB-modified magnetic biochar: efficacy and environmental impact. J. Clean, Prod 474, 143606. https://doi.org/10.1016/j.jclepro.2024.143606.
Pikula, K., Chaika, V., Zakharenko, A., Markina, Z., Vedyagin, A., Kuznetsov, V., Gusev, A., Park, S., Golokhvast, K., 2020. Comparison of the level and mechanisms of toxicity of carbon nanotubes, carbon nanofibers, and silicon nanotubes in bioassay with four marine microalgae. Nanomater. (Basel) 10. https://doi.org/10.3390/nano10030485.
Pitt, J.A., Kozal, J.S., Jayasundara, N., Massarsky, A., Trevisan, R., Geitner, N., Wiesner, M., Levin, E.D., Di Giulio, R.T., 2018. Uptake, tissue distribution, and toxicity of polystyrene nanoparticles in developing zebrafish (Danio rerio). Aquat. Toxicol. 194, 185–194. https://doi.org/10.1016/j.aquatox.2017.11.017.
PlasticEurope, Plastics—the facts 2024, an analysis of European latest …. (2024).
Primpke, S., Christiansen, S.H., Cowger, W., De Frond, H., Deshpande, A., Fischer, M., Holland, E.B., Meyns, M., O'Donnell, B.A., Ossmann, B.E., Pittroff, M., Sarau, G., Scholz-Böttcher, B.M., Wiggin, K.J., 2020. Critical assessment of analytical methods for the harmonized and cost-efficient analysis of microplastics. Appl, Spectrosc. 74, 1012–1047. https://doi.org/10.1177/0003702820921465.
Ramirez Arenas, L., Ramseier Gentile, S., Zimmermann, S., Stoll, S., 2021. Nanoplastics adsorption and removal efficiency by granular activated carbon used in drinking water treatment process. Sci, Total Env. 791, 148175. https://doi.org/10.1016/j.scitotenv.2021.148175.
Ravi Kumar, M.N.V., Sameti, M., Mohapatra, S.S., Kong, X., Lockey, R.F., Bakowsky, U., Lindenblatt, G., Schmidt, H., Lehr, C.M., 2004. Cationic silica nanoparticles as gene carriers: synthesis, characterization and transfection efficiency in vitro and in vivo. J. Nanosci, Nanotechnol 4, 876–881. https://doi.org/10.1166/jnn.2004.120.
Rodrigues, M.O., Abrantes, N., Gonçalves, F.J.M., Nogueira, H., Marques, J.C., Gonçalves, A.M.M., 2018. Spatial and temporal distribution of microplastics in water and sediments of a freshwater system (Antuã River, Portugal). Sci, Total Env. 633, 1549–1559. https://doi.org/10.1016/j.scitotenv.2018.03.233.
Román, S., Ledesma, B., González, J.F., Al-Kassir, A., Engo, G., Álvarez-Murillo, A., 2013. Two stage thermal regeneration of exhausted activated carbons. Steam gasification of effluents. J. Anal, Appl, Pyrolysis 103, 201–206. https://doi.org/10.1016/j.jaap.2012.08.017.
Samsudin, M.H., Mohd Yusoff, M.Z., Roslan, A.M., Hassan, M.A., Idris, J., Ahmad Farid, M.A., Yoshihito, S., 2025. Economic evaluation of woodchip-derived bio-adsorbent production: a case study using a self-sustained pilot-scale pool-type carbonization reactor. Env., Sci, Pollut, Res., Int. 32, 20414–20426. https://doi.org/10.1007/s11356-025-36859-6.
H.P. Schmidt, T. Bucheli, C. Kammann, B. Glaser, European biochar certificate-guidelines for a sustainable production of biochar, (2016).
Sheha, R.R., El-Zahhar, A.A., 2008. Synthesis of some ferromagnetic composite resins and their metal removal characteristics in aqueous solutions. J. Hazard, Mater 150, 795–803. https://doi.org/10.1016/j.jhazmat.2007.05.042.
Shen, M., Hu, T., Huang, W., Song, B., Zeng, G., Zhang, Y., 2021. Removal of microplastics from wastewater with aluminosilicate filter media and their surfactant-modified products: performance, mechanism and utilization. Chem. Eng. J. 421, 129918. https://doi.org/10.1016/j.cej.2021.129918.
Shi, Q., Guo, S., Tang, J., Lyu, H., Ri, C., Sun, H., 2023a. Enhanced removal of aged and differently functionalized polystyrene nanoplastics using ball-milled magnetic pinewood biochars. Env. Pollut 316, 120696. https://doi.org/10.1016/j.envpol.2022.120696.

Shi, Y., Du, J., Zhao, T., Feng, B., Bian, H., Shan, S., Meng, J., Christie, P., Wong, M.H., Zhang, J., 2023b. Removal of nanoplastics from aqueous solution by aggregation using reusable magnetic biochar modified with cetyltrimethylammonium bromide. Env. Pollut 318, 120897. https://doi.org/10.1016/j.envpol.2022.120897.

Shi, C., Wu, H., Wang, W., Zhao, J., Niu, F., Geng, J., 2024. Microplastic removal from water using modified maifanite with rotating magnetic field affected. J. Clean, Prod 434, 140111. https://doi.org/10.1016/j.jclepro.2023.140111.

Singh, N., Tiwari, E., Khandelwal, N., Darbha, G.K., 2019. Understanding the stability of nanoplastics in aqueous environments: effect of ionic strength, temperature, dissolved organic matter, clay, and heavy metals. Env., Sci,: Nano 6, 2968–2976. https://doi.org/10.1039/C9EN00557A.

Singh, N., Khandelwal, N., Ganie, Z.A., Tiwari, E., Darbha, G.K., 2021. Eco-friendly magnetic biochar: an effective trap for nanoplastics of varying surface functionality and size in the aqueous environment. Chem. Eng. J. 418, 129405. https://doi.org/10.1016/j.cej.2021.129405.

Singh, R., Samuel, M.S., Ravikumar, M., Ethiraj, S., Kumar, M., 2024. Graphene materials in pollution trace detection and environmental improvement. Env. Res. 243, 117830. https://doi.org/10.1016/j.envres.2023.117830.

Soffian, M.S., Abdul Halim, F.Z., Aziz, F., A.Rahman, M., Mohamed Amin, M.A., Awang Chee, D.N., 2022. Carbon-based material derived from biomass waste for wastewater treatment. Environ. Adv. 9, 100259. https://doi.org/10.1016/j.envadv.2022.100259.

Sridharan, S., Kumar, M., Singh, L., Bolan, N.S., Saha, M., 2021. Microplastics as an emerging source of particulate air pollution: a critical review. J. Hazard. Mater. 418, 126245. https://doi.org/10.1016/j.jhazmat.2021.126245.

Sun, C., Wang, Z., Chen, L., Li, F., 2020. Fabrication of robust and compressive chitin and graphene oxide sponges for removal of microplastics with different functional groups. Chem. Eng. J. 393, 124796. https://doi.org/10.1016/j.cej.2020.124796.

Sun, C., Wang, Z., Zheng, H., Chen, L., Li, F., 2021. Biodegradable and re-usable sponge materials made from chitin for efficient removal of microplastics. J. Hazard, Mater 420, 126599. https://doi.org/10.1016/j.jhazmat.2021.126599.

Sun, M., Yang, Y., Huang, M., Fu, S., Hao, Y., Hu, S., Lai, D., Zhao, L., 2022. Adsorption behaviors and mechanisms of antibiotic norfloxacin on degradable and nondegradable microplastics. Sci, Total Env. 807, 151042. https://doi.org/10.1016/j.scitotenv.2021.151042.

Tang, Y., Zhang, S., Su, Y., Wu, D., Zhao, Y., Xie, B., 2021. Removal of microplastics from aqueous solutions by magnetic carbon nanotubes. Chem. Eng. J. 406, 126804. https://doi.org/10.1016/j.cej.2020.126804.

Tang, Y., Ford, J., Cockerill, T.T., 2026. Environmental and economic assessment of biochar production systems from agricultural residues. Biochar 8, 24. https://doi.org/10.1007/s42773-025-00527-2.

Tong, M., He, L., Rong, H., Li, M., Kim, H., 2020. Transport behaviors of plastic particles in saturated quartz sand without and with biochar/Fe3O4-biochar amendment. Water Res. 169, 115284. https://doi.org/10.1016/j.watres.2019.115284.

Torboli, A., Foladori, P., Bruni, L., 2025. Enhanced removal of small microplastics (1–5 μm) from secondary-treated wastewater using Spent Coffee Grounds biochar: application of flow cytometry. J. Water Process Eng. 71, 107270. https://doi.org/10.1016/j.jwpe.2025.107270.

Tumwet, F.C., Serbe, R., Kleint, T., Scheytt, T., 2022. Effect of fragmentation on the transport of polyvinyl chloride and low-density polyethylene in saturated quartz sand. Sci, Total Env. 836, 155657. https://doi.org/10.1016/j.scitotenv.2022.155657.

Wadhawan, S., Jain, A., Nayyar, J., Mehta, S.K., 2020. Role of nanomaterials as adsorbents in heavy metal ion removal from waste water: a review. J. Water Process Eng. 33, 101038. https://doi.org/10.1016/j.jwpe.2019.101038.

Waldschläger, K., Schüttrumpf, H., 2020. Infiltration behavior of microplastic particles with different densities, sizes, and shapes-from glass spheres to natural sediments. Env., Sci, Technol 54, 9366–9373. https://doi.org/10.1021/acs.est.0c01722.

Wan, H., Wang, J., Sheng, X., Yan, J., Zhang, W., Xu, Y., 2022. Removal of polystyrene microplastics from aqueous solution using the metal-organic framework material of ZIF-67. Toxics 10. https://doi.org/10.3390/toxics10020070.

Wang, Z., Sedighi, M., Lea-Langton, A., 2020a. Filtration of microplastic spheres by biochar: removal efficiency and immobilisation mechanisms. Water Res. 184, 116165. https://doi.org/10.1016/j.watres.2020.116165.

Wang, H., Zhao, W., Chen, Y., Li, Y., 2020b. Nickel aluminum layered double oxides modified magnetic biochar from waste corncob for efficient removal of acridine orange. Bioresour, Technol 315, 123834. https://doi.org/10.1016/j.biortech.2020.123834.

Wang, J., Sun, C., Huang, Q.-X., Chi, Y., Yan, J.-H., 2021a. Adsorption and thermal degradation of microplastics from aqueous solutions by Mg/Zn modified magnetic biochars. J. Hazard. Mater 419, 126486. https://doi.org/10.1016/j.jhazmat.2021.126486.

Wang, J., Zhao, X., Wu, A., Tang, Z., Niu, L., Wu, F., Wang, F., Zhao, T., Fu, Z., 2021b. Aggregation and stability of sulfate-modified polystyrene nanoplastics in synthetic and natural waters. Env., Pollut 268, 114240. https://doi.org/10.1016/j.envpol.2020.114240.

Wang, C., Wei, W., Zhang, Y.-T., Ni, B.-J., 2022. Evaluating the role of biochar in mitigating the inhibition of polyethylene nanoplastics on anaerobic granular sludge. Water Res. 221, 118855. https://doi.org/10.1016/j.watres.2022.118855.

Wang, P., Duan, P., Mao, D., Kong, X., Hu, M., Wang, C., Piao, Y., 2025. Robust polyaniline coating magnetic biochar nanoparticles for fast and wide pH and temperature range removal of nanoplastics and achieving label free detection. Water Res. 277, 123313. https://doi.org/10.1016/j.watres.2025.123313.

Winterton, R.H.S., 1970. Van der Waals forces. Contemp, Phys 11, 559–574. https://doi.org/10.1080/00107517008202194.

Xing, X., Zhang, Y., Zhou, G., Zhang, Y., Yue, J., Wang, X., Yang, Z., Chen, J., Wang, Q., Zhang, J., 2023. Mechanisms of polystyrene nanoplastics adsorption onto activated carbon modified by ZnCl2. Sci. Total Env. 876, 162763. https://doi.org/10.1016/j.scitotenv.2023.162763.

Xing, Y., Zhang, B., Niu, Q., Ji, G., 2024. Enhanced adsorption of polystyrene nanoplastics by cetyltrimethylammonium bromide surface-modified magnetic rice straw biochar: efficient performance and adsorption mechanisms. Sep Purif Technol 344, 127264. https://doi.org/10.1016/j.seppur.2024.127264.

Yao, C., Wang, B., Zhang, J., Faheem, M., Feng, Q., Hassan, M., Zhang, X., Lee, X., Wang, S., 2024. Formation mechanisms and degradation methods of polycyclic aromatic hydrocarbons in biochar: a review. J. Env. Manage 357, 120610. https://doi.org/10.1016/j.jenvman.2024.120610.

Yi, Y., Tu, G., Zhao, D., Tsang, P.E., Fang, Z., 2019. Biomass waste components significantly influence the removal of Cr(VI) using magnetic biochar derived from four types of feedstocks and steel pickling waste liquor. Chem. Eng. J. 360, 212–220. https://doi.org/10.1016/j.cej.2018.11.205.

Zhang, X., Lv, D., Liu, Z., Xu, D., Yang, F., Wang, X., Tan, Z., Gao, W., Liu, R., Su, C., 2024a. Removal of polystyrene microplastic from aqueous solutions with London Plane bark biochar: pyrolysis temperature, performance and mechanism. Colloids Surf. A: Physicochem. Eng. Asp. 694, 134159. https://doi.org/10.1016/j.colsurfa.2024.134159.

Zhang, J., Chen, Z., Liu, Y., Wei, W., Ni, B.-J., 2024b. Removal of emerging contaminants (ECs) from aqueous solutions by modified biochar: a review. Chem. Eng. J. 479, 147615. https://doi.org/10.1016/j.cej.2023.147615.

Zhao, H., Huang, X., Wang, L., Zhao, X., Yan, F., Yang, Y., Li, G., Gao, P., Ji, P., 2022a. Removal of polystyrene nanoplastics from aqueous solutions using a novel magnetic material: adsorbability, mechanism, and reusability. Chem. Eng. J. 430, 133122. https://doi.org/10.1016/j.cej.2021.133122.

Zhao, W., Su, Z., Geng, T., Zhao, Y., Tian, Y., Zhao, P., 2022b. Effects of ionic strength and particle size on transport of microplastic and humic acid in porous media. Chemosphere 309, 136593. https://doi.org/10.1016/j.chemosphere.2022.136593.

Zhao, H., Song, F., Ji, P., 2024. Dissolved organic matter decreases the interaction between polystyrene nanoplastics and magnetic biochar in multi-solute systems. Desalination 592, 118207. https://doi.org/10.1016/j.desal.2024.118207.

Zheng, Q., Xue, Q., Yan, K., Hao, L., Li, Q., Gao, X., 2007. Investigation of molecular interactions between SWNT and polyethylene/polypropylene/polystyrene/polyaniline molecules. J. Phys, Chem, C 111, 4628–4635. https://doi.org/10.1021/jp066077c.

Zhou, G., Huang, X., Xu, H., Wang, Q., Wang, M., Wang, Y., Li, Q., Zhang, Y., Ye, Q., Zhang, J., 2022. Removal of polystyrene nanoplastics from water by CuNi carbon material: the role of adsorption. Sci. Total Env. 820, 153190. https://doi.org/10.1016/j.scitotenv.2022.153190.

Zhu, S., Ho, S.-H., Huang, X., Wang, D., Yang, F., Wang, L., Wang, C., Cao, X., Ma, F., 2017. Magnetic nanoscale zerovalent iron assisted biochar: interfacial chemical behaviors and heavy metals remediation performance. ACS Sustain, Chem, Eng 5, 9673–9682. https://doi.org/10.1021/acssuschemeng.7b00542.

Zhu, K., Chen, C., Xu, M., Chen, K., Tan, X., Wakeel, M., Alharbi, N.S., 2018. In situ carbothermal reduction synthesis of Fe nanocrystals embedded into N-doped carbon nanospheres for highly efficient U(VI) adsorption and reduction. Chem. Eng. J. 331, 395–405. https://doi.org/10.1016/j.cej.2017.08.126.

Zhu, N., Yan, Q., He, Y., Wang, X., Wei, Z., Liang, D., Yue, H., Yun, Y., Li, G., Sang, N., 2022. Insights into the removal of polystyrene nanoplastics using the contaminated corncob-derived mesoporous biochar from mining area. J. Hazard, Mater 433, 128756. https://doi.org/10.1016/j.jhazmat.2022.128756.

Zhu, D., 2023. Carbon nanotube production from CO2 via high temperature electrolysis | events | Imperial College London. https://www.imperial.ac.uk/events/167563/carbon-nanotube-production-from-co2-via-high-temperature-electrolysis/ accessed March 9, 2026.